LINKING BROWN ADIPOSE TISSUE AND NAFLD BY METABOLOMICS IN ADULTS AND CHILDREN

INVESTIGATING THE PLASMA METABOLOME IN RELATION TO BROWN ADIPOSE TISSUE AND NON-ALCOHOLIC FATTY LIVER DISEASE IN ADULTS AND CHIDLREN

By NINA VARAH, B.Sc.

A Thesis Submitted to the School of Graduate Studies in Partial Fulfilment of the Requirements for the Degree of Master of Science

MASTER OF SCIENCES (Department of Medical Sciences, 2020)

McMaster University, Hamilton, Ontario

TITLE: Investigating the plasma metabolome in relation to brown adipose tissue and Non-Alcoholic Fatty Liver Disease in adults and children

AUTHOR: Nina Varah, BSc (McMaster University)

SUPERVISOR: Dr. Katherine Morrison

COMMITTEE MEMBERS: Dr. Katherine Morrison, Dr. Gregory Steinberg, Dr. Jonathan Schertzer

NUMBER OF PAGES: xv, 118

ABSTRACT

BACKGROUND: Brown adipose tissue (BAT) has emerged as an attractive target to address the dramatic rise in obesity and non-alcoholic fatty liver disease (NAFLD) in adults and children due to its ability to clear lipids through thermogenesis when activated with cold stimulation. Cross-sectional studies have identified an inverse relationship between BAT and NAFLD in adults, although no linking mechanism or relevance in children is known. Metabolomics provides a non-invasive platform to investigate BAT physiology and its relationship with hepatic fat in an effort to identify potential targets for further investigation.

PROJECT OBJECTIVES:

1) To explore the associations between the plasma metabolome and BAT in adults and children.
2) To explore the associations between the plasma metabolome and hepatic fat in adults and children.
3) To identify metabolites associated with both BAT and hepatic fat as potential linking mechanisms for further study.

METHODOLOGY: We recruited 63 male and female adults aged 18 to 57 years and 25 healthy male children aged 8 to 10 years into this cross-sectional study. Study participants underwent blood work, body composition measurement (dual energy X-ray absorptiometry; DXA) and magnetic resonance imaging (MRI) - proton density fat fraction (PDFF) measurements of whole liver hepatic fat, pre- and post-cold supraclavicular fat. BAT activity was calculated as the percent change between post and pre-cold BAT PDFF with the cold stimulus consisting of a water-perfused suit maintained at 18°C for 3-hours (adult) or 1-hour (pediatric). Targeted liquid-chromatography/mass spectrometry metabolomics of 102 metabolites was conducted on fasted

plasma and multivariate linear regression with multiple testing correction was used to examine metabolite predictors of BAT measures and hepatic fat.

RESULTS: In the adult cohort (n=63, median age 25.9 years, median body mass index (BMI) 25.4 kg/m^2), five metabolites were associated with baseline BAT lipid content, where an elevated lipid content may indicate a whiter adipose tissue-like phenotype. Aconitate and creatine commonly predict increased baseline BAT lipid content (β=0.420, *P*=0.001 and β=0.408, *P*=0.001, respectively), and reduced BAT activity (β=-0.462, *P*=0.002 and (β=-0.402, *P*=0.002, respectively). Alanine and two acyl-carnitines also predicted reduced BAT activity. Glutamic acid was similarly related to higher baseline BAT (β=0.480, *P*<0.001) and hepatic lipid content independent of age and sex (β=0.392, *P*=0.002). Three other metabolites were directly related to hepatic fat, and serine inversely. In children (n=25, median age 9.89 years, mean BMI Z-score 1.25), cysteine and cystine were trending towards a significant relationship with higher baseline BAT lipid content, and were both related to elevated hepatic fat independent of adiposity (cysteine: quadratic β=-0.714, p<0.001 and cystine: quadratic β=0.592, p<0.001). Two hydroxy-proline isomers and L-carnitine were associated with reduced BAT activity.

CONCLUSION: In adults, several metabolites were associated with reduced BAT activity and with a higher baseline BAT lipid content in the non-stimulated state – aconitate and creatine were related to both. Acylcarnitines or their metabolites related to BAT in both children and adults, which may suggest areas for subsequent investigation of BAT metabolism. Glutamic acid in adults and cysteine and cystine in children were weakly related to elevated baseline BAT and hepatic fat content. Further, amino acids such as glutamic acid and cysteine may be markers of increased ectopic fat accumulation – and are also associated with a whiter ambient BAT phenotype. Cumulatively, these findings highlight targets for further investigation into BAT physiology and the link to the liver.

ACKNOWLEDGEMENTS

There are so many people that were crucial in making this journey possible with their constant support and positivity. First, I am deeply grateful for everything that my supervisor Dr. Katherine Morrison has done for me over the past two years - your mentorship through this challenging process was essential to help me to grow into a better student, researcher, and person. Thank you for teaching and challenging me through the research process and supporting me in all aspects of life as a graduate student.

I'd also like to extend my gratitude to my committee members, Dr. Gregory Steinberg and Dr. Jonathon Schertzer for your inspiration, knowledge and encouragement through this process. Research is a team effort, and your feedback and support allowed me to create as robust of a project as possible while developing academically.

Next, a HUGE thank you to my amazing GETBAT team – Dr. Basma Ahmed, Elizabeth Gunn, Frank Ong and Prasiddha Parthasarathy, you are all rock stars! I cannot emphasize enough how much unwavering support you've given me. Basma – the best work mom ever – being able to learn from and lean on a mentor/friend like you means more than words can describe. Elizabeth, thank you for our weekly lunch dates, for being my #1 cheerleader, and being the biggest source of support in the good times and even more so the bad. Thank you, Frank, for teaching me the ropes of the brown fat world and helping me find my feet in grad school, and, Prasiddha, for being ever-so helpful, lovely and always encouraging.

I am especially lucky and thankful to also have been surrounded by all of the other wonderful people on our research team – Josée, Chiara, Efrah, Vivian, Selena and Patrick. Obsessing over CrossFit across the office with Josée and fighting over the nachos vs. fries debate with Efrah are just a couple of the things that made this experience about way more than just

research. Thank you, Patrick, for being so willing to help me every time I bugged you about another statistics question (and there were a lot). Thank you everyone for being the best second family I could've asked for!

I would also like to acknowledge Dr. Edward Chouchani and Dr. Evanna Mills at the Dana Farber Cancer Institute for their collaboration in the metabolomics arm of this project.

Most importantly, the biggest thank you of all has to go to my support system of family and friends. To my parents, words cannot describe how grateful I am for all of your unconditional encouragement, love and confidence in me, especially during this challenging past year. Finally, thank you, Andrew, for being my partner in crime through everything and for every time you believed in me more than I did myself.

"Baby got BAT!" – Josée Ivars

TABLE OF CONTENTS

LIST OF FIGURES AND TABLES

LIST OF ABBEVIATIONS

12,13-diHOME: 12,13-dihydroxy-9Z-octadecenoic acid

AA: amino acid

AAA: aromatic amino acid

ALT: alanine aminotransferase

AST: aspartate aminotransferase

ATGL: adipose triglyceride lipase

ATP: adenosine triphosphate

BA: bile acid

BAT: brown adipose tissue

BCAA: branched-chain amino acid

BH: Benjamini-Hochberg

BIA: bioelectrical impedance analysis

BMI: body mass index

CT: computed tomography

DNL: *de novo* lipogenesis

DXA: dual energy X-ray absorptiometry

ESI: electrospray ionization

FA: fatty acid

FDR: false-discovery rate

^{18}F-FDG: ^{18}F-flurodeoxyglucose

FOV: field of view

GC: gas chromatography

GETBAT: Gene Environment Team on Brown/Beige Adipose Tissue

GGT: gamma-glutamyltransferase

GSH: glutathione

HCC: hepatocellular carcinoma

HDL: high-density lipoprotein

HNS: head/neck/spine

ICC: intra-class correlation coefficient

IQR: interquartile range

IRT: infrared thermography

LC: liquid chromatography

LysoPC: lysophosphatidylcholine

MALDI: matrix-assisted laser desorption ionization

MetS: metabolic syndrome

MS: mass spectroscopy

MRE: magnetic resonance elastography

MRI: magnetic resonance imaging

MRS: magnetic resonance spectroscopy

mTORC1: mechanistic target of rapamycin complex 1

MUFA: monounsaturated fatty acid

m/z: mass-to-charge ratio

NAFLD: non-alcoholic fatty liver disease

NASH: non-alcoholic steatohepatitis

NMR: nuclear magnetic resonance

Nrg4: neuroregulin-4

NST: non-shivering thermogenesis

OGTT: oral glucose tolerance test

PC: phosphatidylcholine

PCA: principal component analysis

PDFF: proton-density fat fraction

PET: positron-emission tomography

POX: proline oxidase

ROI: region of interest

ROS: reactive oxygen species

SD: standard deviation

SCV: supraclavicular

T2*: T2* relaxation

TCA: tricarboxylic acid

UCP-1: uncoupling protein-1

US: ultrasound

WAT: white adipose tissue

CHAPTER 1: LITERATURE REVIEW

Obesity has risen to epidemic levels across Canada and the world. Statistics Canada has reported almost two-thirds of Canadian adults and one-third of children are overweight or obese[1]. Furthermore, obesity is associated with cardiometabolic and other complications increasing the morbidity and mortality related to this condition[1]. One major comorbidity is non-alcoholic fatty liver disease (NAFLD), consequently becoming the most common cause of liver disease in adults with an estimated world-wide prevalence of 25%[2]. The prevalence of NAFLD in children is also progressively rising, which is now estimated to be between 3-10% or up to 40-70% in children with obesity[3]. NAFLD is an umbrella term of liver diseases along a spectrum ranging from simple hepatic steatosis (≥ 5% lipid content) to hepatic inflammation (i.e., non-alcoholic steatohepatitis, NASH), fibrosis, cirrhosis and hepatocellular carcinoma (HCC)[4]. Progression along that spectrum is, however, not fully understood and treatment options are limited.

Obesity is classically defined as excess adiposity, but it is important to recognize that two types of adipose tissue exist. Best known is white adipose tissue (WAT), which is the storage vessel for excess energy as fat. Brown adipose tissue (BAT), on the other hand, has a largely opposite role from WAT. Rather than energy storage, BAT takes up circulating glucose and lipids and metabolizes them as fuel for non-shivering thermogenesis (NST) when sympathetically activated by cold exposure. BAT is prevalent in varying amounts in adults and children and, amongst adults, BAT activity is lowest in those with obesity and/or diabetes with insulin resistance[5–7]. The physiological significance of ambient and cold-stimulated BAT is not fully elucidated in humans and much of our mechanistic understanding comes from pre-clinical models. Metabolomics may provide valuable insight into BAT physiology or targets for novel BAT biomarkers as metabolites are produced and consumed in the process of NST. Research

relating the circulating metabolome to BAT presence or activity is very limited in adults, and completely absent in children. Therefore, one objective of this project is to fill the gap in knowledge of human BAT physiology from a metabolomic perspective and propose novel biomarkers of BAT presence or activity to be tested further.

As noted above, the underlying risk factors and pathophysiology of NAFLD are not fully elucidated and treatment options remain limited[2]. Therefore, novel strategies to fully understand, diagnose and treat NAFLD in adults and children are being investigated. Given the thermogenic and lipid-clearing potential of BAT, several investigators have considered whether stimulation of BAT tissue might improve NAFLD. Cross-sectional data provides evidence that BAT and NAFLD are inversely related in adult humans, although the mechanistic connection has yet to be discovered[8,9]. This relationship has not yet been investigated in a pediatric population. Pre-clinical studies have utilized metabolomics to propose a causal relationship between BAT activity and reduced hepatic fat accumulation, with acyl-carnitine and branched-chain amino acid (BCAA) metabolism among the pathways of interest[10,11]. An overarching objective of this project is thus to examine the metabolome associated with BAT activity and hepatic fat accumulation in humans and to compare these and identify if there are any potential metabolic connections that may prompt future mechanistic studies.

1.1 Brown Adipose Tissue

Adipose tissue can be divided into two distinct and unique populations: WAT and BAT. WAT is much more widely regarded as ‘classic’ fat in that its main role is the storage of lipids. Thus, WAT is key in the development of obesity. BAT, however, has a unique role in NST due to the high abundance of uncoupling protein-1 (UCP-1) and other thermogenic genes. UCP-1 effectively uncouples mitochondrial respiration from energy production enabling fuel sources to

flux through the mitochondria and produce heat rather than be stored as energy (i.e., adenosine triphosphate; ATP). BAT is maximally activated under both acute and chronic environmental cold conditions, and activity is reversed to baseline when returned to warmth[12]. BAT contains a high abundance of mitochondria and is highly vascularized by sympathetic nerve fibres[13]. In contrast, WAT cells are composed of one large storage vacuole and are largely poorly vascularized. Given these characteristics of BAT, it may have therapeutic potential for treatment of obesity and related health issues due to its ability to metabolize and clear lipids through thermogenesis. Brown adipocytes are also found within WAT depots and so called 'brite' or 'beige' adipocytes, represent an intermediary phenotype.

In humans, BAT was thought to be only present in infants and to progressively disappear in adulthood. However, the use of positron-emission tomography (PET) with computed tomography (CT) and labelled glucose (^{18}F-fluorodeoxyglucose, ^{18}F-FDG) has allowed researchers to confirm the presence of BAT depots in adult humans[5–7]. These depots of high metabolic activity and immunoreactivity for UCP-1 were found in the supraclavicular (SCV), mediastinal, paravertebral and perirenal regions[14]. Human BAT activity was classically assessed by ^{18}F-FDG PET-CT after acute cold exposure, with researchers finding a very high prevalence of active BAT (>95%) in a cohort of healthy male volunteers[7]. BAT activity in this study also positively correlated with resting metabolic rate in cold and thermoneutral conditions, further supporting the involvement of BAT in whole-body energy metabolism[7]. The ability to detect cold-stimulated BAT activity by PET-CT was further supported by Yoneshiro *et al.*[15] in a larger cohort of 162 male and female adults across a wide age range of 20 to 73 years.

1.2 Measuring BAT

1.2.1 PET-CT

The use of PET-CT with ^{18}F-FDG is considered the gold standard to assess BAT activity. ^{18}F-FDG is a radiolabelled analogue of glucose and is taken up by tissues in the same manner as glucose, and specifically in BAT when sympathetically activated. The tracer becomes phosphorylated and trapped in the tissue allowing quantification of BAT volume and metabolic activity. However, the main fuel source for BAT is fatty acids from intracellular lipolysis rather than glucose and therefore this tracer is not the most accurate at reflecting BAT activity[16,17]. Glucose uptake by BAT is also insulin-dependent and therefore the use of ^{18}F-FDG in subjects with diabetes or insulin resistance may further compromise this as a measure of BAT activity.

Additional challenges with this method include exposure to ionizing radiation and costs and together these have limited the usefulness of ^{18}F-FDG PET-CT in research, especially in a pediatric population. In children, most BAT studies are in retrospectively analyzed PET-CT images in those who have otherwise required a PET-CT scan. Retrospective analysis has contributed to low reproducibility in that, of 2934 participants with a retrospective analysis of PET-CT images, only 13.3% of patients with an initial positive BAT scan had a positive result on repeated scanning[5]. Thus, ^{18}F-FDG PET-CT has limited usefulness for assessing BAT in humans, especially in the pediatric population.

1.2.2 Magnetic Resonance Imaging

More recent studies have made use of non-invasive imaging modalities such as magnetic resonance imaging (MRI) to evaluate BAT activity to avoid radiation exposure[18]. This technique makes use of the physiological differences between BAT, WAT and other tissues in terms of water and fat content. MRI uses a strong magnetic field to create oscillations which provide

energy to excite hydrogen atoms which then emit a radiofrequency detectable by the scanner and translatable into an image[19]. These protons resonate with a different frequency based on their origin, such that protons in fat produce a higher resonance than those in water. The fat-water composition is used to create a proton-density fat fraction map (PDFF%= fat/(fat+water)) and is then used in MRI image analysis for BAT quantification. BAT has a higher water and lower fat content than WAT, as confirmed by histology, which can be used to distinguish the tissues[20,21]. This was also confirmed in more recent studies noting a significantly lower PDFF% in BAT versus WAT in both adults and children, which was then reflected in the ^{18}F-FDG PET-CT signal differences between these tissues[22–24]. Researchers have thus attempted to reproducibly standardize PDFF% values for BAT and WAT, but challenges exist due to the overlapping PDFF% ranges and heterogeneity between children and adults[23–27]. There is unlikely to be a simple solution to this challenge, though, due to the heterogenous mixture of brown, beige and white adipocytes in human SCV fat pads and variations across age groups[15,28]. Therefore, a higher baseline PDFF% within the SCV region is generally considered a "whiter" BAT phenotype, but difficulties still exist in creating rigid guidelines for MRI analysis of human BAT.

Furthermore, as opposed to ^{18}F-FDG PET-CT which is only used to measure glucose uptake by BAT in an active state, MRI PDFF% can be used to detect both baseline fat fraction and cold-stimulated BAT activity. BAT activity is quantified by the reduction in PDFF% after cold exposure as triglycerides are oxidized as thermogenic fuel by BAT[29,30]. This marker of BAT activity was then validated by researchers noting both a significant correlation with PET-CT-assessed activity and no paralleled change in WAT PDFF%[31,32]. This PDFF% decline may be confounded by an increased blood perfusion upon cold exposure, however, but a brief warming period was shown to eliminate this effect while still accurately quantifying BAT activity[31,33]. Overall, the ability of MRI to accurately detect both a baseline BAT phenotype and cold-induced

activity, along with the lack of ionizing radiation exposure, are favourable properties of this imaging modality as compared to PET-CT[23,34].

In our laboratory, MRI analysis of BAT was conducted in 64 adults (61% male) before and after a 3-hour cold exposure[35]. The mean (standard deviation, SD) pre-cold SCV PDFF% was 72.14 (7.91) % and post-cold SCV PDFF% was 69.46 (9.72) %, resulting in a PDFF% reduction of 2.98% (pre-post difference $P<0.001$, paired samples t-test). No change was seen in subcutaneous abdominal PDFF% (i.e., a predominately WAT depot). Additionally, a higher pre-cold SCV PDFF% (i.e., a whiter BAT phenotype) correlated with a smaller cold-stimulated PDFF% decline ($r=-0.616$, $P<0.001$). These results are consistent with the notion that upon BAT activation with cold, PDFF% values will decline due to the increased utilization of triglycerides. Subcutaneous abdominal adipose tissue has a significantly higher PDFF% than the SCV region reflecting the higher fat content of WAT ($P<0.001$, paired samples t-test). These findings are similar to those of Holstila *et al.*[22] who reported a lower baseline SCV PDFF% compared to that of WAT, and Gifford *et al.*[23] who similarly reported a significant difference between BAT and WAT PDFF% and between pre- to post-cold SCV PDFF%.

1.2.3 Other Imaging Modalities

Infrared thermography (IRT) is another potential safe imaging technique to quantify the change in BAT activity with cold exposure based on infrared radiation emitted by overlying skin in the SCV region when BAT is activated. Although BAT activity assessed by IRT strongly correlated with that from PET-CT imaging in adult males, there is questionable validity of IRT use in those with obesity due to the overlying subcutaneous WAT in the SCV region[36]. Proton magnetic resonance spectroscopy is another radiation-free imaging modality shown to correlate with PET-CT-assessed BAT activity in a small adult cohort, but similar limitations to use in

those with obesity exist[37] . Therefore, MRI appears to be the gold standard for non-invasive BAT imaging.

1.3 Therapeutic Potential of BAT in Obesity and NAFLD

As mentioned previously, BAT is an attractive target to combat obesity and related complications due to its ability to consume circulating glucose and lipids as thermogenic fuel. In fact, BAT presence or activity as assessed by ^{18}FDG PET-CT or MRI is repeatedly reported to be inversely correlated to BMI or body fat in humans[7,38,39]. This relationship was replicated in children, where lean children exhibited a significantly lower baseline SCV PDFF% than children with overweight or obesity[25]. Furthermore, researchers have also noted significantly higher insulin sensitivity and glucose and free fatty acid (FA) oxidation in those with detectible cold-induced BAT activity on PET-CT, again inversely correlating with adiposity[33,40]. Rodent models were then used to causally examine this relationship, such as by Lowell *et al*.[41] using two lines of transgenic mice with reduced BAT and obesity, with one line undergoing BAT regeneration after 16 days. The mice with BAT regeneration displayed a resolution of obesity, suggesting the ability of BAT to individually support metabolic homeostasis[41]. Overall, beyond its thermogenic capacity, little is known about the physiological mechanisms by which BAT exerts its beneficial metabolic effects in humans.

Furthermore, NAFLD is one of the most significant comorbidities of obesity with an estimated worldwide prevalence of 80-90% in adults with obesity[3]. There is limited evidence that BAT may show therapeutic potential against NAFLD as well, as two cross-sectional studies have retrospectively analyzed PET-CT images for BAT activity and hepatic fat content[8,9]. A significantly lower prevalence of NAFLD was identified in adults with active BAT compared to those lacking active BAT, independent of age, gender, BMI and serum glucose[8,9]. It is important

to note that both studies found an extremely low population of participants with discernable BAT activity (2% or below of all scans analyzed), likely as a result of the use of non-cold-stimulated imaging[8,9]. Additionally, MRI analysis of 61 male and female adults showed a significant positive correlation between SCV PDFF% at ambient temperature and hepatic fat content (i.e., liver PDFF%) independent of age and sex[42]. Thus, further investigation is required to understand the connection between these tissues. In pre-clinical models, BAT transplantation or activation downregulates hepatic lipogenic genes, and reverses hepatic steatosis and other adverse metabolic outcomes in obese mice[43–45]. Metabolomics is an interesting non-invasive platform to investigate the physiological relevance of human BAT and the mechanistic link with hepatic fat accumulation. This platform will thus be outlined below prior to a discussion about the current literature relating the metabolome with BAT and NAFLD, both individually and in connection.

1.4 Metabolomics

Metabolomics is the method of using analytical chemistry to examine a large number of low-molecular weight molecules (i.e., metabolites) in a wide range of biological samples. The human metabolome is downstream of the genome, transcriptome and proteome and therefore can provide functional information on human health or pathophysiology[46]. Metabolites are used and produced by metabolic processes, such as BAT thermogenesis, and thus can provide insight into wide-reaching physiological roles[47]. Metabolomics can also be used to correlate particular metabolites to specific physiological or pathological states to provide non-invasive biomarker discovery[48].

Biological samples such as tissue extracts, blood, urine and stool can be used in a targeted metabolic profiling or untargeted metabolic fingerprinting[46]. Targeted metabolomics relies on *a priori* knowledge of specific metabolic pathways of interest, which can then be sensitively and

selectively analyzed with optimized methodology, and will be the focus of this report[47]. Untargeted metabolomics provides an unbiased analysis of the biological sample, resulting in a large and complex data set requiring bioinformatic tools for metabolic identification and correlation[47]. Untargeted datasets must be interpreted with caution, however, as metabolite identities have not been verified to a reference standard to be confident in the true identity. Some of the other difficulties in running untargeted metabolomics are that analytical conditions (i.e., pH, solvent, ionization technique, etc.) affect which metabolites are recovered, and a large number of metabolites remain unidentified[47]. A targeted approach to specific metabolites often follows an initial exploratory untargeted approach to verify exact concentrations of metabolites in the sample[47].

1.4.1 Metabolomics Methodology

Nuclear magnetic resonance (NMR) and mass spectrometry (MS) are the two main methods for metabolomic analysis[49]. NMR relies on the energy absorption and re-emission of a targeted atomic nuclei, most often hydrogen (i.e., ^{1}H-NMR) due to its natural abundance[50]. NMR approaches require little-to-no sample preparation and are highly reproducible and quantitative, but lack sensitivity[51]. I will direct the reader to recent relevant review papers for further NMR metabolomics methodology[52]. MS-based methods, on the other hand, are the most common due to the extremely high sensitivity and reliability, and will be the focus of this report[51]. Samples in the liquid or gaseous form are introduced into the MS system, vaporized, and then ionized by an electric source[49]. Such ionization methods include electrospray ionization (ESI) and matrix-assisted laser desorption ionization (MALDI)[53,54]. The mass analyzer (i.e., Orbitraps, quadrupole mass analyzers) then uses electric and/or magnetic fields to deflect the ions onto a detector based on their unique mass-to-charge ratio (m/z)[55]. Integrated computational software uses the detector

data to produce a spectral peak for each ion based on the *m/z* ratio and the retention time, which will be described below[53].

Due to the high complexity of biological samples, a sample separation step precedes the MS analysis. Liquid and gas chromatography (LC and GC, respectively) are the most common separation techniques, both of which rely on the partitioning of a sample between a stationary phase (i.e., a column) and a mobile phase (i.e., liquid or gas, respectively)[56]. Compounds within the sample will partition along the stationary phase column at different times (i.e., retention time) based on a specific property, such as molecular size or mass. Therefore, metabolites within the sample will be produce a spectral peak at their specific retention time as determined by the chromatography step and *m/z* by MS[56]. Tandem MS can then be used as a second MS analysis on isolated ions to identify molecular fragments and distinguish ions from structural isomers[47]. The additional sample preparation required for an MS-based method with a separation step may cause metabolite loss and slightly lower reproducibility[57].

After collecting the *m/z* and retention time, the metabolite identities can be determined with the help of computational software and metabolite databases, and in the case of targeted metabolomics, confirmed with reference standards[47,58]. For example, as will be further described in **Methodology Section 2.4**, the TraceFinder software used in this project collects the *m/z* ratio and retention time for a pre-determined set of known metabolite standards loaded with the biological samples. This way, the software is pre-set to integrate the spectral peaks at the known retention times and *m/z* such that these targeted metabolites can be confidently identified within the biological samples. This clearly limits the fraction of the vast human metabolome covered in this dataset and is thus better suited for hypothesis testing rather than creation as compared to untargeted metabolomics, but significantly increases the quantitative reliability[59]. Metabolite abundance is then quantified as the area under the spectral peak relative to heavy labelled

internal standards. Metabolomic data can be analyzed further by placing metabolites into relevant pathways and networks, which is done by referencing metabolite pathway databases such as MetaboAnalyst[60,61]. Currently, however, these databases only capture a subset of the human metabolome and therefore may be a source of bias towards the pathways available[61].

1.5 Metabolomics and BAT in Humans

BAT presence and activity are reliably measured by ^{18}F-FDG PET-CT and MRI techniques in humans. However, BAT is highly metabolically active and consumes and produces metabolites in the thermogenic process when sympathetically stimulated and therefore metabolomics may provide novel information about BAT physiology[62]. There are very few studies done to date relating the human metabolome to BAT presence and/or activity. Firstly, Boon *et al.*[63] aimed to discover a novel biomarker of BAT activity in serum from 22 lean, healthy male adults (mean age 24 years) using a targeted metabolomic approach. A strong positive correlation was found between ^{18}F-FDG PET-CT-measured BAT activity after a 2-hour cold exposure and the three metabolites lysophosphatidylcholine (LysoPC)-acyl C16:1 ($r=0.35$, $P<0.001$), LysoPC-acyl C16:0 ($r=0.22$, $P=0.002$), and PC-diacyl C32:1 ($r=0.08$, $P=0.04$) in non-cold stimulated serum[63]. Similar relationships with cold-induced BAT volume were noted[63]. After replication in three similar cohorts consisting of 37 male participants in total, LysoPC-acyl C16:0 remained robustly correlated with BAT activity and metabolite concentration tended to increase after cold exposure[63]. LysoPC-acyl C16:0 is likely generated by the esterification of cholesterol with fatty acids (FA) liberated from a phosphatidylcholine during reverse cholesterol transport[64]. This process links to BAT as BAT activation reportedly strongly enhances high-density lipoprotein (HDL)-cholesterol turnover and reverse cholesterol transport in mice[65] and was positively correlated with HDL-cholesterol levels in men[66].

Lynes and colleagues provided evidence for a second novel biomarker for BAT activity in human plasma; also with a targeted metabolomic approach[67]. They found that the oxygenated FA (i.e., oxylipin) 12,13-dihydroxy-9Z-octadecenoic acid (12,13-diHOME) is significantly increased in circulation after a 1-hour cold exposure at 14°C (P=0.003), and is correlated with cold-induced BAT activity as determined by ^{18}F-FDG PET-CT in nine healthy male and female adults (r=0.63, P=0.005)[67]. The researchers also noted that these results were consistent with their pre-clinical observations[67]. However, in a lipidomics study of BAT and WAT biopsies from 14 participants, the global oxylipin profile could not distinguish BAT and WAT, unlike the findings in a murine model[68]. These investigators concluded that the global oxylipin profile may be a surrogate marker of the abundance of brown adipocytes in a homogenous BAT depot, as is often found in mice, but the heterogeneity within human BAT depots (i.e., a mix of white and brown adipocytes) limits this ability[68].

Yoneshiro *et al.*[11] recently undertook an untargeted metabolomic analysis of baseline and cold-stimulated (19°C, 2-hours) serum from 33 healthy male adults. The cohort was divided, based on ^{18}F-FDG PET-CT into high BAT and low BAT activity groups based on the median tracer uptake[11]. They focused on BCAA (i.e., valine, leucine, isoleucine) metabolism and demonstrated that circulating valine levels decreased after cold exposure in high BAT participants (P=4x10^{-4}) , and cold-induced declines in valine, leucine and total BCAA correlated with BAT activity (r=-0.530, P=0.0015)[11]. Importantly, there was no correlation between these reductions and skeletal muscle mass, another organ that readily metabolizes such amino acids[11]. These authors concluded that cold-induced BAT acts as a sink for BCAA oxidation and clearance from circulation, which then has significant metabolic benefits in terms of energy balance and nutrient homeostasis[11].

Finally, one other study examined cold-induced changes in circulating FA levels in 15 healthy male adults, with only three subjects also undergoing ^{18}F-FDG PET-CT imaging for cold-induced BAT activity[69]. Interestingly, one saturated FA increased in circulation after a 100-minute adaptation period at 18°C (P=0.04), while one saturated FA and two monounsaturated FAs decreased after a 300-minute euglycemic steady state period at 18°C (P=0.02, P<0.001 and P<0.001, respectively)[69]. The cold-stimulated ^{18}F-FDG PET-CT BAT imaging was used as a proof-of-concept to assume the FA alterations occur concurrently with BAT activation[69]. Overall, the authors suggested that BAT is a mediating factor in the cold-induced lipidomic alterations, although without direct correlations with BAT activity[69]. To summarize the above work, a limited number of metabolites from diverse biological pathways were shown to be correlated with PET-CT-assessed BAT activity, specifically in healthy adults (**Figure 1).** However, no comparisons have been made in children, and underlying mechanisms regulating these metabolomic changes are still unknown. It will be interesting to contrast the findings of this project to those above due to the inclusion of children and use of MRI for BAT analysis.

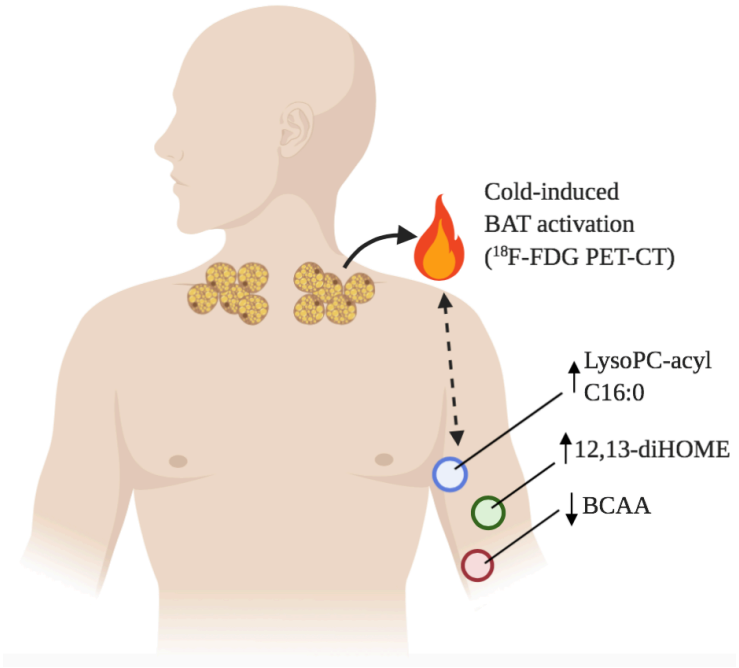

Figure 1. Summary of the literature relating the metabolome to BAT activity in adults. Abbreviations: *LysoPC-acyl* lysophosphatidylcholine-acyl, *12,13-diHOME* 12,13-dihydroxy-9Z-octadecenoic acid, *BCAA* branched-chain amino acid.

1.6 Metabolome and BAT in Rodents

Rodent models allow for analyses of both the metabolome in circulation and in tissue extracts, the latter of which is clearly limited in human studies, and therefore a broader understanding of the relationship with BAT in rodents is available. Findings from pre-clinical metabolomic research are summarized in

Figure 2. Multiple studies have found an alteration of glucose and lipid oxidation pathways and associated metabolites in BAT with cold stimulation[10,58,70,71]. For example, Hiroshima *et al.*[70] analyzed the metabolome of rat BAT extracts at thermoneutrality and after a 48-hour cold exposure, noting a cold-induced reduction in glycolysis/gluconeogenesis intermediates (with no change in the glycolytic end-product pyruvic acid) and an increase in metabolites of the tricarboxylic acid (TCA) cycle, β-oxidation, and FA uptake. Similarly, Lu *et al.*[71] compared the cold-induced metabolomic effects in murine BAT and WAT extracts and noted an enhanced upregulation of pathways of amino acid, purine and pyrimidine metabolism and redox regulation in BAT versus WAT. More specifically, metabolites of mitochondrial metabolism were shown to be critical in the BAT thermogenic process. For example, succinate, a TCA cycle intermediate and regulator of cellular redox status, is specifically highly expressed in BAT, enhanced with cold exposure in mice, and promotes BAT thermogenesis upon treatment[58]. Additionally, liver-derived acyl-carnitines, required for mitochondrial FA oxidation, were found to increase robustly in circulation and were taken up and metabolized specifically by BAT after cold stimulation[10].

Although the findings in humans are not as comprehensive as those in rodents, certain similarities can be found. As discussed previously, the oxylipin 12,13-diHOME was found to be correlated with BAT activity and elevated in circulation and BAT tissue after acute or prolonged cold in mice, mirroring the authors' results in humans[67]. The authors also noted that 12,13-diHOME is synthesized and released from BAT after cold exposure to then promote BAT lipid uptake and UCP-1 activity, which emphasizes the role of BAT in lipid oxidation when sympathetically activated[67]. Yoneshiro *et al*.[11] also supported their human findings of BCAAs as a thermogenic fuel for BAT in pre-clinical models, by noting that labelled leucine was primarily taken up and oxidized mouse BAT mitochondria after cold exposure, and BAT-specific BCAA oxidation-deficient mice exhibited cold and glucose intolerance, weight and fat gain, and increased liver fat[11]. Cumulatively, clinical and pre-clinical metabolomics research points towards a mechanistic role of BAT in glucose, lipid and amino acid uptake and catabolism when sympathetically stimulated, particularly involving mitochondrial oxidation. How BAT-specific functional changes may influence whole-body energy balance and chronic disease development, such as obesity and NAFLD, however, requires further investigation.

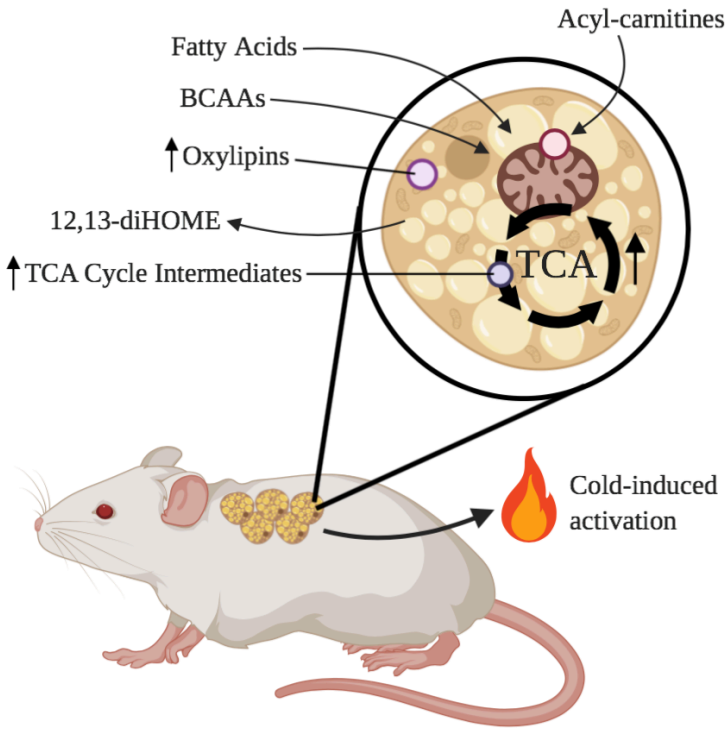

Figure 2. Summary of the literature relating the metabolome to BAT activity in rodents. Also associated with increased TCA cycle flux is β-oxidation activity. Abbreviations: *BCAA* branched-chain amino acid, *12,13-diHOME* 12,13-dihydroxy-9Z-octadecenoic acid, *TCA* tricarboxylic acid.

1.7 Non-Alcoholic Fatty Liver Disease

It is clear that NAFLD places a significant burden on the health of the world's population, and both adults and children are susceptible to this chronic disease. It is therefore critical to understand the pathophysiology of NAFLD across the disease spectrum to enable accurate diagnosis and effective treatments. Although continued research is required, it is generally accepted that hepatic steatosis develops due to a chronic excess hepatic uptake and synthesis of FAs and other metabolic substrates[72–74]. This leads to the accumulation of toxic lipid species (i.e., FA metabolites), which then promote hepatocyte oxidative stress, injury, and death[72–74]. Insulin resistance is generally accepted as having a major central role in this lipotoxic cascade in two manners: (1) dysregulated adipose tissue lipolysis causing release of excess free FAs into the circulation and delivery to the liver, and (2) decreased peripheral glucose disposal

and promoting hepatic update and subsequent *de novo* lipogenesis (DNL)[74–76]. This increased flux of free FAs into the liver and incomplete lipid oxidation also promotes hepatocellular production of reactive oxygen species (ROS) beyond homeostatic levels, thereby inducing inflammation and cellular injury[74].

1.8 Risk Factors Associated with NAFLD

It is also important to understand factors that drive the development and progression of NAFLD to aid in disease screening, treatment and management. Generally accepted risk factors for development of NAFLD include metabolic syndrome, ethnicity, genetic factors, age and sex[77]. However, the presence of metabolic syndrome (MetS; i.e., obesity, hyperglycemia, dyslipidemia, systemic hypertension) is largely considered to have the strongest overall influence[2]. A meta-analysis conducted in 2016 by Younossi *et al.*[78] concluded that the pooled estimated prevalence of MetS in patients with NAFLD and NASH were 42.5% and 70.7%, respectively. The specific pooled prevalence estimates for components of MetS in NAFLD and NASH, respectively, were as follows: obesity; 51.3% and 81.8%, dyslipidemia; 69.2% and 72.1%, and type 2 diabetes; 22.5% and 43.6%[78]. This relationship between NAFLD and comorbidities is likely bi-directional, as another meta-analysis concluded that there was 65% increased risk of fatal or nonfatal cardiovascular events in the 34,000 patients with NAFLD included in the study[79].

Ethnicity and genetic factors are also risk factors for NAFLD development. In a recent meta-analysis of 368569 participants, the prevalence of NAFLD (as defined by hepatic steatosis on ultrasound or MRI or elevated liver enzymes) was highest in those of Hispanic descent, intermediate in Whites, and lowest in African-Americans[80]. These differences between groups were minimized in high-risk cohorts (i.e., cohorts composed of predominantly those with

obesity, diabetes, or a history of liver disease)[80]. While lifestyle factors are believed to partially account for these inter-ethnic differences, a number of genetic polymorphisms are associated with NAFLD as well, of which the best characterized is the *PNPLA3* gene polymorphism[81].

Male sex and increased age are other generally accepted risk factors for NAFLD development[78,82]. The overall prevalence of NAFLD is higher in males than in females, as was concluded in the recent systematic review by Ballestri *et al.*[83]. These authors concluded this was due to the protective effects of estrogen in premenopausal women. The influence of age and gender may differ based on ethnicity, however. NAFLD is more common at a younger age in Asian and Indian populations compared to Western populations[77]. Discrepancies also exist in the age of NAFLD development by gender, as the prevalence of ultrasound-diagnosed NAFLD was shown to increase consistently across the lifespan in females but remained consistent in males of a Korean descent[84]. NAFLD can, however, occur at all ages, and the prevalence of NAFLD in pediatric populations is rapidly increasing world-wide and is now considered the most common pediatric chronic liver disease[85]. In general, although there exists a plethora of epidemiological research conducted on world-wide NAFLD prevalence, more knowledge about the influence of these, and other, driving factors on development and progression across disease stages is needed.

1.9 Measurement and Diagnosis of NAFLD

Considering the huge burden that NAFLD management places on the world's population, reliable imaging techniques are required for accurate diagnosis across the disease stages and implementation of the appropriate treatment. The choice of appropriate diagnostic technique must be chosen in light of its unique strengths and limitations, as will be discussed below.

1.9.1 Liver Biopsy

Currently, liver biopsy is the gold standard for assessing NAFLD disease severity, specifically in the diagnosis of NASH and fibrotic stage. Unfortunately, major limitations exist with the use of histological assessment, as liver biopsy is invasive, costly and prone to sampling variability[86]. The risk of complications such as pain, bleeding, and morbidity as well as the lack of suitability for screening of low-risk individuals further promotes the need for continued development of non-invasive techniques for NAFLD assessment[87]. Biopsy is still required for definitive diagnosis of NAFLD and disease staging but application to a broader patient population is challenging for the reasons described above.

1.9.2 Magnetic Resonance-Based Techniques

In contrast to liver biopsy, magnetic resonance-based techniques provide a non-invasive platform to accurately measure liver triglyceride content (i.e., hepatic steatosis). The gold standard for quantification of hepatic steatosis is magnetic resonance spectroscopy (MRS), where NAFLD is defined as a hepatic fat content of 5.6% or higher[88]. MRS is highly sensitive to even trace amounts of hepatic fat, as measured by the differing signal intensities corresponding to water versus fat proton resonance. However, some challenges with MRS exist including that the analysis is dependent on the location of the single voxel chosen and thus is susceptible to sampling variability[87].

In contrast, MR-based imaging techniques without spectroscopy were developed to estimate hepatic fat across the entire liver using PDFF%. As described above, the PDFF% method accurately quantifies whole-liver fat content by detecting the ratio of fat protons to total fat and water protons. This method is advantageous as it is much less labour- and time-intensive, and whole-liver images allow for longitudinal monitoring of patients as the region of interest

where fat was measured is exactly known[87]. PDFF% was also shown to strongly correlate with histologically-measured steatosis grade and outperforms ultrasonography for quantitative hepatic steatosis assessment[89,90]. The MRI PDFF% method is therefore a strong, non-invasive alternative to liver biopsy for hepatic steatosis assessment but is not capable of NASH diagnosis or fibrotic staging. To combat this limitation, MR elastography (MRE) is an emerging technique that takes advantage of the mechanical properties (i.e., stiffness and elasticity) of the liver, which strongly correlate with biopsy-assessed fibrosis[91].

1.9.3 Other Techniques

Finally, circulating concentrations of liver enzymes involved in glucose and amino acid metabolism such as alanine aminotransferase (ALT), aspartate aminotransferase (AST) and gamma-glutamyltransferase (GGT) were once attractive targets as surrogate markers of liver injury[92]. This notion was largely refuted though as several studies report that aminotransferase levels are highly variable in NAFLD patients and have a poor predictive value[93,94]. Composite scores may combine liver enzymes with other known NAFLD indicators of age, body composition and blood chemistry to increase the predictive value of these measures on presence or severity of NAFLD with varying efficacy[95]. Metabolomics may be an easy and relatively non-invasive tool to identify novel circulating NAFLD biomarkers to add predictive value to established scoring systems.

1.10 The Metabolome in NAFLD

While numerous accurate and reliable techniques exist for assessment of liver pathology, such as MRI-PDFF% for hepatic steatosis, there are still limitations in non-invasive diagnosis and monitoring across the stages of NAFLD. Metabolomics however allows further analysis of NAFLD pathophysiology to aid in development of effective interventions and identify novel

biomarkers. Much of the work in this field is currently focused on the latter objective, concluding that individual metabolites and combined biomarker panels exist to aid in non-invasive disease diagnosis with varying degrees of efficacy. However, as this project is not focused on biomarker discovery, we will direct readers to recent comprehensive reviews[96,97]. We will instead highlight the main alterations in amino acid, lipid, carbohydrate and bile acid metabolism associated with NAFLD in adults from a metabolomic point of view in the following sections and summarized in **Figure 3**. Then, any relevant literature from pediatric populations will be summarized for comparison to adults. A recent narrative review of the adult serum metabolomic profile in NAFLD is also available by Gitto *et al*.[98].

1.10.1 Amino Acids

To begin, the liver is a main site of amino acid (AA) regulation and is therefore intricately entwined with whole-body metabolism. Broad alterations to circulating AAs were noted in NAFLD such as BCAAs, aromatic AAs (AAA), and multiple non-essential AAs. Firstly, increased plasma and hepatic BCAAs are found in adults with NAFLD, with or without obesity, in numerous metabolomic studies[99,100]. However, Kawanaka *et al*.[101] reported a correlation between decreased plasma BCAAs (measured by an amino assay rather than metabolomics) and increasing liver fibrosis grade in adults, highlighting the complexity of NAFLD as a disease spectrum. In general, it was proposed that BCAAs and NAFLD are linked through an impaired cross-talk between hepatic and/or peripheral mitochondrial TCA cycle leading to inefficient BCAAs catabolism and cellular stress[98,102].

Additionally, the liver is the main site of AAA catabolic enzymes so hepatocyte function is required for AAA regulation[100]. In fact, increased AAAs such as tyrosine and phenylalanine were seen in plasma in adults with NAFLD, and was even cited as the most dysregulated pathway in adolescents with NAFLD[99,103]. This may be a result of increased hepatic oxidative

stress from the incomplete catabolism of excess metabolic substrates, which drives an increased intracellular demand for anti-oxidant molecules such as glutathione (GSH)[104]. This is because cysteine acts as both an intermediate in GSH production and an inhibitor of hepatic tyrosine transaminase (i.e., inhibitor of tyrosine breakdown); results by Kalhan *et al*.[99] supported this notion as circulating cysteine-GSH conjugate was decreased while tyrosine was increased in adults with hepatic steatosis.

Finally, the non-essential AAs glycine and serine are also critical to GSH production as rate-limiting substrates, and glutamate is released into circulation after GSH is transaminated by GGT[100]. Consequently, glycine and serine levels are decreased and glutamate levels are increased in the circulation of adults with NAFLD[99,100,104]. Gaggini *et a*l.[100] also eloquently summed up this relationship in their novel glutamate-serine-glycine-index (glutamate/[serine+glycine]). Glutamate is also considered an anaplerotic substrate for the TCA cycle when converted to α-ketoglutarate, which has shown to accumulate in circulation of adults with NAFLD[105,106]. Thus, the broad changes in circulating AAs associated with NAFLD provide insight into hepatocellular impairments and likely have wide-spread impacts in whole-body metabolic health.

1.10.2 Lipid Metabolism

NAFLD is also well-known to be characterized by alterations in the complex process of lipid metabolism, but fortunately metabolomics has allowed for analysis of a wide spectrum of lipid classes in patients with NAFLD and NASH. A lipidomic analysis was conducted in participants with biopsy-proven NAFLD or NASH compared to healthy controls by Puri *et al*.[107], and patients with NAFLD had increased total, saturated and monounsaturated FAs (MUFA; specifically palmitoleic and oleic acids). An elevated rate of DNL in adults with NAFLD and NASH was suggested as evidenced by an increased incorporation of MUFA relative to

polyunsaturated FAs into circulating lipid pools through increased activity of lipogenic enzymes[107–109]. Furthermore, LysoPCs are considered toxic metabolites of FA oxidation and thus an indirect mediator of hepatic cytotoxicity seen in NAFLD[110]. Papandreou *et al.*[111] found that adults with a reversion of NAFLD after a Mediterranean diet intervention and mean follow-up period of 3.8 years showed reduced circulating LysoPC species as a possible result of reduced hepatic lipotoxicity[111]. Phosphatidylcholines (PC) and LysoPCs were generally reported to be most prevalent in favourable high-density lipoprotein cholesterol which is reduced in NAFLD and thus may partially explain an increase in these lipids in circulation[112,113]. However, phospholipid metabolism is highly complex and may differ with disease severity as researchers have noted reduced LysoPCs in adults with NASH versus healthy controls[99]. Finally, several studies have reported increases in circulating or hepatic carnitine species in patients with NAFLD and NASH[99,107,114]. An increased acylcarnitine production is considered to be due to the high FA load and mitochondrial lipotoxicity associated with NAFLD[115]. Increased plasma long chain acylcarnitines is reported to be strongly correlated with the NAFLD-associated rise in circulating BCAAs as fuel for increased mitochondrial TCA flux[102]. Overall, changes to circulating total lipid load and composition, phospholipid metabolism and mitochondrial FA uptake are characteristic of NAFLD, but continued metabolomic investigation is warranted to fully understand the role of the lipidome in liver pathophysiology.

1.10.3 Carbohydrate Metabolism

NAFLD is likely to be accompanied with insulin resistance, hyperglycemia and hyperinsulinemia[2]. Consequently, metabolomic studies in both mice[116,117] and adult humans[99,118] have reported increased circulating lactate concentrations in NAFLD, likely explained by the above metabolic disturbances and resulting shift towards anaerobic metabolism. Toye *et al.*[117] stated that increased plasma lactate in mice with high-fat diet-induced NAFLD reflects enhanced

muscle lactate production in a hyperglycemic state and increased availability of gluconeogenic substrates. Increased circulating pyruvate, alanine and mannose were also seen in varying stages of NAFLD, reflecting a proposed rise in cytosolic glycolysis through the use of glucose to produce alanine and lactate via pyruvate[99,117,119].

1.10.4 Bile Acids

Lastly, bile acids (BAs) are metabolites of cholesterol breakdown in liver and have a critical role in glucose and lipid homeostasis[120]. Primary bile acids (i.e., cholic acid and chenodeoxycholic acid) can then be converted into secondary BAs by the gut microbiome or conjugated with amino acids[121]. BAs can alter intestinal fat absorption and induce growth factor expression, which then has a multitude of downstream effects on hepatic insulin signaling, glucose and lipid metabolism, and inflammation[121]. García-Cañaveras *et al*.[122] analyzed the metabolome from steatotic and non-steatotic human liver samples, concluding that elevated total BAs are found in simple steatosis. An altered BA profile is more commonly associated with increased NAFLD severity, though, with researchers regularly noting elevated total serum and hepatic BAs in patients with NASH, but with differing distribution of specific BA species[108,123]. For example, Jiao *et al*.[120] found a four-fold increased percent of serum secondary BAs but reduced percent of chenodeoxycholic acid in adults with NASH versus healthy controls. Therefore, it is clear that changes to BA regulation in adults with NAFLD and/or NASH

accompany the plethora of other metabolomic impairments highlighted above and summarized in **Figure 3**, including amino acids, lipids and carbohydrates.

Figure 3. Summary of the major findings relating the metabolome to NAFLD in adults. Toxic lipid intermediates include PCs and Lyso-PCs. Abbreviations: *ROS* reactive oxygen species, *GSH* glutathione, *BCAA* branched-chain amino acids.

1.10.5 The Metabolome in Pediatric NAFLD

High-throughput methods such as metabolomics have become of great interest in order to

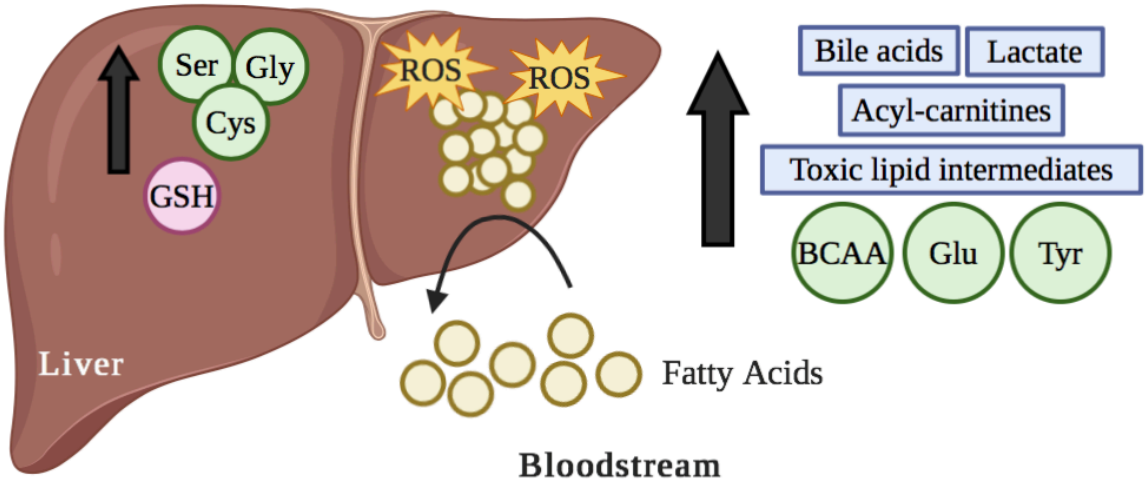

study the differences in NAFLD pathogenesis between adults and children for precise diagnosis and treatment. A number of similarities between adults and younger populations are noted. Goffredo and colleagues[124] noted elevated circulating BCAAs (valine and isoleucine) and tryptophan in 78 male adolescents with hepatic steatosis in a targeted metabolomics study. The authors also reported that circulating valine concentration was predictive of steatosis progression at two year follow-up[124]. Likewise, Jin *et al.*[103] found that while many pathways of FA metabolism and DNL were dysregulated in adolescents with hepatic steatosis, the tyrosine metabolism pathway was the most dysregulated. In a targeted metabolomics study in 76 Chinese children with and without NAFLD on ultrasound, an increase in palmitoleic acid was noted as

was also seen in adults[125]. In contrast to adult studies, no change in total saturated FA, MUFA or BA levels in these children with NAFLD were noted, and the direction of change in a number of BA species (i.e., CDCA) differed between adults and children[125]. Finally, Khusial *et al.*[126] identified a panel of metabolites that were altered in plasma from 222 children (11-18 years) with biopsy- or MRI-diagnosed hepatic steatosis versus 337 control participants in effort to identify pediatric-specific biomarkers[126]. They noted lower serine, increases in the BCAAs leucine/isoleucine and increased tryptophan, consistent with previously described findings in adults[126]. However, these authors also noted a reduced plasma abundance of three LysoPCs, which is contrary to some adult findings[111,126]. In conclusion, research relating the metabolome to pediatric NAFLD highlights a number of similar results as that in adults, such as BCAAs, AAAs, other amino acids and certain FAs. However, discrepancies also exist between adults and children in terms of the BA profile and certain phospholipids, and therefore further investigation into similarities and differences between circulating metabolomic features is warranted.

1.11 The Metabolomic Link Between BAT and NAFLD

Metabolomics may be informative in investigating common biochemical mechanisms linking BAT and liver to support the cross-sectional data that suggests a relationship between these tissues. These findings relate to carnitine metabolism and AA metabolism. Simcox *et al.*[10] identified a robust increase in circulating acylcarnitines derived by the liver after cold stimulation by untargeted lipidomics in mice. Further, labelled acylcarnitines were taken up and metabolized primarily by BAT, and a knock-down of hepatic acylcarnitine genes resulted in cold intolerance[10]. In the discovery of plasma succinate accumulation after cold exposure and its metabolism as a thermogenic substrate in mouse BAT, Mills *et al.*[127] also noted a reduced hepatic lipid deposition in succinate-treated mice. Elevated circulating BCAAs are also characteristic of NAFLD and obesity in humans[99,100,114] and Yoneshiro *et al.*[11] noted that BCAAs

are selectively taken up and oxidized by cold-stimulated BAT in humans and mice. Furthermore, *in vitro* BCAA treatment induces human brown adipocyte oxygen consumption[11]. Mice generated with a BAT-specific catabolic defect not only had increased circulating BCAA and were cold intolerant, but also showed increased body mass, liver mass, and liver fat content[11]. Finally, although not analyzed with metabolomics, reduced peripheral serotonin resulted in decreased liver fat accumulation in a UCP-1-dependant manner in mice (i.e., BAT thermogenesis was required to see such effects)[128]. Collectively, pre-clinical mechanistic studies have identified molecular targets that may mediate the observed inverse relationship between BAT and hepatic fat, such as acylcarnitines for BAT FA uptake and various TCA cycle substrates to support mitochondrial oxidation. It is now crucial to investigate if any of these results are translatable to the human metabolome for further exploration of the BAT-liver connection.

1.12 Summary and Study Significance

BAT may have an important role in combatting the ever-rising rates of obesity, diabetes and NAFLD due to its thermogenic and metabolic capacities. However, many questions about the significance of human BAT still exist, particularly in its role in whole-body energy balance. Metabolomics is a platform that, through the analysis of circulating metabolites, can investigate substrates and products for BAT thermogenesis. Cross-sectional studies have also reported an inverse relationship between BAT and the presence of NAFLD in adults, but potential linking mechanisms are poorly studied and understood[8,9]. Research is available studying NAFLD from a metabolomic perspective in adults and to a lesser extent, children, with notable discrepancies between these age groups. While a handful of pre-clinical studies have proposed linking metabolic processes between BAT and NAFLD, such as the BAT-specific oxidation of acylcarnitines, succinate and BCAAs supporting reduced liver fat and mass, metabolomics studies linking these in humans, especially in children, are currently not available[10,11,58].

Therefore, the purpose of this project was to examine the relationship of the circulating metabolome with BAT and hepatic liver accumulation in both adults and children. This may contribute to increased understanding of the underlying physiology of these tissues and how they may be linked.

CHAPTER 2: STUDY DESIGN AND METHODOLOGY

2.1 Study Objectives and Hypothesis

2.1.1 Study Objectives

We know that BAT is present and can be stimulated to metabolize circulating glucose and lipids for NST in both adults and children. Observational data has reported an inverse correlation between BAT activity and the presence of NAFLD in adults, but the mechanisms at play are unknown. This relationship has also yet to be investigated in a pediatric population. Therefore, this project aims to fill this gap in the literature as an initial evaluation of potential mechanistic links between BAT and hepatic fat accumulation through examination of the circulating metabolome while comparing and contrasting results between adults and children.

Primary Objective 1: To explore the associations between the plasma metabolome and **BAT** in adults and children and to compare and contrast these findings.

Secondary Objective 1: To examine if associations between the metabolome and BAT measures differ between adult female and male participants.

Primary Objective 2: To explore the associations between the plasma metabolome and **hepatic fat** in adults and children and to compare and contrast these findings.

Secondary Objective 2: To examine if associations between the metabolome and hepatic fat differ between adult male and female participants.

Primary Objective 3: To identify metabolites associated with both BAT and hepatic fat in adults or children as potential linking mechanisms for further study.

Sensitivity Analysis: Primary Objectives 1 and 2 will be repeated with an alternative statistical analysis method to compare results.

2.1.2 Study Hypothesis

It was hypothesized that circulating metabolites may be related to either or both baseline BAT lipid content and cold-induced BAT activity due to the highly metabolic process of NST. Additionally, it was hypothesized that the plasma metabolome is related to hepatic fat content as seen in other studies. Finally, considering the observational data that has suggested an inverse connection between BAT activity and NAFLD, it was hypothesized that certain metabolites will similarly predict both baseline BAT and hepatic fat, and/or inversely predict cold-induced BAT activity and hepatic fat[8,9]. With limited literature available on the analysis of human BAT or the BAT-NAFLD axis from a metabolomic perspective, this study is largely exploratory. This means that any identified significant metabolites relating to BAT activity and/or NAFLD may be targets for future mechanistic studies in pre-clinical models to confirm or deny our conclusions

2.2 Study Methodology

To accomplish the above objectives, this project used a subset of the data collected from the Gene Environment Team on Brown/Beige Adipose Tissue (GETBAT) study at McMaster University. This is a cross-sectional study designed to investigate the relationships between BAT presence, cold-stimulated BAT activity, liver fat, the serotonin pathway and the gut microbiome in adults and children. Only data pertaining to BAT activity and hepatic fat will be examined in this study. Two study cohorts exist in the GETBAT study; an adult cohort and a pediatric cohort.

2.2.1. Study Design and Population

The adult cohort included participants 18 to 57 years of age who met the inclusion criteria (**Appendix A1**). The pediatric cohort included male children eight to ten years of age meeting

the eligibility criteria (**Appendix A2**). Briefly, the inclusion criteria for both studies targeted healthy participants of any body size who could have MRI imaging done and who were not on medications thought to influence BAT metabolism or hepatic fat. The study was approved by the Hamilton Health Sciences Research Ethics Board. All adult participants consented, all pediatric participants assented, and their legal guardian provided informed consent. The reason for only including male children was to limit the influence of pubertal status and sex on outcomes as reported by previous studies[129,130]. Upon consent, each participant was provided with a participant identification number, and any potentially-identifiable information was stored in locked cupboards or in password-protected spreadsheets.

Subject Recruitment. Study participants were recruited from the community utilizing approved recruitment posters and social media advertising and from clinics at Hamilton Health Sciences. Adults with diabetes were recruited through the Boris Diabetes and Endocrinology clinic at McMaster University Medical Centre after receiving consent to contact. Pediatric participants were recruited through the Children's Exercise and Nutrition Centre, Growing Healthy Pediatric Weight Management program at McMaster Children's Hospital after consent to contact was obtained from clinic personnel.

All participants completed two visits less than one month apart: Visit 1 held at McMaster University Medical Centre and Visit 2 held at St. Joseph's Healthcare Hamilton. Participants were contacted by email and phone prior to each visit with reminders to refrain from vigorous physical activity 48 hours prior, avoid caffeine 12 hours prior, and avoid serotonergic foods 24 hours prior to each visit, and arrive fasted for at least 8 hours prior to each visit. Female adult participants with regular menstruation or using oral contraceptives were scheduled within seven days of their next anticipated menstrual cycle. For those with irregular menstruation, participants were asked to contact the research team at the start of their next menstruation to limit the

hormonal influence on thermoregulation. The following methods only include study components relevant to the current investigation/analysis.

2.2.1 Adult Study Visit Breakdown

Visit 1 Breakdown. Written informed consent was first obtained from each participant and all participants were re-screened for eligibility. Trained research personnel then collected height and weight measurements, repeated three times. Weight (kg) was measured by an electronic platform scale (BMI Scale Model 882; Seca, Hamburg, Deutschland) and height (cm) by a wall-mounted stadiometer (Height Measuring Rod Model 240; Seca, Hamburg, Deutschland). BMI was subsequently calculated as weight (kg) divided by squared height (m) (BMI=kg/m^2), where the WHO classifies normal weight as BMI < 25 kg/m^2, overweight as BMI ≥ 25 kg/m^2, and obese as BMI ≥ 30 kg/m^2 [131]. Body composition, including body fat and lean mass, was assessed using dual energy X-ray absorptiometry (DXA) on a GE Lunar Prodigy Advance (Model #8743) scanner. Fasting blood work was collected for measures of glucose, insulin, lipids, liver enzymes, and metabolomic analysis. A 75g oral glucose tolerance test (OGTT) was obtained for participants without known Type 2 diabetes. See **Appendix A5** for a full Visit 1 timeline.

***Visit 2 Breakdown*.** Visit 2 began with re-screening for eligibility and collection of all sensors, logs, and urine and stool samples. Participants then acclimatized to the room temperature for 30 minutes, prior to the baseline MRI scanning sessions. Cold was then applied through a full-body water-perfused suit connected to a water bath for 180 minutes at 18°C. Post-cold MRI scanning sessions were completed immediately following cold exposure. See **Appendix A6** for a Visit 2 timeline.

2.2.2 Pediatric Study Visit Breakdown

Visit 1 Breakdown. Written informed assent from each child and consent from their parent or guardian were first obtained, and all participants were re-screened for eligibility. Height and weight were collected using the same protocol as in the adult cohort. Average height and weight measures were subsequently used to calculate BMI Z-score, which is a value of standard deviations from the median BMI for a given sex and pediatric age-group. BMI Z-score was calculated using the WHO AnthroPlus anthropometric calculator, with the World Health Organization defining normal weight as a Z-score < 1, overweight as a Z-score ≥ 1 and obese as a Z-score ≥ 2[132,133]. Fasting blood work was collected for measures of glucose, insulin, lipids, liver enzymes, and metabolomic analysis. An OGTT was obtained for all participants, dosed appropriately to the child's body weight (1.75 g glucose/kg body weight to a maximum of 75 g). Body composition was assessed using DXA. See **Appendix A7** for a full Visit 1 timeline.

Visit 2 Breakdown. Visit 2 began with re-screening for eligibility and collection of all sensors, logs, and urine and stool samples. Participants then acclimatized to the room temperature for 30 minutes, prior to the baseline MRI scanning sessions. Cold was applied for 60 minutes at 18°C through a child-sized, full-body water-perfused suit connected to a water bath. Post-cold MRI scanning sessions were completed immediately following cold exposure. See **Appendix A6** for a timeline of Visit 2.

2.3 Primary Outcome Measures

The primary outcomes of this project are: (1) baseline BAT lipid content as quantified by pre-cold SCV PDFF%; (2) cold-stimulated BAT activity as quantified by the change in SCV PDFF% after cold exposure relative to baseline; and, (3) baseline hepatic lipid content. MRI was used for evaluation of all primary outcomes, and the methodology has been outlined below.

2.3.1 Pre- and Post-Cold BAT Lipid Content

***Acquisition*.** A 3-Tesla whole-body MRI scanner (Discovery 750; GE Healthcare, Waukesha, WI, USA) was used with an HNS (Head/Neck/Spine) coil for the acquisition of images from the C3 to T5 region. Subjects underwent MRI scanning before and after a three-hour (adult cohort) or one-hour (pediatric cohort) cold exposure at 18°C.

***Sequence*.** A commercially available chemical-shift based fat-water separation MRI sequence (IDEAL-IQ) was used for PDFF% imaging. This sequence provides three-dimensional volumetric imaging to create triglyceride fat fraction and R2* maps, and corrects for T2* decay to accurately measure triglyceride content[134]. See **Appendix A9** for specific MRI parameters.

***Analysis*.** The software program Analyze Pro (Version 1.0; Mayo Clinic, Biomedical Imaging Resource, AnalyzeDirect, Overland Park, KS, USA) was used for all MRI analysis. Analysis of all adult images was completed by GETBAT study personnel Dr. Basma Ahmed, Frank Ong and Stephan Oreskovich with high inter-rater reliability demonstrated by excellent intra-class correlation coefficient (ICC) values (i.e., $ICC_{consistency}$ and $ICC_{agreement} \geq 90\%$). Analysis of all pediatric images was subsequently completed by Dr. Basma Ahmed.

***Fat Mask Application*.** To ensure the adipose tissue is isolated from surrounding non-fatty tissues (i.e., muscle) in the image analysis, a fat mask was applied. It relies on the inherent intensity differences between adipose and non-adipose tissues in MR images and lessens the fat-water swaps that occur in this region. The fat mask was applied to all participants at the C7/T1 vertebral disk for standardization.

Fat Fraction Threshold Application. After application of the fat mask, thresholding of the fat fraction map to between the range of 30-100% was applied to further ensure adipose tissue is differentiated from non-adipose tissues.

Defining the SCV ROI. The ROI for BAT analysis was contained within the supraclavicular (SCV) fossa as delineated by the *trapezius* muscle posteriorly, *sternocleidomastoid* muscle medially and the clavicle inferiorly. The C5/C6 disk of the vertebral column was used as the reference for the start of segmentation, and the T1/T2 disk was used as a reference for the end of segmentation. The SCV region of interest (ROI) was delineated with the "free-hand draw" tool within the 30-100% fat fraction threshold in the axial plane view. All slices between the C5/C6 disk and T1/T2 disk were used for ROI application in the adult cohort. However, we noticed that the pediatric participants were often not in the exact same placement in the MRI from pre- to post-cold scanning, potentially due to increased shivering from the cold exposure. Thus, to avoid missing some of the SCV ROI in the post-cold images by using the above method, the end of the SCV region segmentation would be determined by visual comparison to the pre-cold SCV region. This resulted in slight discrepancies between slice numbers in pre- versus post-cold ROIs, but there was no significant difference in SCV ROI volume between analyses (mean pre-cold SCV volume = 24.03 cm^3, mean post-cold SCV volume = 23.67 cm^3, P=0.623; paired-samples t-test).

Erosion of the ROI. The "erosion" function was used as a post-processing step after the ROIs were defined to correct for any inherent partial volume effects present in the image. The 2D-Erode (1x3 jack structural element) function was used to remove a single voxel (i.e., a single layer) from the image (1 voxel = 1.4844mm^3). Voxel sizes may change dependant on the field of view (FOV) and acquisition matrix size, but care was taken to attempt to maintain consistency in all MRI parameters across the study. In instances of fat-water swaps present in the images altering the FOV may attenuate this issue, but then it was important to use similar parameter settings between pre- and post-cold MRI images. It should be noted that the research staff were not blinded to the pre- or post-cold scans during image acquisition or analysis.

Application of a T2* Mask. Just as the 30-100% fat fraction threshold was applied to distinguish adipose from surrounding non-adipose tissues, a mask was applied to discriminate BAT from WAT in the SCV region. This T2* relaxation (T2*) mask was applied to the FF mask to select voxels between 2 and 25 ms. The T2* map was originally obtained from the R2* map generated by the IDEAL-IQ sequence and transformed into T2* values with the formula T2* (ms) = 1000/R2* (s^1). This range was chosen because previous reports have concluded that a T2* value ≥ 26 ms includes mostly muscle, fluids and white adipose tissue, while 2 ms falls at the lower limit of this MR sequence's ability to detect T2* values[135]. The pre-cold SCV PDFF% values were then collected and averaged for quantification of the baseline BAT lipid content.

2.3.2 Cold-induced BAT Activity

After the analysis of pre- and post-cold SCV PDFF%, BAT activity was quantified as the percent change (Δ) in SCV PDFF% from pre- to post-cold relative to the baseline SCV PDFF% (i.e., ΔSCV PDFF%/pre-cold SCV PDFF% * 100). This quantification is in line with the studies by Lundström *et al.*[31] and Ang *et al*.[136], where the cold-stimulated BAT activity measured by MRI or infrared thermography, respectively, were represented by the change in PDFF% or skin surface temperature as a percentage of the baseline level. No current consensus in the literature exists as to what is the most physiologically-relevant measure of MRI-measured BAT activity, though. For example, Gashi *et al*.[137] recently used the absolute change in SCV PDFF% from pre- to post-cold as the marker of BAT activity, and therefore this data will also be presented as a comparator outcome.

2.3.3 Baseline Hepatic Lipid Content

In the completion of the second primary objective of this project, baseline hepatic fat was quantified by MRI as outlined below.

***Acquisition*.** The same 3-Tesla whole-body MRI scanner as above was used with a 32-channel torso array coil for acquisition of the liver in the axial plane.

***Sequence and Analysis*.** Liver analysis also used the IDEAL-IQ MRI sequence to measure liver triglyceride content as quantified by PDFF% and the Analyze Pro (Version 1.0; Mayo Clinic, Biomedical Imaging Resource, AnalyzeDirect, Overland Park, KS, USA) software. See **Appendix A9** for specific MRI parameters. Analysis of all adult images was completed by GETBAT study personnel Frank Ong, and all pediatric images by Dr. Basma Ahmed. There again was high inter-rater reliability as demonstrated by $ICC_{consistency}$ and $ICC_{agreement} \geq 90\%$.

Segmentation and ROI. The whole liver was segmented after a brief breath-hold (approximately 17 seconds) to reduce motion artifacts. The ROI was drawn over the entire liver using a "smart trace" tool to ensure that the edge of the ROI is "snapped" to the point where voxel intensity differs significantly. The number of slices differed between participants in order to segment the entire liver.

Erosion of the ROI. A similar 2D 3x3 jack structural element was used as an erosion tool to correct for inherent partial volume effects. Liver PDFF% values were then collected and averaged for each participant without the application of PDFF% thresholds or masks.

2.4 Main Exposure: Metabolite Identity and Relative Abundance

In order to assess the relationship of BAT and hepatic fat with the circulating metabolome, participant samples were analyzed by the laboratory of Dr. E Chouchani, Harvard University, Boston, MA, USA.

Sample Collection. Fasted bloodwork was collected in a 4mL EDTA-coated vacutainers, then centrifuged at 3000rpm for 10 minutes at 4°C by research staff. After processing, plasma was collected in either 300µL (adults) or 200µL (children) aliquots and snap frozen and stored at -

80°C. The timeline of the study visits differed between the adult and pediatric cohorts in that the blood samples were centrifuged and aliquoted up to three hours after collection in the adult cohort, but most often done within 30 minutes in the pediatric cohort. Within each cohort, time to snap freezing for plasma was fairly consistent between participants but may have been delayed in some cases dependant on research staff availability, although exact timing was not collected.

2.4.1 LC-MS Metabolomics

An LC-MS system was used for targeted metabolomic analysis in this project, composed of an UltiMate 3000 Ultra-High Performance LC (Thermo Fisher Scientific; Waltham, MA) with a Luna NH2 column (Phenomenex; Torrance, CA) coupled to a Q Exactive Plus Hybrid Quadrupole-Orbitrap mass spectrometer (Thermo Fisher Scientific; Waltham, MA).

Metabolite Preparation and Analysis. Participant samples were analyzed using an LC-MS model as described previously by Mills *et al.* (2018)[58]. Briefly, analytes were extracted in buffer composed of 80% methanol containing inosine-$^{15}N_4$, thymine-d_4 and glycocholate-d_4 internal standards (Cambridge Isotope Laboratories; Andover, MA). The analytes were injected onto the separation column and then eluted with 10% mobile phase A (20 mM ammonium acetate and 20 mM ammonium hydroxide in water), 90% mobile phase B (10 mM ammonium hydroxide in 75:25 v/v acetonitrile/methanol) and final linear gradient to 100% mobile phase A. Electrospray ionization in the negative ion mode was then used for mass spectrometry analysis. For certain metabolites that were not detectable in negative ion mode, the positive ion mode was used. Specific mass spectrometry settings are also described by Mills *et al.*[58]. Progenesis Qi software version 1.0 (NonLinear Dynamics) was used for raw data processing (i.e., feature alignment and signal detection/integration). Finally, TraceFinder software version 4.1 (Thermo Fisher Scientific) was used to integrate a targeted set of known metabolite and isotopologue peaks so

that detected peaks within the biological samples could be confirmed by comparison to these reference standards. Heavy-labelled internal standards were also loaded to correct for any human errors. Metabolite abundance is quantified as the area under their spectral peak relative to the average area under the peak of the heavy-labelled internal standards.

2.4.2 Covariates

Several covariates were included in our analyses due to their previously identified relationships with our primary outcomes. These include **age, sex** and **body fat percentage**. Age is a significant predictor of BAT presence in humans, with increasing age correlated to decreasing BAT activity or mass[15,38,39,138]. A controversial relationship between sex and BAT has been proposed by a number of studies reporting higher BAT prevalence in females[6,38], while others show no sex dimorphism[139,140] or a male bias in youth participants[130]. Measures of adiposity such as body mass index (BMI), body fat percentage and visceral fat accumulation are strongly inversely related to BAT presence in multiple studies.[6,33,141]. We were thus interested in examining the relationship of the metabolome with ambient and cold-induced BAT, and considered this relationship with, and without, these covariates in the model.

Similarly, as described above, NAFLD prevalence is higher with increasing age, in males and in those with obesity – so age, sex and body fat percentage were also considered in examining the relationship between the metabolome and hepatic fat. Thus, to maintain consistency in both primary objectives, age, sex and percent body fat were included as covariates in all adult analyses. Only percent body fat was included for the pediatric analysis as all participants were male within a narrow age range. We decided to assess body composition by body fat percentage rather than BMI as BMI is an indirect estimate of adiposity that cannot differentiate between fat and lean mass. Body fat percentage, as measured by DXA, provides a highly accurate and precise quantification of adiposity in both adults and children with a very low radiation dose[142–

[144]. DXA is considered the gold standard for body composition assessment as it is an easy and direct measurement of fat mass in a single region or a whole-body scan, and is well correlated to CT, MRI and bioelectrical impedance analysis (BIA)[145].

2.5 Statistical Analysis

All statistical analysis has been completed using SPSS Statistics 23 and GraphPad Prism 8.4.0. Participant demographics are presented as n or n (%) with mean (standard deviation, SD) for normally-distributed variables or median [interquartile range, IQR] for non-normally-distributed variables. Normality was assessed for all variables using the Shapiro-Wilk test, which has been proposed by some researchers as the best choice for normality test as it provides better power than the alternative Kolmogorov-Smirnov test[146]. Metabolite values represent the relative abundance of each metabolite in the plasma of each participant, and all metabolite variables were log transformed for normalization of the scale and normality was subsequently assumed. Any participant with a metabolite relative abundance of 0 was assumed to be below the detectable limit of the LC-MS platform. The minimal detectable value was predicted to be the minimum value in the dataset for that particular metabolite, and this value was then halved and imputed for any zero value to avoid missing data due to methodological limitations.

To investigate the associations between metabolite abundance and BAT or hepatic fat, metabolites were used as explanatory variables in univariate linear regression models for each primary outcome variable described previously. As this dataset includes 102 distinct metabolites, 102 univariate linear regressions were run in parallel to assess each metabolite individually. Considering the high risk of false positives (Type I error) when numerous comparisons are being testing in parallel, a multiple testing correction via false-discovery rate (FDR) with the Benjamini-Hochberg (BH) procedure was used[147]. The FDR is defined as the proportion of tests

within a set that are falsely considered as significant[148]. The p-corrected value (q-value) was set a 0.05, where a q-value of 0.05 means that only 5% of metabolomic features with $p < q$ will be false positives[147]. An important property of the q-value to keep in mind is that it sets an FDR at the designated level for each set of comparisons (i.e., statistical tests) rather than individual comparisons, and thus the significance level is not consistent between different statistical analyses[148]. All p-values reported are raw values, and grey shading in the *Results* tables represents significance after BH correction. Any metabolites with $p < q$ in univariate models were included in multivariate linear regression models with step-wise inclusion of the three covariates age, sex and total percent body fat (only percent body fat for children). In all regression models, a scatterplot was used to visually inspect for linearity. Quadratic terms were included if a non-linear relationship was evident. In all multivariate analyses (i.e., other than initial univariate test), $P<0.05$ was considered statistically significant.

To address secondary objectives in the adult cohort, sex interaction effects were included into all multivariate regression models in step-wise manner where sex interaction = metabolite abundance * sex to determine if sex is a mediating factor[149]. For any significant sex interaction terms, sex-stratified multivariate regression models were performed. This sex interaction term was included to identify the presence or absence of interaction between two independent variables – metabolite relative abundance and sex[150]. In other words, this is a method to identify if the metabolome is impacted directly by sex when analyzed in relation to BAT or hepatic fat. This is different than just including each independent variable in the linear regression, which evaluates the impact of each independent variable on the dependent outcome (i.e., the impact of sex on BAT activity).

2.5.1 Sensitivity Analysis

Due to the large number of metabolites available for analysis compared to the number of participants, studies in the metabolomics field often rely on dimension reduction techniques[151]. Dimension reduction refers to the grouping of independent, linearly correlated variables into distinct "components" to reduce the complexity of the dataset while maintaining maximal variation[152]. One such example is Principal Component Analysis (PCA). This was implemented in this study as an alternative sensitivity analysis for comparison to univariate testing described above for the primary analysis. By clustering metabolites into components, the relevant metabolome of each participant can be explained with fewer correlated variables to reduce the FDR[152]. PCA is an unsupervised data reduction technique, meaning that components are dependant only on explanatory variables without user intervention or participant groupings[152].

While there is no consensus on minimum required sample size for PCA, it is largely accepted that the number of participants must exceed the number of variables[153]. As this dataset does not adhere to this rule, an initial metabolite screening step was employed in the adult cohort. Pearson or spearman correlation coefficients were assessed for each metabolite, and any metabolites with a very weak correlation (r or $rho < 0.250$) with all outcomes were excluded. PCA was not performed in the pediatric cohort as the sample size of 25 was too small.

To define each component by a group of metabolites, each metabolite received a "factor loading" representing its correlation with the component, where the magnitude of the factor loading shows the strength of this correlation[154]. Varimax (orthogonal) rotation was then applied to increase the simplicity and interpretability of the final structure by maximizing factor loadings and minimizing overlap between components[154]. Factor scores were derived as new explanatory variables by multiplying each factor loading by the original relative abundance and summing

these products for all metabolites within the component[154]. This is a standardized z-score and indicates each participant's metabolome profile adheres to the component pattern[154].

As a PCA identifies an equal number of components as there are original variables, a choice must be made as to how many components will be retained to explain maximal variation. This is one of the limitations of PCA, as there is a degree of subjectivity in the process of selecting components to retain. Common and valid examples include retaining all components with an "eigenvalue" (i.e., the amount of variation captured by said component) greater than one or those before the inflection point of the scree plot arm (i.e., eigenvalues plotted against their component number)[155]. In this project, the scree plot method was used for component selection.

After selecting the total number of components and derivation of the factor scores, multivariate linear regressions were performed to assess the relationship of each metabolite component with the same outcome variables and covariates as above. Similar methodology has been used previously in metabolomic studies[154,156].

2.5.2 Calculation of Sample Size

A "rule of thumb" model was used to determine sample size required for the outlined statistical analyses, which states that ten subjects had to be recruited per variable included in each model[157]. In the adult study, 60 participants were recruited to provide sufficient power for the following variables to be included in regression analyses: age, sex, body fat percentage, and the BAT or liver primary outcome. In the pediatrics study, 25 children were recruited to allow for inclusion of percent body fat and the BAT or liver primary outcome.

CHAPTER 3: RESULTS

3.1 Adult Cohort Recruitment

This project consists of two cohorts of the GETBAT study: (1) an adult cohort and (2) a pediatric cohort, and the data will be discussed by cohort before comparisons are made. To begin, adult recruitment took place between June 2016 and March 2018 and is shown in **Figure 4,**. A total of 483 potential participants from the community (415) or the Boris Diabetes and Endocrinology clinic (68) were in contact with research staff. A total of 73 participants met eligibility criteria, consented to the GETBAT study and completed Visit 1 (15% enrollment rate), and 64 participants completed both study visits (88% completion rate).

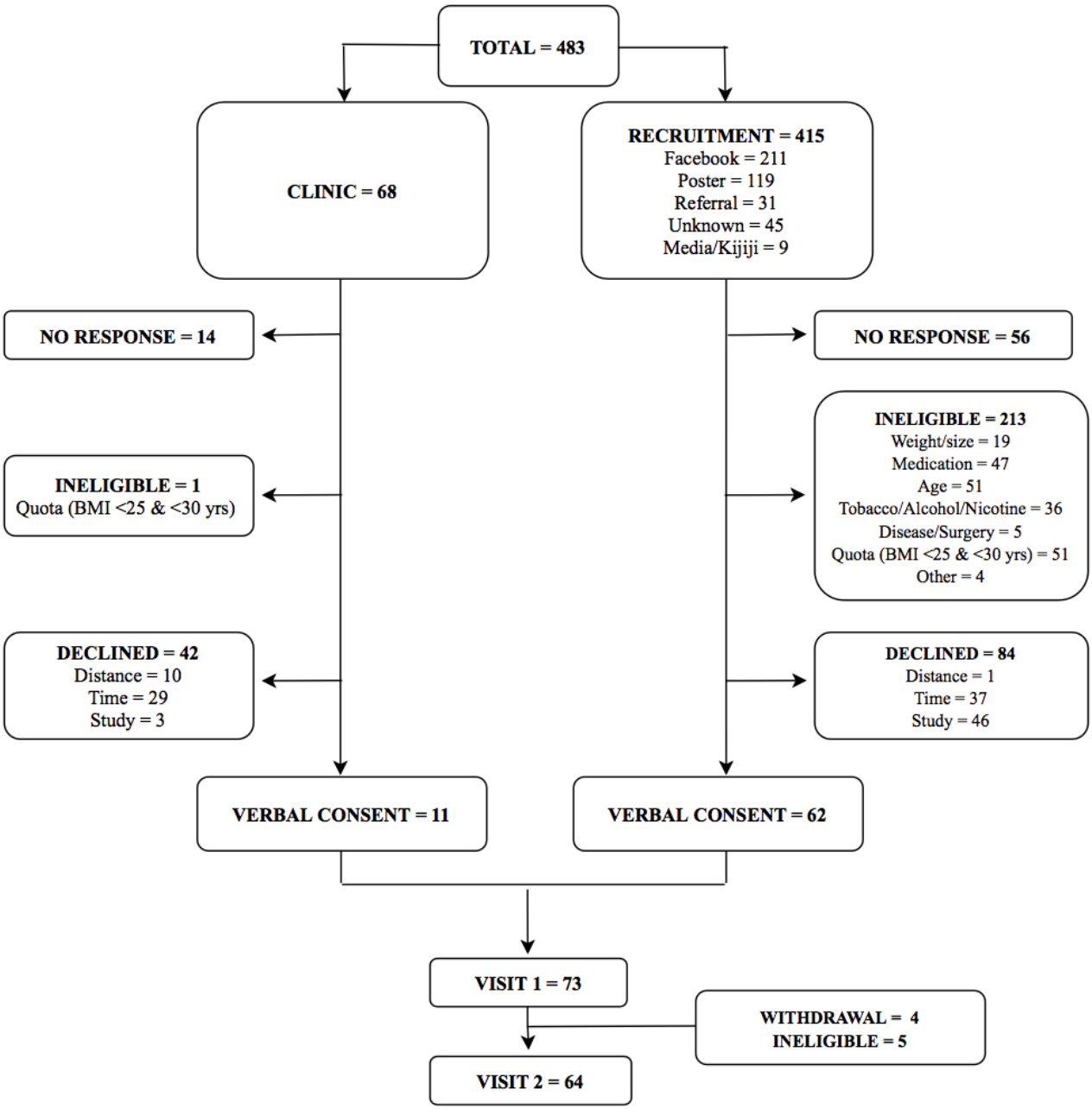

Figure 4. Adult GETBAT recruitment and study flow. Study recruitment took place between June 2016 and March 2018. Abbreviations: *BMI* body mass index.

3.2 Adult Cohort Demographics

The adult cohort consisted of 63 male and female participants between the ages of 18 and 57 years (one participant was excluded due to missing metabolomic data). The median age was 25.9 years and 62% were male and 38% were female. The median [IQR] BMI was 25.4 kg/m^2 [22.4, 31.7] with 52% of the participants being classified as overweight or obese according to WHO cut-offs, and the median percent body fat was 28.5%, with one participant exceeding the weight threshold of the DXA scanner, so no body composition was available[131].

The MRI based BAT and liver measures are described in **Table 1**. All participants underwent pre-cold MRI scanning and had a baseline BAT lipid content measurement (i.e., pre-cold SCV PDFF%); mean value of 72.1 ± 7.96%. It is important to note that an increased pre-cold SCV PDFF% represents a less "brown" phenotype in this BAT depot. Of the 63 participants, 59 participants had complete post-cold MRI data enabling the calculation of the absolute change in BAT lipid content with cold stimulation (i.e., SCV PDFF% reduction); mean value of 2.95 ± 2.43%. The median value for the percent change in SCV PDFF% was 3.44% [1.49, 6.53]. The post-cold MRI images from four participants could not be analyzed due to excess motion (shivering) in the scanner.

As described in **Methodology Section 2.3.3**, participants also underwent measurement of hepatic lipid content in the pre-cold state. In the 62 who completed this measure, the median baseline hepatic lipid content (pre-cold liver PDFF%) was 5.37% [4.54, 6.71]. Furthermore, 55% of participants were NAFLD- and 45% of participants were NAFLD+ based on the established hepatic fat cut-off value of 5.6%[88].

Table 1. Adult participant demographics, BAT and hepatic fat measures.

	n (%)	Mean (SD) Median [Q1, Q3]

Participant Demographics		
Age, y	63	25.92 [22.75, 35.80]
Sex	63	-
Male	39 (62%)	-
Female	24 (38%)	-
BMI (kg/m^2)	63	25.4 [22.4, 31.7]
Normal	30 (48%)	22.2 (1.6)
Overweight/Obese	33 (52%)	31.7 [26.6, 36.6]
Percent Body Fat	62	28.5 [19.5, 38.0]
MRI Results		
Pre-Cold SCV PDFF%	63	72.09 (7.96)
SCV PDFF% Reduction	59	2.95 (2.43)
Percent Change SCV PDFF%	59	3.44 [1.49, 6.53]
Pre-Cold Liver PDFF%	62	5.37 [4.54, 6.71]
NAFLD-	34 (54%)	4.62 (0.57)
NAFLD+	28 (46%)	7.24 [6.23, 8.73]

3.3 Association Between BAT and the Plasma Metabolome in Adults

The adult plasma metabolome was analyzed in relation to BAT to investigate if any metabolomic features are able to predict each BAT measure. Results for measures of baseline BAT lipid content and cold-stimulated BAT activity are presented below, and similarities and differences are highlighted. As mentioned previously, the percent change in BAT PDFF% is considered the BAT activity outcome in this project, and data for the absolute reduction in BAT PDFF% is presented for comparison.

In the initial univariate analysis relating pre-cold SCV PDFF% to each metabolite with correction for multiple testing, five metabolites significantly predict this BAT measure: aconitate, asparagine, glutamic acid, methionine and creatine (**Table 2**). Aconitate, glutamic acid and creatine were directly related to baseline SCV PDFF% suggesting that higher values of these are associated with a "whiter" BAT phenotype. Higher levels of asparagine and methionine were

related to a lower baseline SCV PDFF% representing a "browner" BAT phenotype. The direct relationship of aconitate and glutamic acid and inverse relationship of asparagine persisted even when age and sex were included in the model. There was a significant sex interaction for aconitate with baseline BAT lipid content, such that aconitate was directly related to pre-cold SCV PDFF% in males only (**Table 3)**. Glutamic acid was related to increased baseline BAT lipid content independent of age, sex and total body fat percentage. See **Figure 5** for scatter plots of the correlation between each of these five metabolites with baseline BAT lipid content.

Table 2. Stepwise linear regression models for **Pre-Cold SCV PDFF%** in adults**.** *Denotes that a quadratic function was used as it fit better than a linear function for labeled variables. Grey shading and bolding denote $P<0.05$.

	Model 1 Univariate			**Model 2** + Age			**Model 3** + Age + Sex			**Model 4** + Age + Sex + % Body Fat		
Predictor	β	t	p-value	β	t	p-value	β	t	p-value	β	t	p-value
Aconitate	**.420**	**3.584**	**.001**	**.224**	**2.072**	**.043**	.213	1.873	.066	.074	.973	.335
Creatine: Linear	**.408**	**3.503**	**.001**	.198	1.775	.081	.185	1.606	.114	-.019	-.238	.813
Creatine: Quadratic*	.170	1.463	.149	.110	1.078	.285	.110	1.071	.289	-.051	-.720	.474
Glutamic Acid: Linear	**.480**	**4.241**	**<.001**	**.374**	**3.997**	**<.001**	**.488**	**5.164**	**<.001**	**.214**	**2.758**	**.008**
Glutamic Acid: Quad*	**-.198**	**-1.751**	**.085**	**-.180**	**-1.961**	**.055**	**-.217**	**-2.510**	**.015**	**-.157**	**-2.508**	**.015**
Asparagine	**-.441**	**-3.808**	**<.001**	**-.282**	**-2.740**	**.008**	**-.321**	**-3.080**	**.003**	-.066	-.847	.400
Methionine	**-.409**	**-3.474**	**.001**	-.184	-1.634	.108	-.176	-1.547	.127	-.060	-.793	.431

Table 3. Sex-stratified aconitate regression models for **Pre-Cold SCV PDFF%**. Grey shading and bolding denote $P<0.05$.

	Model 1 Univariate			**Model 2** + Age			**Model 3** + Age + % Body Fat		
Predictor	β	t	p-value	β	t	p-value	β	t	p-value

Aconitate - Male	**.425**	**2.860**	**.007**	**.297**	**2.119**	**.041**	.174	1.997	.054
Aconitate - Female	.284	1.355	.190	.071	.394	.698	-.116	-1.090	.290

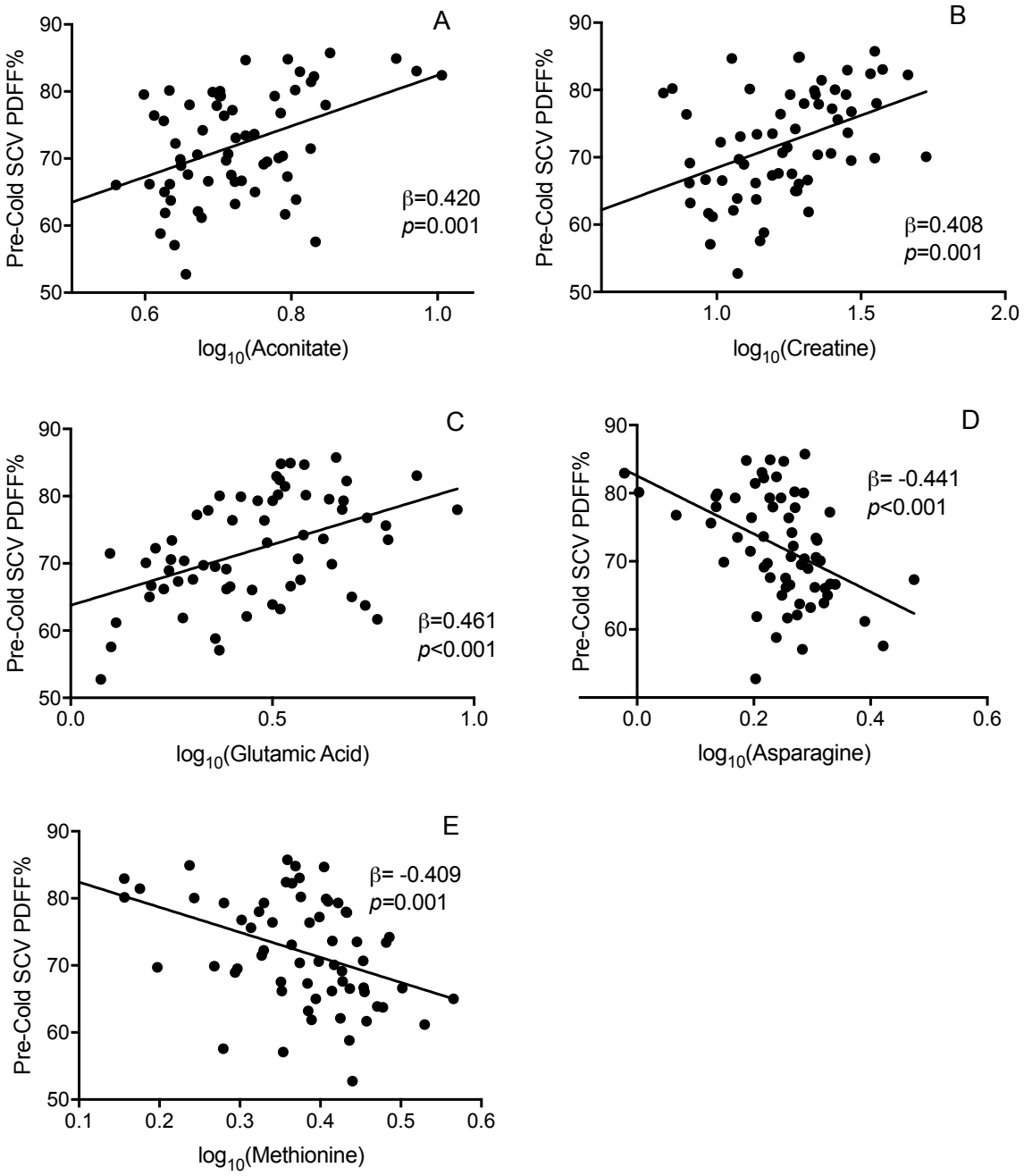

Figure 5. Correlation scatter plot for **Pre-Cold SCV PDFF%** in adults. (A) Aconitate, (B) creatine, (C) glutamic acid, (D) asparagine, and (E) methionine.

For BAT activity (i.e., the percent change in PDFF% reduction from baseline), no metabolites were significant after multiple testing correction. **Table 4** and **Figure 6** however presents any significant metabolites from the absolute reduction SCV PDFF% models with relative SCV PDFF% decline for comparison. Five metabolites were negatively related to absolute SCV PDFF% reduction: aconitate, alanine, acetyl-carnitine, creatine and hexanoyl-carnitine (

Table 5, Figure 7). This suggests that a higher abundance of these metabolites predicts lower cold-induced BAT activity when the absolute decline in SCV PDFF% is considered. Although very similar patterns can be seen in univariate and age-corrected models for the relative SCV PDFF% decline, these metabolites did not meet the significance criteria after adjustment for multiple comparisons. Graphically, the relationship of each of these metabolites to both BAT activity variables is also similar. Aconitate and both carnitine species remained significant even when age, sex and percent body fat were included in the model. Alanine remained significant with age and sex correction, and creatine with age in the model. No sex interaction for aconitate with change in SCV PDFF% was seen. Thus, aconitate, alanine, acetyl-carnitine, hexanoyl-L-carnitine and creatine were lower in adults with higher BAT activity, but significance was lost when the baseline SCV PDFF% was included in the analysis (i.e., when looking at decline relative to baseline).

Table 4. Stepwise linear regression models for **Percent Change SCV PDFF%** in adults. Abbreviations: *NS* non-significant after multiple testing correction (raw p-value).

	Model 1 Univariate			**Model 2** + Age			**Model 3** + Age + Sex			**Model 4** + Age + Sex + % Body Fat		
Predictor	β	t	p-value	β	t	p-value	β	t	p-value	β	t	p-value
Aconitate	-.371	-2.991	NS (.004)	-.243	-1.892	.064	-.211	-1.59	.118	-.127	-1.083	.284

Creatine	-.412	-3.386	NS (.001)	-.281	-2.165	.035	-.255	-1.92	.060	-.129	-1.068	.290
Alanine	-.419	-3.45	NS (.001)	-.310	-2.531	.014	-.285	-2.251	.028	-.165	-1.429	.159
Acetyl-carnitine	-.413	-3.391	NS (.001)	-.288	-2.259	.028	-.258	-1.93	.059	-.210	-1.817	.075
Hexanoyl-L-carnitine	-.412	-3.382	NS (.001)	-.350	-3.064	.003	-.320	-2.697	.009	-.285	-2.874	.006

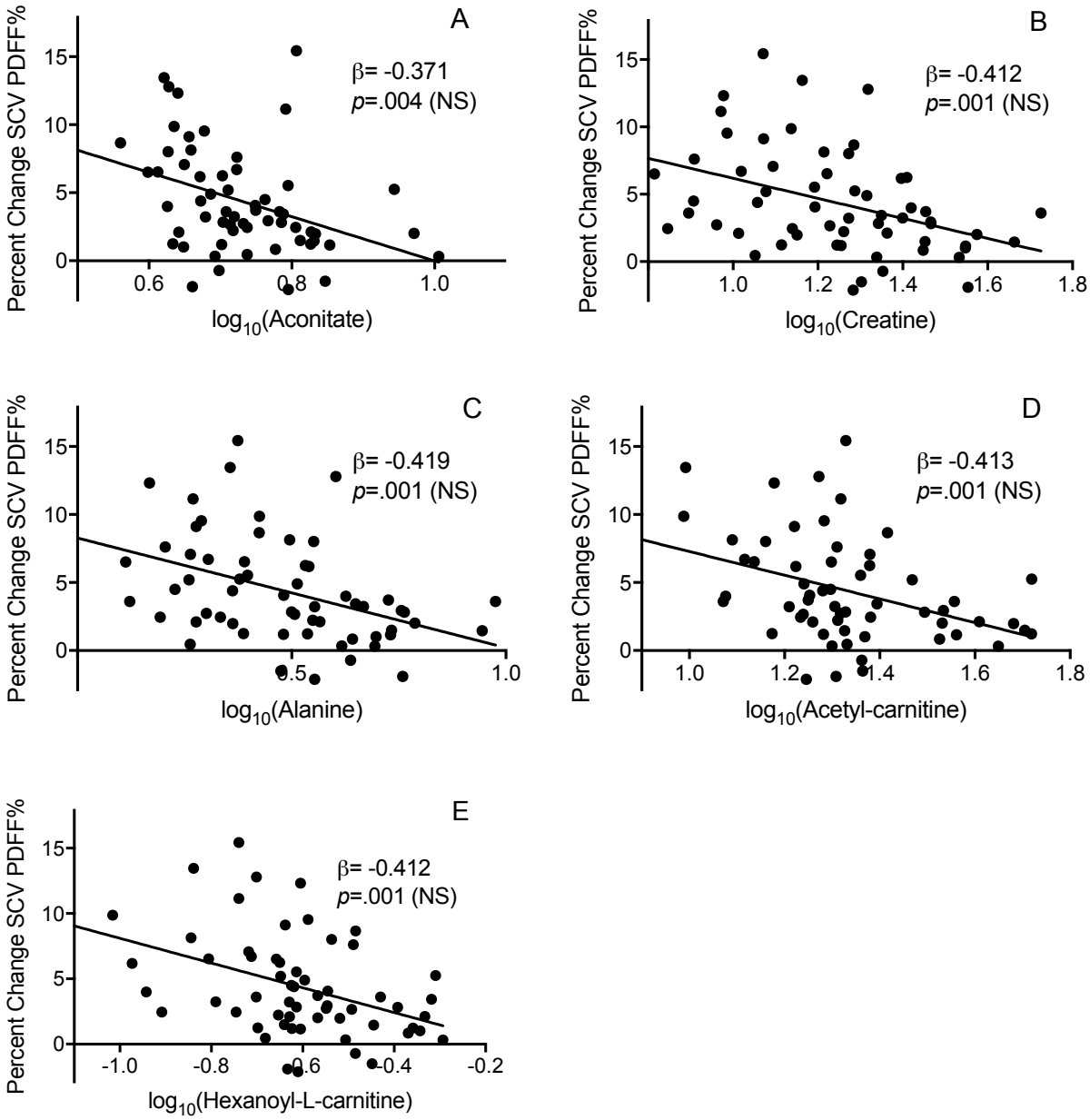

Figure 6. Correlation scatter plot for **Percent Change SCV PDFF%** in adults. (A) Aconitate, (B) creatine, (C) alanine, (D) acetyl-carnitine and (E) hexanoyl-L-carnitine.

Table 5. Stepwise linear regression models for **SCV PDFF% Reduction** in adults. *Denotes that a quadratic function was used as it fit better than a linear function for labeled variables. Grey shading and bolding denote $P<0.05$.

	Model 1 Univariate			**Model 2** + Age			**Model 3** + Age + Sex			**Model 4** + Age + Sex + % Body Fat		
Predictor	β	t	p-value	β	t	p-value	β	t	p-value	β	t	p-value
Aconitate: Linear	**-.462**	**-3.183**	**.002**	**-.363**	**-2.554**	**.014**	**-.331**	**-2.245**	**.029**	**-.278**	**-2.152**	**.036**
Aconitate: Quadratic*	.201	1.381	.173	.274	1.958	.055	.265	1.882	.065	**.327**	**2.652**	**.011**
Creatine	**-.402**	**-3.285**	**.002**	**-.282**	**-2.143**	**.037**	-.255	-1.899	.063	-.141	-1.123	.267
Alanine: Linear	**-.411**	**-3.217**	**.002**	**-.312**	**-2.395**	**.020**	**-.290**	**-2.171**	**.034**	-.203	-1.652	.105
Alanine: Quadratic*	-.011	-.084	.934	-.013	-.110	.913	-.002	-.019	.985	.112	.962	.340
Acetyl-carnitine: Linear	**-.453**	**-3.464**	**.001**	**-.337**	**-2.467**	**.017**	**-.305**	**-2.149**	**.036**	**-.256**	**-2.015**	**.049**
Acetyl-carnitine: Quadratic*	.167	1.278	.207	.167	1.324	.191	.171	1.347	.184	.154	1.368	.177
Hexanoyl-L-carnitine: Linear	**-.423**	**-3.447**	**.001**	**-.362**	**-3.099**	**.003**	**-.357**	**-3.073**	**.003**	**-.305**	**-2.906**	**.005**
Hexanoyl-L-carnitine: Quadratic*	-.003	-.024	.981	.033	.285	.777	.026	.225	.823	.012	.119	.906

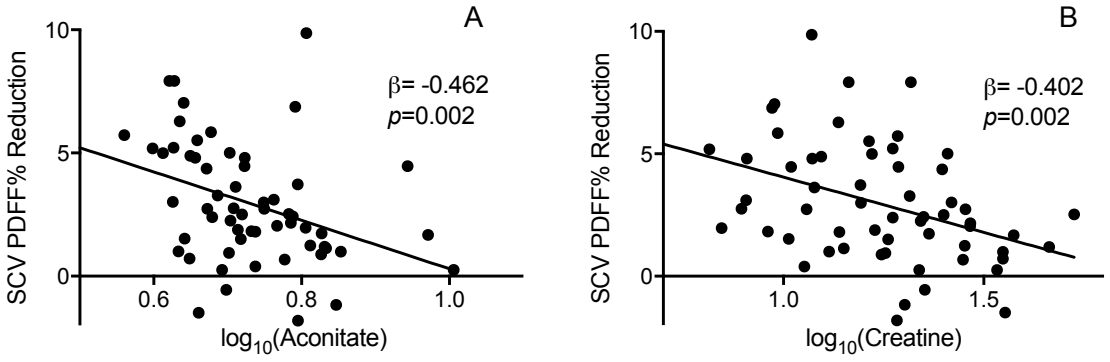

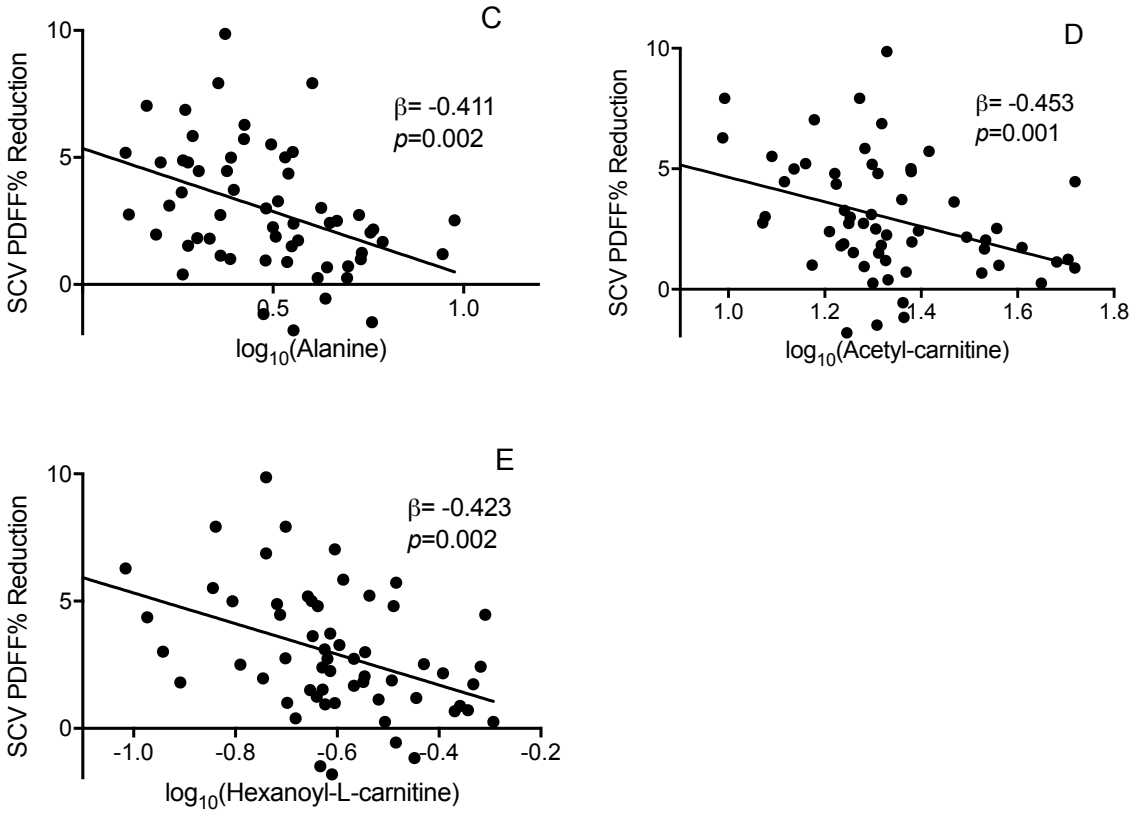

Figure 7. Correlation scatter plot for **SCV PDFF% Reduction** in adults. (A) Aconitate, (B) creatine, (C) alanine, (D) acetyl-carnitine, and (E) hexanoyl-L-carnitine.

Aconitate and creatine were associated with both baseline SCV PDFF% and cold-induced SCV PDFF% reduction, suggesting some consistency in the findings of their relationship to BAT.

As discussed in **Methodology Section 2.5.1**, in addition to the analysis described, a sensitivity analysis was carried out in which the metabolites were grouped using a PCA in an effort to reduce the number of variables examined. In this analysis, metabolites that are correlated become grouped into a component (see **Appendix B1-B4**). The metabolites grouped into 11 components and these explained 74% of the variability in the data. Some of the components had many metabolites grouped under them reducing the usefulness of this analysis. The analytes highlighted in the analysis above for pre-cold SCV PDFF% and the components they were

within are: glutamic acid (component 8), aconitate (component 3), creatine (component 4), asparagine (component 6) and methionine (component 6 and 8). In examining the relationship between these components and pre-cold SCV PDFF% (**Appendix B5**), findings from our primary analysis were re-confirmed. Specifically, components 3 and 4, which include aconitate and creatine respectively, were directly related to pre-cold SCV PDFF% and component 6, containing asparagine and methionine, was inversely related. These findings support the observation from the primary analysis that aconitate and creatine are higher in those with higher baseline BAT lipid content (i.e., a whiter BAT phenotype), and asparagine and methionine are lower in those with higher baseline BAT lipid content. Component 8, which includes glutamic acid was not, however, related.

Components 2 and 4 were inversely related to both the relative and absolute reduction in SCV PDFF% in response to cold; in other words, those with higher levels of these components had less cold-induced BAT activity (**Appendix B6-B7**). This is consistent with the observation that creatine (component 4), alanine (component 4), acetyl-carnitine (components 2 and 4) and hexanoyl-L-carnitine (component 4 and 7) are also higher in those with less decline in SCV PDFF% (non-significant for component 7). Thus, the sensitivity analysis confirms some of the findings from the analysis of individual metabolites. However, two components that were significant for all three BAT measures (components 9 and 11) had no metabolites within them that were significant in the primary analysis. These components include the metabolites thymine, aminobenzoic acid, hippurate, orotate, propionate and succinate in component 9 and cysteine, cystine and orotate in component 11.

3.4 Association Between Hepatic Fat and the Plasma Metabolome in Adults

In examining the relationship of the metabolome to hepatic fat, we were interested especially in those metabolites that were also related to hepatic fat independent of age, sex and body fat percentage (i.e., metabolites that may predict hepatic fat accumulation independent of obesity status). Three metabolites, tyrosine, xanthine and pyridoxal, were elevated in those with increased hepatic fat, while higher serine levels were associated with lower hepatic fat independent of all covariates (**Table 6**). Glutamic acid also significantly predicted higher hepatic fat, but this relationship was not independent of total body fat percentage. Scatter plots for each identified metabolite are presented in **Figure 8**. None of the below significant metabolites showed a sex interaction and therefore no sex-stratified regression models were performed.

Table 6. Stepwise linear regression models for **Pre-Cold Liver PDFF%** in adults**.** *Denotes that a quadratic function was used as it fit better than a linear function for labeled variables. Grey shading and bolding denote $P<0.05$.

	Model 1 Univariate			**Model 2** + Age			**Model 3** + Age + Sex			**Model 4** + Age + Sex + % Body Fat*		
Predictor	β	t	p-value	β	t	p-value	β	t	p-value	β	t	p-value
Glutamic Acid	**.392**	**3.305**	**.002**	**.326**	**2.858**	**.006**	**.367**	**2.978**	**.004**	.201	1.566	.123
Tyrosine: Linear	**.405**	**3.604**	**.001**	**.374**	**3.535**	**.001**	**.384**	**3.487**	**.001**	**.283**	**2.734**	**.008**
Tyrosine: Quadratic*	**.271**	**2.408**	**.019**	**.231**	**2.174**	**.034**	**.225**	**2.084**	**.042**	**.216**	**2.218**	**.031**
Pyridoxal	**.387**	**3.253**	**.002**	**.296**	**2.502**	**.015**	**.306**	**2.543**	**.014**	**.241**	**2.206**	**.032**
Xanthine	**.428**	**3.664**	**.001**	**.322**	**2.645**	**.010**	**.323**	**2.612**	**.011**	**.272**	**2.487**	**.016**
Serine	**-.390**	**-3.279**	**.002**	**-.289**	**-2.398**	**.020**	**-.289**	**-2.377**	**.021**	**-.223**	**-2.048**	**.045**

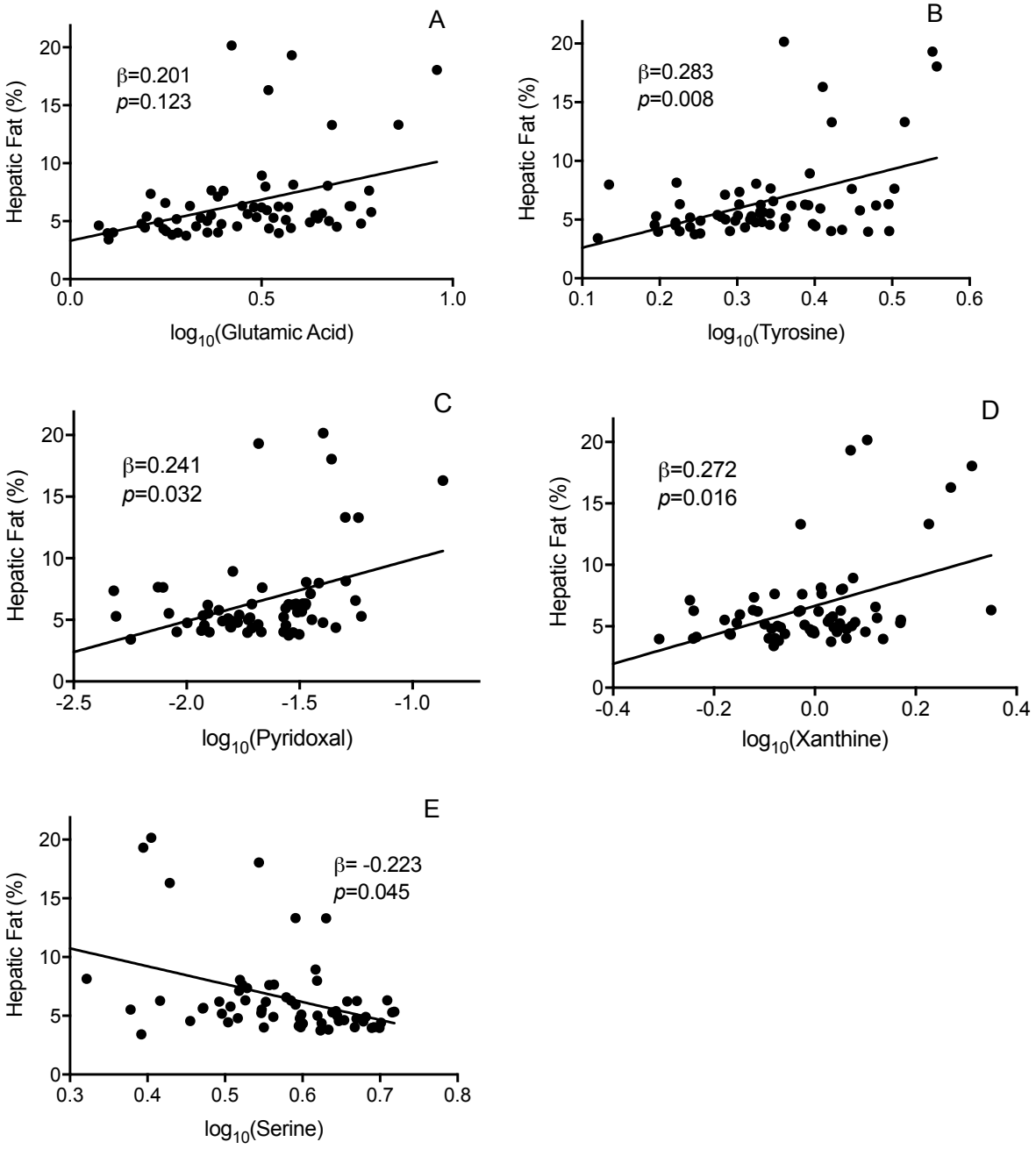

Figure 8. Correlation scatter plot for **hepatic fat (%)** in adults. (A) Glutamic acid, (B) Tyrosine, (C) pyridoxal, (D) xanthine, and (E) serine.

In the sensitivity analysis (**Appendix B8**), component 8 was directly related and component 9 was indirectly related to hepatic fat independent of all covariates. Thus, our findings for tyrosine (components 1 and 8) and glutamic acid (component 8) were confirmed in this sensitivity analysis. Component 6 was inversely related to hepatic fat similar to serine which is within this

component, but the relationship was no longer significant when body fat percentage was included in the model. Xanthine and pyridoxal were both included in component 4, which was non-significantly trending (P=0.055) towards a positive relationship with hepatic fat, although only in the univariate model.

Glutamic acid was the sole metabolite that predicted both higher baseline BAT lipid content and hepatic fat content after controlling for the influence of age and sex. Interestingly, component 9 was inversely related to hepatic fat independent of age, sex and body fat, and was similarly related to elevated baseline BAT lipid content. None of the individual metabolites in this component (thymine, aminobenzoic acid, hippurate, orotate, propionate, succinate) were significant in the individual metabolite analysis, although succinate has been previously noted to be associated with BAT metabolism[58].

In summary, in adults, five metabolites of the 102 tested were related to baseline BAT lipid content and two of these, aconitate and creatine were also related to BAT activity (in terms of absolute SCV PDFF%). The directionality of these models was in line with expectations (i.e., higher metabolite abundance predicts a whiter baseline BAT phenotype and decreased cold-induced BAT activity). Alternative statistical analysis (i.e., PCA) also corroborates these results for creatine with both BAT measures and aconitate with pre-cold SCV PDFF%, further supporting both metabolites linkage to BAT activity. Of the 5 metabolites associated with BAT activity (measured as the absolute cold-induced decline in SCV PDFF%), three (alanine, hexanoyl-L-carnitine and acetyl-carnitine) were not associated with baseline BAT lipid content. None of these metabolites were also linked to hepatic fat accumulation, however. Glutamic acid is a candidate metabolite linked to both increased baseline BAT and hepatic lipid content but lost its relationship with hepatic fat when adiposity was included in the model thus weakening the evidence.

3.5 Pediatric Study Recruitment

Next, each of the primary objectives of this project were similarly analyzed in the pediatric GETBAT cohort and these results were compared to those from the adult cohort. Recruitment for the pediatric cohort took place between February 2018 and August 2019; flowchart presented in **Figure 9.** Of the 152 children in contact with research staff, 54 were from the Children's Exercise and Nutrition Clinic at McMaster Children's Hospital, and 98 were from the community. A total of 35 children consented to the GETBAT study and completed the first study visit (23% enrollment rate), and 26 children completed both study visits (74% completion rate). Of the nine participants who did not complete both study visits, two participants either withdrew or were lost to follow-up after the first study visit. Seven participants did not complete the second visit due to claustrophobia in the MRI.

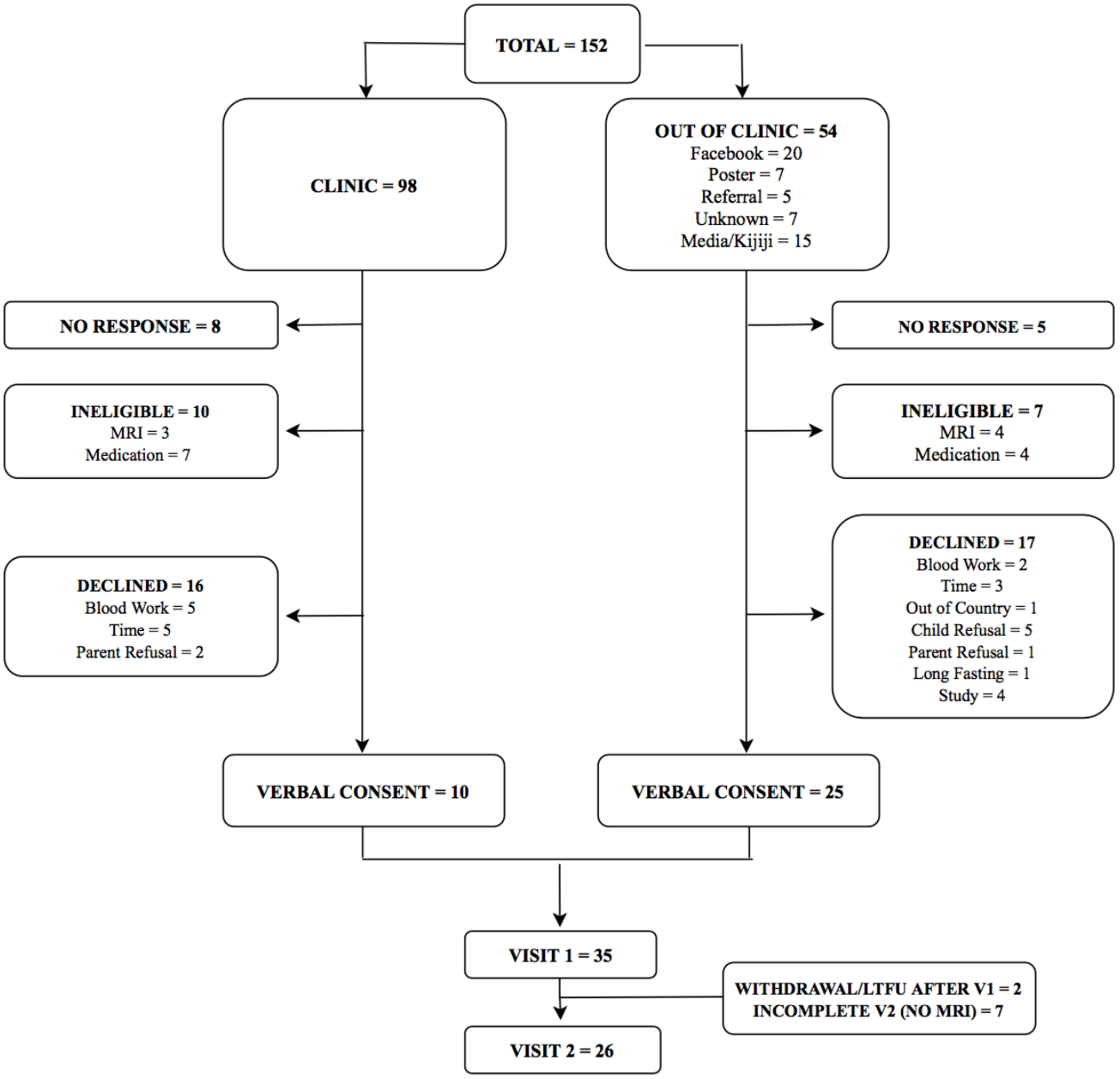

Figure 9. Pediatric GETBAT study recruitment. Study recruitment took place between February 2018 and August 2019. Abbreviations: *LTFU* lost to follow-up, *V1* visit 1, *V2* visit 2, *MRI* magnetic resonance imaging.

3.6 Pediatric Cohort Demographics

The pediatric cohort consisted of 25 male children between the ages of eight and ten years (median age 9.89 years) who completed the pre-cold MRI. Of those who completed the baseline MRI, three participants did not have metabolomics data due to the completion of the initial metabolomics analysis before the completion of recruitment and were thus excluded. The mean BMI Z-score, a standardized scale of BMI for children, was 1.25 ± 2.06; 48% of the participants were overweight or obese according to WHO cut-offs[132]. The median body fat percentage was 25.0% [15.40, 43.35].

MRI-based measures of BAT and hepatic fat are available in **Table 7**. All participants underwent baseline MRI scanning for pre-cold SCV PDFF%; mean value of 63.03 ± 11.48%. This value is lower than the mean baseline value from the adult cohort, representing a "browner" BAT phenotype, which is in line with previously-reported age-related BAT decline[15]. Twenty-three participants also completed post-cold imaging, and the mean decline in BAT lipid content (i.e., SCV PDFF% reduction) with cold stimulation was 1.86 ± 2.48%. The relative decline in BAT lipid content from baseline (i.e., percent change SCV PDFF%) was then calculated; mean value of 3.12 ± 4.02%. Two participants did not undergo post-cold imaging due to claustrophobia. Finally, the same 23 participants also underwent MRI scanning for baseline liver fat; median value of 3.25% [2.83, 4.61]. Thus, 17% of participants were NAFLD+ using the same threshold of PDFF ≥ 5.6% as for the adult cohort.

Table 7. Pediatric participant demographics, BAT and hepatic fat measures.

	n (%)	Mean (SD) Median [IQR]
Participant Demographics		
Age, y	25	9.89 [9.16, 10.60]

% Body Fat	25	25.00 [15.40, 43.35]
BMI Z-score	25	1.25 (2.06)
Normal	13 (52%)	-0.49 (0.66)
Overweight/Obese	12 (48%)	3.14 (1.13)
MRI Results		
Pre-Cold SCV PDFF%	25	63.03 (11.48)
SCV PDFF% Reduction	23	1.86 (2.48)
Percent Change SCV PDFF%	23	3.12 (4.02)
Pre-Cold Liver PDFF%	23	3.25 [2.83, 4.61]
NAFLD-	19 (83%)	3.38 (0.85)
NAFLD+	4 (17%)	15.94 (10.39)

3.7 Association Between BAT and the Plasma Metabolome in Prepubertal Males

One of the main goals of this project was to investigate if there are differences in the plasma metabolome in relation to BAT measures in children compared to adults. Thus, a similar analysis was undertaken except that no correction for age or sex was required due to the single sex and tight age group of this cohort.

No metabolites were significantly related to pre-cold SCV PDFF% after multiple testing correction. However, multivariate regression analysis was performed for two metabolites approaching significance, cysteine and cystine (**Table 8, Figure 10**), as it was interesting to note that they were both significantly related to hepatic fat (see **Results Section 3.8**). It is crucial to interpret these results with caution as neither metabolite was significant after BH adjustment.

Table 8. Stepwise linear regression models for **Pre-Cold SCV PDFF%** in children. Abbreviations: *NS* non-significant after multiple testing correction (raw p-value).

	Model 1	**Model 2**
Predictor	Univariate	+ % Body Fat

	β	t	p-value	β	t	p-value
Cysteine	.585	3.462	NS (.002)	.095	.820	.421
Cystine	.541	3.084	NS (.005)	.058	.503	.620

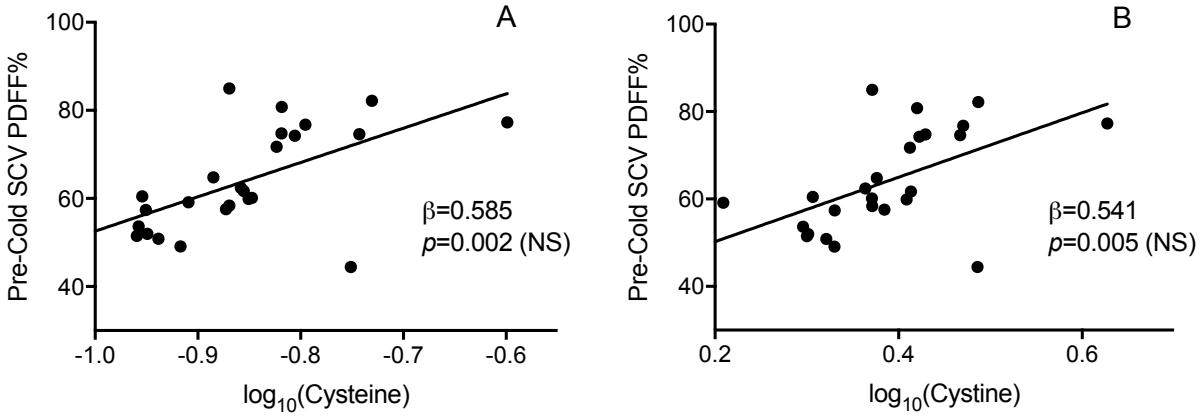

Figure 10. Correlation scatter plot for **Pre-Cold SCV PDFF%** in children. (A) Cysteine, and (B) cystine. Abbreviations: *NS* non-significant after multiple testing p-value correction.

Three metabolites, 4-hydroxy-L-proline, cis-4-hydroxy-D-proline and L-carnitine were inversely related to percent change in SCV PDFF% in the univariate model and after correction for percent body fat (**Table 9, Figure 11**). Similarly, 4-hydroxy-L-proline, cis-4-hydroxy-D-proline were also inversely related to the absolute change in SCV PDFF% in this cohort (**Appendix B9-B10**). Unlike in the adult cohort, there were no metabolite similarities between baseline or cold-stimulated BAT measures. No sensitivity analysis was performed due to the small sample size.

Table 9. Stepwise linear regression models for **Percent Change SCV PDFF%** in children. Grey shading and bolding denote $P<0.05$.

	Model 1 Univariate			**Model 2** + % Body Fat		
Predictor	β	t	p-value	β	t	p-value
4-Hydroxy-L-proline	**-.702**	**-4.516**	**< .001**	**-.646**	**-3.736**	**.001**

cis-4-Hydroxy-D- proline	**-.699**	**-4.483**	**< .001**	**-.642**	**-3.709**	**.001**
L-carnitine	**-.642**	**-3.841**	**.001**	**-.591**	**-3.701**	**.001**

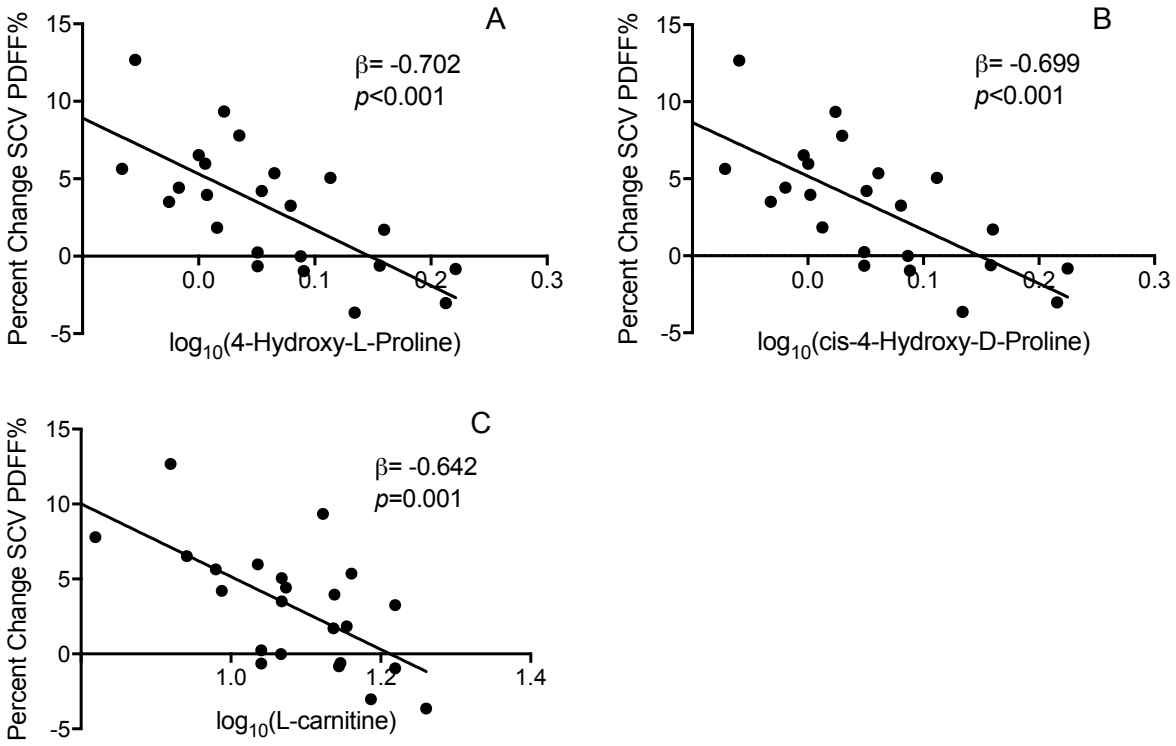

Figure 11. Correlation scatter plot for **Percent Change SCV PDFF%** in children. (A) 4-hydroxy-L-proline, (B) cis-4-hydroxy-proline, and (C) L-carnitine.

3.8 Association Between Hepatic Fat and the Plasma Metabolome in Prepubertal Boys

Two metabolites, cysteine and cystine, were directly related to hepatic fat accumulation in these boys after multiple testing correction. Increased levels of both were quadratically associated with increased hepatic fat and this relationship was independent of total body fat. (**Table 10, Figure 12**). This is particularly interesting as these metabolites were also trending towards significantly related to a higher pre-cold BAT lipid content, or a whiter BAT phenotype.

Table 10. Stepwise linear regression models for **Pre-Cold Liver PDFF%** in children. *Denotes that a quadratic function was used as it fit better than a linear function for labeled variables. Grey shading and bolding denote $P<0.05$.

Predictor	Model 1 Univariate			Model 2 + % Body Fat		
	β	t	p-value	β	t	p-value
Cysteine: Linear	.305	2.069	.052	.035	.218	.829
Cysteine: Quadratic *	**.628**	**4.265**	**< .001**	**.714**	**5.425**	**< .001**
Cystine: Linear	**.445**	**3.319**	**.003**	.257	1.721	.101
Cystine: Quadratic *	**.563**	**4.202**	**< .001**	**.592**	**4.800**	**< .001**

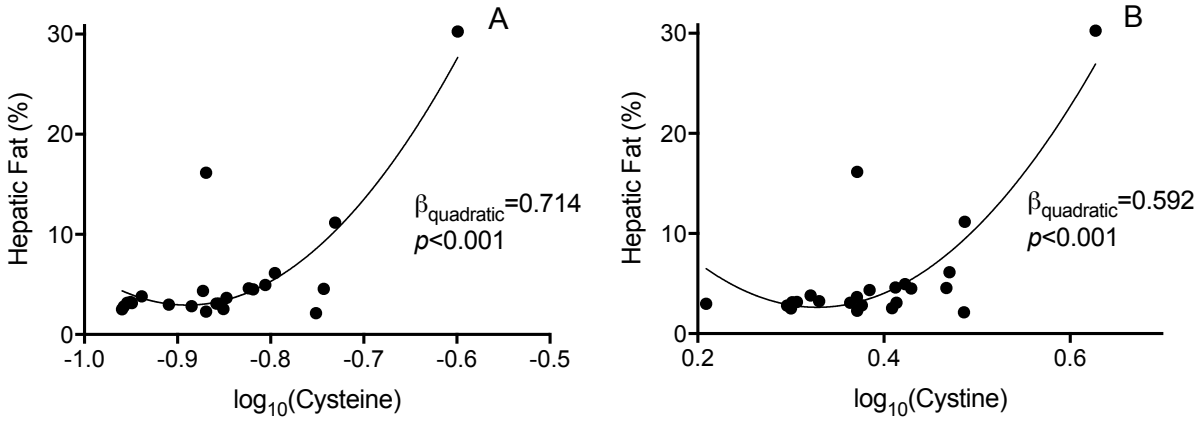

Figure 12. Correlation scatter plot for **hepatic fat (%)** in children. (A) Cysteine, and (B) cystine.

It is important to compare and contrast our findings in adults and in children. A summary figure of these results is presented in **Figure 13**. Interestingly, there were no exact consistencies in any of the BAT or liver analyses between the children and adults. However, the most notable similarity was in the BAT activity analyses, where acetyl-carnitine and hexanoyl-L-carnitine were associated with SCV PDFF% decline and trending towards significance in relative SCV PDFF% decline in the adults. In the children, neither of these carnitine species were significantly related to BAT activity, but a metabolite of hexanoyl-L-carnitine, L-carnitine, was similarly associated to relative SCV PDFF%. Thus, higher circulating levels of carnitine related

metabolites were associated with lower cold-induced decline in BAT lipid content suggesting a potential role of circulating carnitines in BAT physiology regardless of age.

Notable findings in the adult cohort only included the relationship of aconitate and creatine with both increased baseline BAT lipid content and less absolute cold-induced change in BAT lipid content. Glutamic acid was the sole metabolite that predicted both baseline BAT and liver measures in the adult cohort, independent of age and sex. In contrast, in the pediatric cohort, aconitate was not related to pre-cold BAT lipid content (β=0.125, *P*=0.551) or absolute BAT activity (β=-0.461, *P*=0.027) after multiple testing correction though the directionality of the relationship was similar to that seen in the adult findings. Creatine was also not related to BAT in the children. Glutamic acid, similarly, was not a significant predictor of pre-cold BAT lipid content (β=0.135, *P*=0.521) or pre-cold hepatic fat (β=0.372, *P*=0.080) in the children though the relationship with hepatic fat neared significance.

On the other hand, in children, both cystine and cysteine trended toward a relationship with BAT and were related to hepatic fat. In adults, neither cysteine nor cystine were related to pre-cold BAT lipid content after multiple testing correction (β=0.284, *P*=0.024 and β=0.300, *P*=0.017, respectively). In adult liver analysis, neither metabolite was significantly associated, but it is interesting to note that they both appear to be trending towards significance (β=0.903, *P*=0.005 and β=0.721, *P*=0.004) when correcting for multiple testing. Cysteine and cystine were both included in component 11 in the adult sensitivity analysis which predicted increased pre-cold BAT lipid content independent of all covariates, but not cold-induced BAT activity or hepatic fat. Taken together, these findings suggest a potential role of cysteine and cystine in both BAT and liver physiology across age groups, though the evidence from this study is relatively weak and inconsistent.

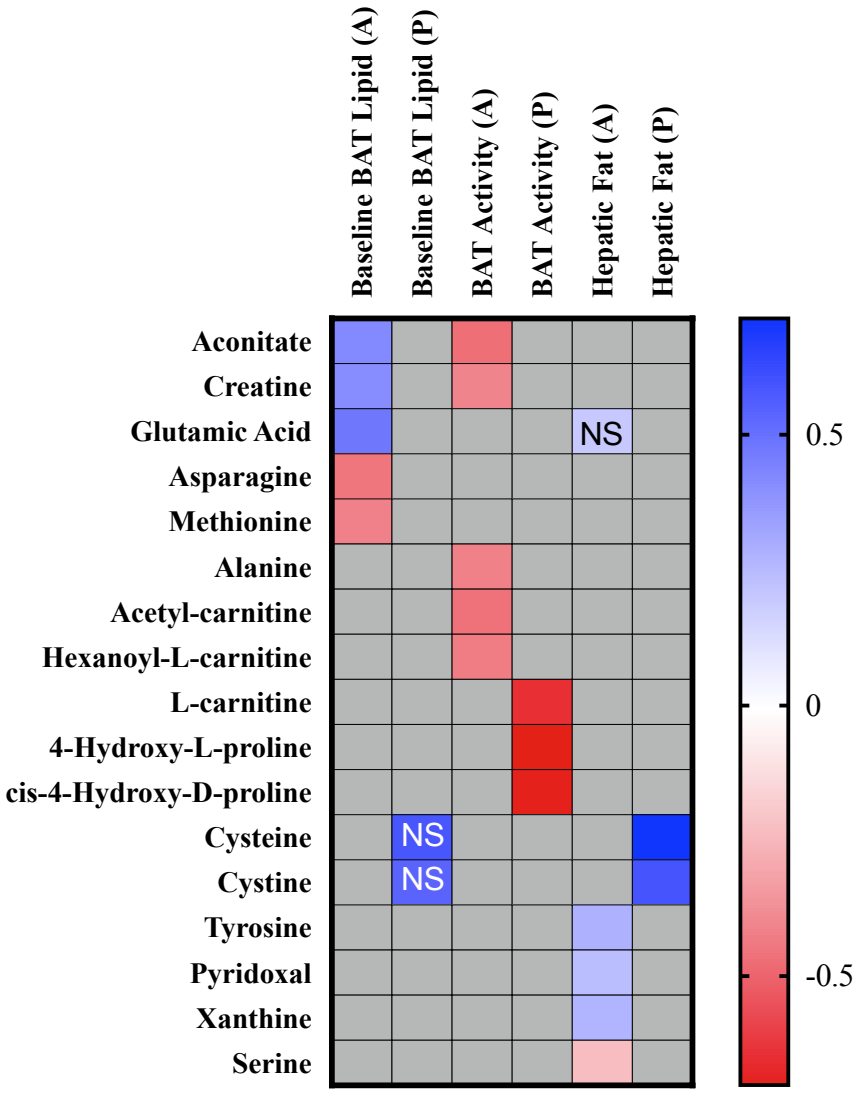

Figure 13. Summary of significant study findings. Values refer to standardized linear or quadratic regression coefficients for the univariate model in all BAT analyses (P < BH adjusted P) and covariate-adjusted model for hepatic fat analyses (P<0.05). Abbreviations: *A* adult, *P* pediatric *NS* non-significant trend.

CHAPTER 4: DISCUSSION

4.1 Associations Between BAT and the Plasma Metabolome in Adults

The first primary objective of this project was to investigate the associations between the plasma metabolome and baseline and cold-stimulated BAT in adults and children. See **Figure 14** for a summary of the metabolites identified in adults or children that may play a role in supporting a "browner" baseline BAT phenotype or increased cold-induced BAT activity. Considering that the results differed between cohorts, however, the findings in the adults will be discussed first.

As previously mentioned, five metabolites (aconitate, asparagine, glutamic acid, methionine and creatine) were related to baseline BAT lipid content in adults. Similarly, five metabolites (aconitate, alanine, acetyl-carnitine, hexanoyl-L-carnitine and creatine) were related to BAT activity measured as the absolute decline in lipid content. Of these metabolites, aconitate and creatine predicted both elevated baseline BAT lipid content and reduced cold-induced BAT activity. We also show that these relationships hold with alternative statistical modeling to emphasize the significance of aconitate and creatine as candidate metabolites to characterize BAT in adults. Although none of these metabolites have been reported in the literature as related to human BAT, I will attempt to interpret the findings in light of what we know about BAT physiology from pre-clinical research.

Aconitate is a critical metabolite in the TCA cycle as an intermediate of the conversion of citrate to isocitrate. We know BAT primarily uptakes and metabolizes lipids for thermogenesis, so β-oxidation and specifically the TCA cycle are crucial pathways for regulation of BAT activity[158]. Increased concentration of numerous TCA cycle intermediates, including cis-aconitic acid (i.e., the unconjugated form of aconitate), were elevated in rat BAT tissue after cold

exposure indicating increased β-oxidation[70]. Other intermediates such as succinate and fumaric acid have also been found to be increased in BAT tissue with cold exposure in pre-clinical models by these authors and others[58,70]. This methodology is different from our study though, as we are analyzing the circulating aconitate abundance rather than that in BAT tissue, and have only measured this in the pre-cold, fasted state. However, our reported positive association between circulating aconitate level and elevated BAT lipid content and decreased BAT activity may suggest decreased aconitate oxidation within BAT as is proposed in the above pre-clinical studies. This causal relationship, however, cannot be explored in a cross-sectional study.

Additionally, creatine plays a critical role in energy (ATP) production and cycling from the mitochondria particularly in skeletal muscle and brain tissues. It has been recently proposed that creatine also regulates brown and beige fat energy expenditure in a UCP-1-independent manner[159]. Murine beige adipocytes, considered more reflective of human brown fat, and human brown adipocytes both showed increased mitochondrial respiration, energy expenditure and thermogenic induction with creatine treatment, which was further validated in a murine *in vivo* model[159]. Although again no causal relationship can be proposed in our study, higher baseline BAT lipid content (i.e., a whiter BAT phenotype) and decreased BAT activity were associated with higher creatine levels in this adult cohort, which may represent decreased creatine-dependent BAT energy expenditure.

Another interesting concept to consider when interpreting these findings is the role that mechanistic target of rapamycin complex 1 (mTORC1) plays in cell growth and nutrient sensing in many different tissues, including BAT. Cold exposure activates mTORC1 in BAT and is necessary for cold-induced BAT expansion and oxidative metabolism of glucose and lipids[160]. In addition to the BAT thermogenic impairment with an mTORC1 defect, Labbé *et al.*[160] reported a reduced abundance of many TCA cycle intermediates in BAT suggesting defective pyruvate

catabolism. It has also been reported that mTORC1 can be activated by multiple amino acids, such as glutamine, asparagine, methionine and alanine[161]. In our findings, reduced ambient BAT lipid content (i.e., a browner BAT phenotype) was associated with increased circulating methionine and asparagine; both proposed activators of mTORC1 for BAT function. On the other hand, Labbé *et al*.[160] also suggested increased glutaminolysis of mTORC1-defective mice considering their reported increase in α-ketoglutarate, glutamine and glutamate in BAT. Our reported higher circulating glutamic acid levels associated with higher baseline BAT lipid content is also in line with these findings. Finally, we report an inverse relationship between two carnitine species and BAT activity. Mitochondrial lipid oxidation relies on acylcarnitine function for FA uptake and catabolism; the production of which was shown to be blunted with an mTORC1 defect[160]. Here, we report higher carnitine associated with lower cold-induced change in BAT triglyceride suggesting potential challenges in uptake of acylcarnitines into BAT for lipid oxidation. Pre-clinical studies have also shown a cold-induced increase in circulating acylcarnitines and subsequent uptake and metabolism by BAT for β-oxidation[10,58].

4.2 Association Between Hepatic Fat and the Plasma Metabolome in Adults

Three metabolites were directly associated with increased hepatic fat; tyrosine, xanthine and pyridoxal, and serine with reduced hepatic fat independent of age, sex and adiposity. Glutamic acid was related to increased hepatic fat independent of age and sex, but this relationship was lost with inclusion of total body fat percentage. All of these metabolites have been established in the literature as playing a causal or consequential role in NAFLD development in humans, consistent with our findings.

Glutamic acid and serine are extensively studied in the NAFLD metabolomic literature as critical metabolites in the maintenance of hepatic redox balance; an especially central process in

NAFLD. Glutamic acid, serine and glycine are all substrates for GSH production, which is the central anti-oxidant compound in the hepatocyte and is upregulated in a state of oxidative stress such as NAFLD[100]. Glycine and serine have been found to be rate-limiting GSH substrates and therefore are often reported as reduced in circulation in NAFLD[100,104,162]. Glutamic acid, although also a GSH substrate, is readily transaminated from GSH by GGT, aspartate by AST and α-ketoglutarate by ALT for release into circulation. Therefore, an increased abundance of glutamic acid in circulation is often noted in NAFLD, both due to redox regulation and TCA cycle alterations from lipid overload[99,100,124]. Our findings for both glutamic acid and serine are thus consistent with the literature, and the significance of glutamic acid is further strengthened by the consistency seen in our sensitivity analysis. Unfortunately, since our dataset uses a relative abundance of each metabolite within the cohort, no conclusions can be drawn on the circulating concentration of these notable metabolites compared to previous work.

Furthermore, pyridoxal is a critical component of the active form of vitamin B6, which is a cofactor for many reactions such as all of the amino acid transaminations noted above[163]. Vitamin B6 is also known to be a necessary cofactor in the transsulfuration pathway regulating homocysteine and cysteine concentration, both clearly implicated in NAFLD in the GSH pathway[164]. Although circulating pyridoxal abundance has not been specifically analyzed in relation to NAFLD presence or hepatic fat content, Sookoian *et al.*[119] noted an interesting relationship between serum pyridoxal 5'-phosphate concentration and liver ALT and AST transcript levels. A significant inverse correlation was found between this cofactor and levels of both enzyme transcripts in liver tissue, which appears to contradict our findings[119]. However, while these authors noted an increase in transcript levels of both enzymes, they also found a corresponding decrease in hepatic protein expression of one isoform each of ALT and AST and therefore concluded that the regulation of such enzymes is overall dysregulated[119]. The

abundance of serum pyridoxal 5'-phosphate was never analyzed in relation to serum ALT or AST, only hepatic transcript levels, which thus makes it difficult to compare our results with this study[119]. The findings in this study and our project do nonetheless expose a potential role that this cofactor may play in NAFLD.

Finally, xanthine is an intermediate metabolite in the uric acid production pathway, which is commonly reported as upregulated as either a cause or consequence of NAFLD[165,166]. Liver-derived xanthine oxidoreductase (XOR) catalyzes this reaction and concomitant rise in ROS, and its activity has also been shown to both be upregulated in response to FA treatment and able to promote triglyceride accumulation in hepatocytes[167,168]. An increase in plasma xanthine associated with elevated hepatic fat as shown in our study thus confirms these notions. Unfortunately, we cannot confirm if this relationship also holds with uric acid or if xanthine individually produces the same detrimental hepatic effects.

Many of these metabolomics studies, however, make use of liver biopsy in those with confirmed NAFLD as the gold standard for hepatic analysis rather than our use of MRI. The consistencies between our findings in this second objective and the NAFLD literature support the validity of analyzing the metabolome in relation to MRI-assessed hepatic steatosis as a non-invasive imaging substitute. Additionally, our ability to detect individual metabolites that predict hepatic fat accumulation on a linear scale is a strength compared to the vast majority of NAFLD studies that rely on discrete groupings between those with and without the disease. We now have reason to believe that the circulating metabolome may be altered with hepatic fat accumulation prior to NAFLD diagnosis, as no participants were being treated for liver disease. It is also a strength of this study that we had a near-equal stratification between participants with and without NAFLD so that the results are not skewed towards one group over the other. In conclusion, while we do report various metabolites that are related to BAT or hepatic fat, we

were unable to find metabolites common to both outcomes. We report that circulating glutamic acid may play a role in both ambient BAT and hepatic fat accumulation, but the evidence is weak as this relationship is lost when considering the influence of adiposity on hepatic fat.

4.3 Association Between BAT and the Plasma Metabolome in Prepubertal Males

The second arm of each primary objective in this project was to replicate the above analyses in our pediatric GETBAT cohort, and then compare and contrast any findings with those in the adults (see **Figure 14** for a summary of adult and pediatric BAT findings). We first examined the metabolome in relation to BAT and found three metabolites that were negatively related to relative BAT activity: two proline isomers and L-carnitine. While no metabolites were related to baseline BAT lipid content, cysteine and cystine were closely trending towards significance and therefore I will discuss them as consistent findings with those in **Section 4.4**.

L-carnitine is a metabolite of hexanoyl-L-carnitine, differing by the lack of acyl group on the common backbone of methionine and lysine[169]. It similarly functions to support mitochondrial function through FA uptake and oxidation[169]. The directionality of the relationship between L-carnitine and BAT activity in the children is in agreement with hexanoyl-L-carnitine and acetyl-carnitine in the adults, and thus consistent with the findings in previous pre-clinical studies. In adults, carnitine levels were associated with absolute rather than relative BAT activity, but both carnitine species were very close to reaching significance in both models. It appears therefore that circulating carnitines are implicated in cold-induced BAT physiology, and that higher circulating levels are associated with lower BAT activity in men, women and boys, in spite of some differences in the cold stimulation protocol which was shorter in children.

The two proline isomers (4-hydroxy-L-proline and cis-4-hydroxy-D-proline) that were inversely related to relative BAT activity in the children are, however, distinct findings from the

adult cohort. Proline is a non-essential proteinogenic amino acid that can be catabolized by proline oxidase (POX), a mitochondrial inner membrane enzyme, into glutamate and α-ketoglutarate[170]. This proline cycle is generally stimulated under conditions of nutrient stress to aid in ATP production and anaplerosis of substrates into the TCA cycle[170]. More specially, POX activation in adipocytes under a state of nutrient stress or hypoxia was shown to induce the expression of adipose triglyceride lipase (ATGL), which promotes mitochondrial oxidative metabolism and prevents adipocyte inflammation and death[171]. A similar role of POX has been seen in the BAT of mice lacking a critical enzyme for nutrient homeostasis after prolonged fasting[172]. Although direct relationships between proline abundance and BAT physiology have not been reported in rodents or humans, it is conceivable to hypothesize that the relationship seen in our study may be due to increased catabolism of proline by BAT for support of the elevated mitochondrial oxidative metabolism for thermogenesis. In light of the relationship with L-carnitine and the above adult BAT analysis, this hypothesis is plausible considering the general trend of our findings relating BAT with mitochondrial metabolism. Additionally, all analyzed plasma samples were collected in the fasted state, which may promote POX activation for proline catabolism within adipocytes. Mechanistic pre-clinical research is required, however, to be able to confirm or deny these notions.

Finally, since this project is largely a hypothesis-generating study, it is interesting to note the trend to a direct relationship between cysteine and cystine and baseline BAT lipid content in light of a similar relationship to hepatic fat accumulation. Importantly, although neither metabolite was a predictor in the adult BAT analysis, cysteine, cystine and orotate made up a component that was significantly positively related to baseline BAT lipid content in our sensitivity analysis in adults. Cysteine is a critical substrate for intracellular GSH production; a potent anti-oxidant molecule known to be upregulated in inflammatory states such as obesity[173].

Since the transamination of GSH into its component amino acids (i.e., cysteine, glutamic acid and glycine) then occurs by GGT at the cell surface, the intracellular redox state is a driving force in regulation of circulating cysteine and its dimerized form, cystine. In a pre-clinical study, Galinier *et al.*[173] found an increased intracellular GSH concentration in WAT from obese mice, as well as enhanced triglyceride deposition, cellular maturation and GSH concentration in pre-adipocytes after anti-oxidant treatment. Taking this one step further, Lettieri Barbato *et al*.[174] studied the role of GSH in both WAT and BAT from mice in basal and cold-stimulated states with consistent findings. BAT, a more pro-oxidant tissue, had lower intracellular GSH than WAT at baseline, but then cold exposure or adrenergic stimulation reduced GSH in WAT to a similar level to BAT as evidence of WAT browning[174]. Finally, GSH depletion promoted weight loss, reduced adipose tissue mass and lipid droplet size, and thermogenic gene induction from WAT depots[174]. These pre-clinical studies support the increased GSH requirement in adipose tissue with a whiter phenotype, which may explain the trend we have reported here with cysteine and cystine. However, there is reason to believe that circulating cysteine may be a determinant of obesity in humans independent of the GSH pathway, as a large cross-sectional study Elshorbagy *et al.*[175] found cysteine was a strong predictor of BMI independent of GGT (i.e., the enzyme required for GSH transamination). This notion is supported by early *in vitro* work that reported the ability of cysteine to independently promote adipose tissue lipogenesis in an oxidative stress-dependent manner[176,177]. Therefore, unanswered questions still exist in terms of cysteine and cystine regulation and their role in human WAT and BAT function and overall metabolic health.

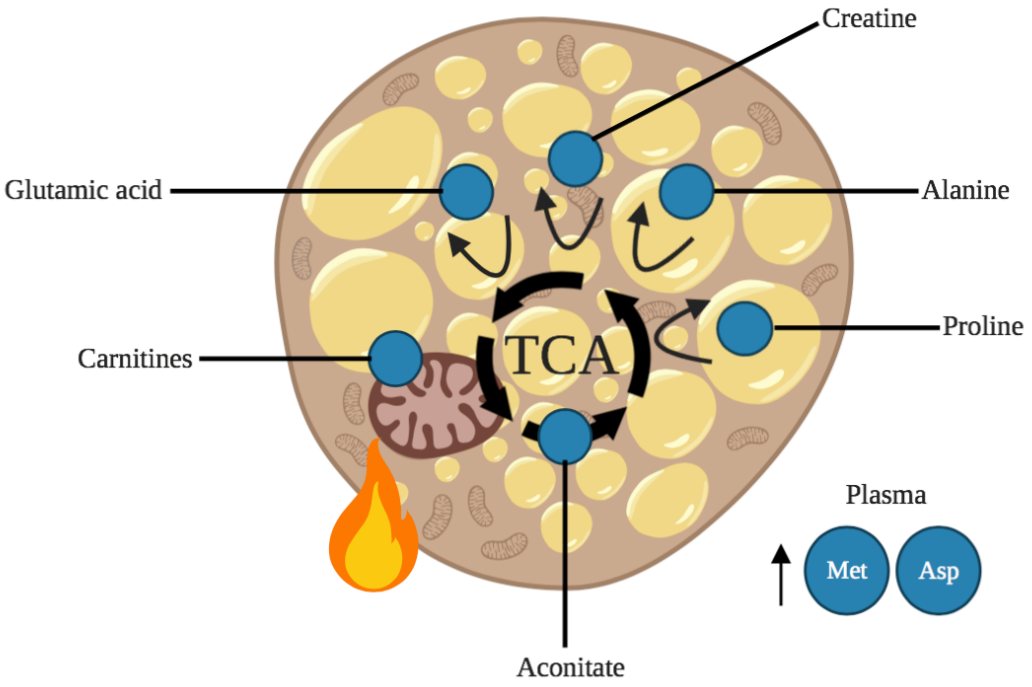

Figure 14. Summary of the metabolites in adults or children associated with ambient or cold-induced BAT. Abbreviations: *TCA* tricarboxylic acid.

4.4 Association Between Hepatic Fat and the Plasma Metabolome in Prepubertal Boys

Finally, analysis of the plasma metabolome in relation to the liver in this cohort of male children identified a positive relationship between both cystine and cysteine and hepatic fat independent of total body adiposity. Cysteine, again, is a sulfur-containing amino acid and is readily dimerized in the extracellular space to produce cystine. Cysteine can be produced from hepatic methionine metabolism, progressing through the intermediary metabolite homocysteine[178]. Cysteine and by extension, cystine, play important roles in hepatic redox balance as substrates for hepatic GSH production particularly in NAFLD[99]. As mentioned previously, GSH can also be transaminated by GGT to release cysteine, glycine and glutamate into circulation[100]. Studies have reported increased homocysteine and cysteine, as well as

decreased GSH in circulation in both children and adults with NAFLD[99,178,179]. Our pediatric findings are therefore in line with the literature, and further support the notion of an increased anti-oxidant requirement with hepatic fat deposition.

Although it is interesting to note that while neither cysteine nor cysteine were related to hepatic fat in adults, both trended towards significance and therefore may warrant further investigation in future studies. This, combined with the significance of glutamic acid and serine in the adults, emphasizes the role of GSH metabolism and redox balance in hepatic fat accumulation in both adults and children. The lack of exact consistency between cohorts may also be a result of the difference in hepatic fat content, where the adults had a significantly higher median baseline hepatic PDFF% than the children ($P<0.05$, Mann-Whitney U-test). This is an expected difference, considering the well-known positive relationship between increasing age and NAFLD development. However, the trend in the adults showing a similar result as the children despite significant differences in cohort characteristics and the small sample size may even further underscore the generalizability of the relationship between cystine, cysteine and hepatic fat. Therefore, although not the exact same metabolites, many of the significant findings from both cohorts have implications in the same biological processes (i.e., glutamic acid, serine, cysteine and cystine) and therefore support the importance of hepatic redox balance in NAFLD across a wide range of ages.

4.5 Linking BAT and the Liver

Cumulatively, we identified three metabolites with a consistent relationship with both baseline BAT and hepatic lipid content; glutamic acid in the adults and cysteine and cystine in the children (trending in the BAT analysis) (**Figure 15**). All three metabolites followed a similar pattern, where an increased abundance was associated with an elevated ambient BAT and liver

fat deposition. This pattern between BAT and hepatic fat is to be expected considering the previously published correlation between these tissues in humans[8,9]. Although cysteine and cystine were not individually related to BAT in adults, they were related to elevated baseline BAT lipid content when analyzed in combination with orotate by PCA. Unfortunately, we cannot know if these metabolites casually link BAT and hepatic fat deposition due to the cross-sectional nature of this study. Alterations to levels of circulating glutamic acid, cysteine or cystine may be simply a result of wide-spread metabolic disturbances such as insulin resistance that promotes lipid deposition. This is particularly relevant for glutamic acid, which was not significantly related to hepatic fat after correction for adiposity. However, the relationship held true with inclusion of all covariates for glutamic acid in the adult BAT analysis and cysteine and cystine in the pediatric hepatic fat analysis, which strengthens our findings.

To the best of our knowledge, this is the first study that analyzed the human metabolome from both a BAT and hepatic fat perspective and identified linking metabolites. In rodents, however, a limited number of studies have reported on compounds that may characterize this relationship, including Nrg4, serotonin, acylcarnitines and BCAAs (see **Introduction Section 1.11**)[10,11,45,128]. In the acylcarnitine case, it was shown that these metabolites were being produced by the liver with cold stimulation and subsequently taken up and metabolized by BAT as a thermogenic fuel[10]. Similarly, BCAAs were found to be BAT-specific thermogenic substrates, and a loss-of-function mutation in BCAA oxidation caused liver derangements[11]. Both of these mechanisms rely on substrate oxidation by BAT mitochondria, and specifically have been shown to require mTORC1 activation[11,160]. Considering this requirement for mitochondrial oxidation for BAT function, and the known alterations in mitochondrial oxidative and anaplerotic fluxes that promote hepatic lipid deposition, it is plausible to think that the link between these tissues lies in the mitochondria[180]. Finally, as highlighted above, glutamic acid,

cysteine and cystine are all involved in maintaining cellular redox balance through the GSH pathway in adipose and hepatic tissues, which is another possible explanatory mechanism[99,171].

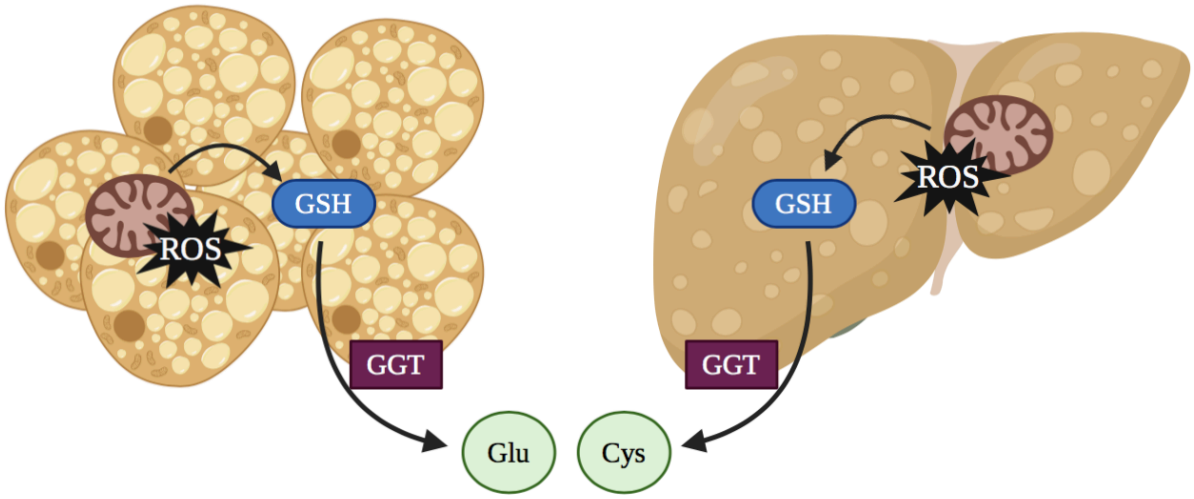

Figure 15. Summary of the common BAT and liver findings in this project and potential mechanistic link. Abbreviations: *ROS* reactive oxygen species, *GSH* glutathione, *GGT* gamma-glutamyltransferase.

4.6 Limitations

There are a number of limitations to comment on in this project. First of all, the cross-sectional nature of this study limits our ability to propose any causal relationships between the metabolome and our primary outcomes beyond speculation. Any proposed mechanisms would have to be studied in pre-clinical models and, eventually, intervention trials. The purpose of this study is thus for hypothesis creation rather than mechanistic testing. Also, all plasma was collected on a different day from the MRI measurements, in the fasted state and without cold stimulation. Therefore, any findings in relation to cold stimulated BAT activity are simply associations, rather than providing evidence how these metabolites might change as BAT is activated.

All metabolomic data used in this project was analyzed by the laboratory of Dr. E. Chouchani using their LC-MS platform, which relied upon previously validated methodology[58]. Though our study is strengthened by the work this team has undertaken to optimize and verify the reference standards, we were limited in the metabolites we could consider, and the focus was primarily on metabolites of mitochondrial metabolism. While this use of internal validated standards to identify the targeted metabolites produces a high-quality dataset, other metabolites shown previously to be associated with BAT or NAFLD like bile acids or oxylipins could not be assessed in this project. Also, as mentioned previously, we cannot compare the absolute concentration of any metabolites in our dataset to those of previous studies, as all metabolites are represented as a relative abundance to the reference metabolite peaks as quantified by the TraceFinder software.

Additionally, although MRI has been validated against liver biopsy as a reliable and reproducible method of hepatic steatosis assessment, this methodology does not tell us anything about other stages along the NAFLD spectrum (i.e., NASH, fibrosis or cirrhosis). Therefore, we cannot draw any conclusions about the plasma metabolome in relation to increasing severity of NAFLD in this cohort.

Methodological differences between the adults and children are also limitations in the comparison of findings across cohorts. The duration of the cold exposure differed between cohorts, with adults undergoing 180 minutes of cold versus only 60 minutes in the children, which may affect the magnitude of change in BAT lipid content with cold stimulation. The effect of this difference may be marginal though, as previous work from our laboratory provides evidence that BAT was maximally activated in 12 healthy adults after only 35 minutes of cold exposure[35]. Also related to BAT imaging limitations, the image analysis program was limited in that the post-cold images could not be automatically aligned to the pre-cold images and thus

slight differences in the SCV region segmentation may exist. This is especially a limitation in the pediatric image analysis, where we noticed many participants were in different positions from pre- to post-cold scanning so that the pediatric segmentation protocol was adjusted to account for this (see **Methodology Section 2.3.1**). This would impact both the absolute and relative change in SCV PDFF%, though not the pre-cold measurement. Finally, there was a sizable difference in the cohort sizes (63 adults versus 25 children) which results in differing statistical power between cohorts and therefore may play a role in the metabolite findings. However, studies in the metabolomics field in relation to both BAT and NAFLD have been published with sample sizes equal or smaller than our pediatric cohort[68,120]. This small pediatric sample size also limited our ability to perform PCA as the sensitivity analysis as well, as it is generally accepted that the sample size should be larger than the number of variables for PCA[181]. The cohorts also differed considerably in the prevalence of NAFLD although this was partially accounted for by using regression models with continuous outcome variables.

4.7 Future Directions

With the limited understanding of the physiological significance of baseline and activated BAT in humans, it is important to continue analyzing this tissue from a variety of different avenues, such as metabolomics. The identified significant metabolites from this project can be used as starting points in further studies to better understand how BAT influences human metabolism. To strengthen our findings, these results must be replicated and validated in larger and more diverse cohorts of adults and children. This would be necessary to be able to assess the ability of any of these identified metabolites to act as sensitive and specific BAT biomarkers. We also focused our pediatric cohort on prepubertal boys to limit the effects of pubertal status on BAT physiology, so a logical next step would be to conduct a similar study in prepubertal females and note any similarities or differences. Ideally, plasma should be collected before and

after the cold exposure to better assess the relationship between cold-stimulated BAT activity and cold-induced changes in the circulating metabolome.

It is also crucial to investigate the proposed mechanisms in pre-clinical models to be able to draw causal relationships between the metabolome and our primary outcomes. For example, it would be interesting to measure BAT thermogenesis or oxygen consumption before and after treatment with one of the related metabolites such as 4-hydroxy-L-proline. The BAT-related metabolites could also be analyzed in a rodent model with a specific BAT knockout model or labelled with an appropriate tracer to determine if they are being taken up or metabolized by BAT with cold or adrenergic stimulation. To assess the proposed link between BAT and NAFLD from this project, such as glutamic acid in the adults and cysteine and cystine in the children, a mouse model of NAFLD could be developed using the methionine and choline deficient diet and samples could be collected before and after cold exposure. This would allow researchers to investigate such metabolites in relation to baseline BAT lipid content and cold stimulated BAT activity in a NAFLD model without the influence of other metabolic syndrome characteristics like obesity or insulin resistance[182].

Finally, although not a specific objective of this project, we have quantified cold-stimulated BAT activity in two different ways and noticed slight discrepancies in the results between them. For example, in the adult cohort, five metabolites were significantly related to absolute BAT PDFF% reduction, but none were related when considering relative BAT PDFF% reduction from baseline after multiple testing correction. It is important to validate both measurements against the gold standard of BAT activity imaging, ^{18}F-FDG PET-CT, or in histological samples from pre-clinical models. This would ideally help us better understand which variable is more representative of BAT physiology in terms of energy expenditure or substrate utilization.

4.8 Conclusion

In this current study, we set out to analyze the relationship between baseline and cold-stimulated BAT as well as hepatic fat and the circulating metabolome in adults and children. We initially identified a lack of research available in the BAT field from a metabolomic perspective in humans as a method to better understand how this tissue influences human metabolic health. Research was particularly absent on this topic in children. Although a plethora of studies have been conducted relating NAFLD to the circulating metabolome, we do not currently understand how hepatic fat is related to ambient and cold-induced BAT despite observing inverse correlations between these. In adults, we observed multiple metabolites predicting baseline BAT lipid content and cold-induced BAT activity, with aconitate and creatine showing consistency between these outcomes. Similarly, glutamic acid predicted both baseline BAT and hepatic lipid content in adults. These notable findings represent novel metabolites in the BAT literature, particularly in the common relationship with hepatic fat.

In children, three metabolites characterized the relationship with BAT activity, with L-carnitine being consistent with findings in the adult cohort. Cysteine and cystine comparably predicted baseline BAT (trending) and hepatic lipid content in the children, again representing novel findings to begin to understand the link between BAT and liver physiology. Further investigation of these metabolites of interest in pre-clinical studies will be important in order to test biochemical mechanisms and establish whether this is a direct or causal relationship. It will also be important to determine whether findings can be replicated in larger more diverse human populations. In conclusion this study has identified multiple metabolites that may be important for BAT and NAFLD in both children and adults and serves as a starting point for future research.

REFERENCES

1. Standing Senate Committee on Social Affairs S and T. *Obesity A Whole-of-Society Approach for a Healthier Canada*. Ottawa; 2016. www.senate-senat.ca/social.asp. Accessed January 4, 2019.
2. Friedman SL, Neuschwander-Tetri BA, Rinella M, Sanyal AJ. Mechanisms of NAFLD development and therapeutic strategies. *Nat Med*. 2018;24(7):908-922. doi:10.1038/s41591-018-0104-9
3. Bellentani S, Scaglioni F, Marino M, Bedogni G. Epidemiology of Non-Alcoholic Fatty Liver Disease. *Dig Dis*. 2010;28(1):155-161. doi:10.1159/000282080
4. Singh S, Allen AM, Wang Z, Prokop LJ, Murad MH, Loomba R. Fibrosis Progression in Nonalcoholic Fatty Liver vs Nonalcoholic Steatohepatitis: A Systematic Review and Meta-analysis of Paired-Biopsy Studies. *Clin Gastroenterol Hepatol*. 2015;13(4):643-654.e9. doi:10.1016/j.cgh.2014.04.014
5. Lee P, Greenfield JR, Ho KKY, Fulham MJ. A critical appraisal of the prevalence and metabolic significance of brown adipose tissue in adult humans. *Am J Physiol Metab*. 2010;299(4):E601-E606. doi:10.1152/ajpendo.00298.2010
6. Cypess AM, Lehman S, Williams G, et al. Identification and importance of brown adipose tissue in adult humans. *Obstet Gynecol Surv*. 2009;64(8):519-520. doi:10.3201/eid1910.130203
7. van Marken Lichtenbelt WD, Vanhommerig JW, Smulders NM, et al. Cold-Activated Brown Adipose Tissue in Healthy Men. *N Engl J Med*. 2009;360(15):1500-1508. doi:10.1056/NEJMoa0808718
8. Yilmaz Y, Ones T, Purnak T, et al. Association between the presence of brown adipose tissue and non-alcoholic fatty liver disease in adult humans. *Aliment Pharmacol Ther*.

2011;34(3):318-323. doi:10.1111/j.1365-2036.2011.04723.x

9. Ozguven S, Ones T, Yilmaz Y, Turoglu HT, Imeryuz N. The role of active brown adipose tissue in human metabolism. *Eur J Nucl Med Mol Imaging*. 2016;43(2):355-361. doi:10.1007/s00259-015-3166-7

10. Simcox J, Geoghegan G, Maschek JA, et al. Global Analysis of Plasma Lipids Identifies Liver-Derived Acylcarnitines as a Fuel Source for Brown Fat Thermogenesis. *Cell Metab*. 2017;26(3):509-522.e6. doi:10.1016/J.CMET.2017.08.006

11. Yoneshiro T, Wang Q, Tajima K, et al. BCAA catabolism in brown fat controls energy homeostasis through SLC25A44. *Nature*. 2019;572(7771):614-619. doi:10.1038/s41586-019-1503-x

12. Christensen CR, Clark PB, Morton KA. Reversal of Hypermetabolic Brown Adipose Tissuein F-18 FDG PET Imaging. *Clin Nucl Med*. 2006;31(4):193-196. doi:10.1097/01.rlu.0000204199.33136.05

13. Harms M, Seale P. Brown and beige fat: development, function and therapeutic potential. *Nat Med*. 2013;19(10):1252-1263. doi:10.1038/nm.3361

14. Nedergaard J, Bengtsson T, Cannon B. Unexpected evidence for active brown adipose tissue in adult humans. *Am J Physiol Metab*. 2007;293(2):E444-E452. doi:10.1152/ajpendo.00691.2006

15. Yoneshiro T, Aita S, Matsushita M, et al. Age-Related Decrease in Cold-Activated Brown Adipose Tissue and Accumulation of Body Fat in Healthy Humans. *Obesity*. 2011;19(9):1755-1760. doi:10.1038/oby.2011.125

16. Labbé SM, Caron A, Bakan I, et al. In vivo measurement of energy substrate contribution to cold-induced brown adipose tissue thermogenesis. *FASEB J*. 2015;29(5):2046-2058. doi:10.1096/fj.14-266247

17. Blondin DP, Frisch F, Phoenix S, et al. Inhibition of Intracellular Triglyceride Lipolysis Suppresses Cold-Induced Brown Adipose Tissue Metabolism and Increases Shivering in Humans. *Cell Metab*. 2017;25(2):438-447. doi:10.1016/j.cmet.2016.12.005

18. Ong FJ, Ahmed BA, Oreskovich SM, et al. Recent advances in the detection of brown adipose tissue in adult humans: a review. *Clin Sci (Lond)*. 2018;132(10):1039-1054. doi:10.1042/CS20170276

19. Izzi-Engbeaya C, Salem V, Atkar RS, Dhillo WS. Insights into Brown Adipose Tissue Physiology as Revealed by Imaging Studies. *Adipocyte*. 2015;4(1):1-12. doi:10.4161/21623945.2014.965609

20. Menschik Z. Histochemical comparison of brown and white adipose tissue in guinea pigs. *Anat Rec*. 1953;116(4):439-455. doi:10.1002/ar.1091160405

21. Reddy NL, Jones TA, Wayte SC, et al. Identification of Brown Adipose Tissue Using MR Imaging in a Human Adult With Histological and Immunohistochemical Confirmation. *J Clin Endocrinol Metab*. 2014;99(1):E117-E121. doi:10.1210/jc.2013-2036

22. Holstila M, Pesola M, Saari T, et al. MR signal-fat-fraction analysis and T2* weighted imaging measure BAT reliably on humans without cold exposure. *Metabolism*. 2017;70:23-30. doi:10.1016/j.metabol.2017.02.001

23. Gifford A, Towse TF, Walker RC, Avison MJ, Welch EB. Characterizing active and inactive brown adipose tissue in adult humans using PET-CT and MR imaging. *Am J Physiol Metab*. 2016;311(1):E95-E104. doi:10.1152/ajpendo.00482.2015

24. Hu HH, Yin L, Aggabao PC, Perkins TG, Chia JM, Gilsanz V. Comparison of brown and white adipose tissues in infants and children with chemical-shift-encoded water-fat MRI. *J Magn Reson Imaging*. 2013;38(4):885-896. doi:10.1002/jmri.24053

25. Hu HH, Yin L, Aggabao PC, Perkins TG, Chia JM, Gilsanz V. Comparison of Brown and

White Adipose Tissues in Infants and Children With Chemical-Shift-Encoded Water-Fat MRI. doi:10.1002/jmri.24053

26. Franssens BT, Eikendal AL, Leiner T, van der Graaf Y, Visseren FLJ, Hoogduin JM. Reliability and agreement of adipose tissue fat fraction measurements with water-fat MRI in patients with manifest cardiovascular disease. *NMR Biomed*. 2016;29(1):48-56. doi:10.1002/nbm.3444
27. Franz D, Karampinos DC, Rummeny EJ, et al. Discrimination Between Brown and White Adipose Tissue Using a 2-Point Dixon Water-Fat Separation Method in Simultaneous PET/MRI. *J Nucl Med*. 2015;56(11):1742-1747. doi:10.2967/jnumed.115.160770
28. Wu J, Boström P, Sparks LM, et al. Beige adipocytes are a distinct type of thermogenic fat cell in mouse and human. *Cell*. 2012;150(2):366-376. doi:10.1016/j.cell.2012.05.016
29. Ouellet V, Labbé SM, Blondin DP, et al. Brown adipose tissue oxidative metabolism contributes to energy expenditure during acute cold exposure in humans. *J Clin Invest*. 2012;122(2):545-552. doi:10.1172/JCI60433
30. Baba S, Jacene HA, Engles JM, Honda H, Wahl RL. CT Hounsfield units of brown adipose tissue increase with activation: preclinical and clinical studies. *J Nucl Med*. 2010;51(2):246-250. doi:10.2967/jnumed.109.068775
31. Lundström E, Strand R, Johansson L, Bergsten P, Ahlström H, Kullberg J. Magnetic resonance imaging cooling-reheating protocol indicates decreased fat fraction via lipid consumption in suspected brown adipose tissue. *PLoS One*. 2015;10(4):e0126705. doi:10.1371/journal.pone.0126705
32. van Rooijen BD, van der Lans AAJJ, Brans B, et al. Imaging Cold-Activated Brown Adipose Tissue Using Dynamic T2*-Weighted Magnetic Resonance Imaging and 2-Deoxy-2-[18F]fluoro-D-glucose Positron Emission Tomography. *Invest Radiol*.

2013;48(10):708-714. doi:10.1097/RLI.0b013e31829363b8

33. Orava J, Nuutila P, Noponen T, et al. Blunted metabolic responses to cold and insulin stimulation in brown adipose tissue of obese humans. *Obesity*. 2013;21(11):2279-2287. doi:10.1002/oby.20456

34. Chen Y-CI, Cypess AM, Chen Y-C, et al. Measurement of human brown adipose tissue volume and activity using anatomic MR imaging and functional MR imaging. *J Nucl Med*. 2013;54(9):1584-1587. doi:10.2967/jnumed.112.117275

35. Oreskovich SM, Ong FJ, Ahmed BA, et al. MRI Reveals Human Brown Adipose Tissue Is Rapidly Activated in Response to Cold. *J Endocr Soc*. 2019;3(12):2374-2384. doi:10.1210/js.2019-00309

36. Law J, Morris DE, Izzi-Engbeaya C, et al. Thermal Imaging Is a Noninvasive Alternative to PET/CT for Measurement of Brown Adipose Tissue Activity in Humans. *J Nucl Med*. 2018;59(3):516-522. doi:10.2967/jnumed.117.190546

37. Koskensalo K, Raiko J, Saari T, et al. Human Brown Adipose Tissue Temperature and Fat Fraction Are Related to Its Metabolic Activity. *J Clin Endocrinol Metab*. 2017;102(4):1200-1207. doi:10.1210/jc.2016-3086

38. Pfannenberg C, Werner MK, Ripkens S, et al. Impact of age on the relationships of brown adipose tissue with sex and adiposity in humans. *Diabetes*. 2010;59(7):1789-1793. doi:10.2337/db10-0004

39. Saito M, Okamatsu-Ogura Y, Matsushita M, et al. High Incidence of Metabolically Active Brown Adipose Tissue in Healthy Adult Humans. *Diabetes*. 2009;58(7):1526-1531. doi:10.2337/DB09-0530

40. Chondronikola M, Volpi E, Børsheim E, et al. Brown adipose tissue improves whole-body glucose homeostasis and insulin sensitivity in humans. *Diabetes*. 2014;63(12):4089-4099.

doi:10.2337/db14-0746

41. Lowell BB, S-Susulic V, Hamann A, et al. Development of obesity in transgenic mice after genetic ablation of brown adipose tissue. *Nature*. 1993;366(6457):740-742. doi:10.1038/366740a0

42. Franz D, Weidlich D, Freitag F, et al. Association of proton density fat fraction in adipose tissue with imaging-based and anthropometric obesity markers in adults. *Int J Obes*. 2018;42(2):175-182. doi:10.1038/ijo.2017.194

43. Liu X, Wang S, You Y, et al. Brown Adipose Tissue Transplantation Reverses Obesity in Ob/Ob Mice. *Endocrinology*. 2015;156(7):2461-2469. doi:10.1210/en.2014-1598

44. Poekes L, Gillard J, Farrell GC, Horsmans Y, Leclercq IA. Activation of brown adipose tissue enhances the efficacy of caloric restriction for treatment of nonalcoholic steatohepatitis. *Lab Investig*. 2019;99(1):4-16. doi:10.1038/s41374-018-0120-x

45. Wang GX, Zhao XY, Meng ZX, et al. The brown fat-enriched secreted factor Nrg4 preserves metabolic homeostasis through attenuation of hepatic lipogenesis. *Nat Med*. 2014;20(12):1436-1443. doi:10.1038/nm.3713

46. Azad RK, Shulaev V. Metabolomics technology and bioinformatics for precision medicine. doi:10.1093/bib/bbx170

47. Johnson CH, Ivanisevic J, Siuzdak G. Metabolomics: beyond biomarkers and towards mechanisms. *Nat Rev Mol Cell Biol*. 2016;17(7):451-459. doi:10.1038/nrm.2016.25

48. Rauschert S, Uhl O, Koletzko B, Hellmuth C. Metabolomic Biomarkers for Obesity in Humans : A Short Review. 2014:314-324. doi:10.1159/000365040

49. Alonso A, Marsal S, JuliÃ A. Analytical Methods in Untargeted Metabolomics: State of the Art in 2015. *Front Bioeng Biotechnol*. 2015;3:23. doi:10.3389/fbioe.2015.00023

50. Bothwell JHF, Griffin JL. An introduction to biological nuclear magnetic resonance

spectroscopy. *Biol Rev*. 2011;86(2):493-510. doi:10.1111/j.1469-185X.2010.00157.x

51. Raftery ZPD. Comparing and combining NMR spectroscopy and mass spectrometry in metabolomics. *Anal Bioanal Chem*. 2007;387:525-527. doi:10.1007/s00216-006-0687-8

52. Smolinska A, Blanchet L, Buydens LMC, Wijmenga SS. NMR and pattern recognition methods in metabolomics: From data acquisition to biomarker discovery: A review. *Anal Chim Acta*. 2012;750:82-97. doi:10.1016/j.aca.2012.05.049

53. El-Aneed A, Cohen A, Banoub J. Mass Spectrometry, Review of the Basics: Electrospray, MALDI, and Commonly Used Mass Analyzers. *Appl Spectrosc Rev*. 2009;44(3):210-230. doi:10.1080/05704920902717872

54. Ho CS, Lam CWK, Chan MHM, et al. Electrospray ionisation mass spectrometry: principles and clinical applications. *Clin Biochem Rev*. 2003;24(1):3-12. http://www.ncbi.nlm.nih.gov/pubmed/18568044. Accessed June 27, 2019.

55. Hu Q, Noll RJ, Li H, Makarov A, Hardman M, Graham Cooks R. The Orbitrap: a new mass spectrometer. *J Mass Spectrom*. 2005;40(4):430-443. doi:10.1002/jms.856

56. Karasek FW, Clement RE. *Basic Gas Chromatography-Mass Spectrometry : Principles and Techniques*. Elsevier; 1988. https://books.google.ca/books?hl=en&lr=&id=_WVDqDII63cC&oi=fnd&pg=PP1&dq=basic+gas+chromatography&ots=7izIelP_lX&sig=-RUtIjnNLNXKZJcrnsg3w-0ei-U#v=onepage&q=basic gas chromatography&f=false. Accessed June 20, 2019.

57. Zhang A, Sun H, Wang P, Han Y, Wang X. Modern analytical techniques in metabolomics analysis. *Analyst*. 2012;137(2):293-300. doi:10.1039/c1an15605e

58. Mills EL, Pierce KA, Jedrychowski MP, et al. Accumulation of succinate controls activation of adipose tissue thermogenesis. *Nature*. 2018;560(7716):102-106. doi:10.1038/s41586-018-0353-2

59. Zhou J, Yin Y. Strategies for large-scale targeted metabolomics quantification by liquid chromatography-mass spectrometry. *Analyst*. 2016;141(23):6362-6373. doi:10.1039/c6an01753c

60. Go EP. Database resources in metabolomics: An overview. *J Neuroimmune Pharmacol*. 2010;5(1):18-30. doi:10.1007/s11481-009-9157-3

61. Xia J, Sinelnikov I V, Han B, Wishart DS. MetaboAnalyst 3.0-making metabolomics more meaningful. *Nucleic Acids Res*. 2015;43:251-257. doi:10.1093/nar/gkv380

62. Cannon B, Nedergaard J. Brown Adipose Tissue: Function and Physiological Significance. *Physiol Rev*. 2004;84(1):277-359. doi:10.1152/physrev.00015.2003

63. Boon MR, Bakker LEH, Prehn C, et al. LysoPC-acyl C16:0 is associated with brown adipose tissue activity in men. *Metabolomics*. 2017;13(5):48. doi:10.1007/s11306-017-1185-z

64. Magill P, Rao SN, Miller NE, et al. Relationships between the metabolism of high-density and very-low-density lipoproteins in man: studies of apolipoprotein kinetics and adipose tissue lipoprotein lipase activity. *Eur J Clin Invest*. 1982;12(2):113-120. http://www.ncbi.nlm.nih.gov/pubmed/6807682. Accessed June 20, 2019.

65. Bartelt A, John C, Schaltenberg N, et al. Thermogenic adipocytes promote HDL turnover and reverse cholesterol transport. *Nat Commun*. 2017;8:15010. doi:10.1038/ncomms15010

66. Matsushita M, Yoneshiro T, Aita S, Kameya T, Sugie H, Saito M. Impact of brown adipose tissue on body fatness and glucose metabolism in healthy humans. *Int J Obes*. 2014;38(6):812-817. doi:10.1038/ijo.2013.206

67. Lynes MD, Leiria LO, Lundh M, et al. The cold-induced lipokine 12,13-diHOME promotes fatty acid transport into brown adipose tissue. *Nat Med*. 2017;23(5):631-637.

doi:10.1038/nm.4297

68. Dieckmann S, Maurer S, Fromme T, Colson C, Richard D. Fatty Acid Metabolite Profiling Reveals Oxylipins as Markers of Brown but Not Brite Adipose Tissue. 2020;11(February). doi:10.3389/fendo.2020.00073

69. Iwen KA, Backhaus J, Cassens M, et al. Cold-Induced Brown Adipose Tissue Activity Alters Plasma Fatty Acids and Improves Glucose Metabolism in Men. *J Clin Endocrinol Metab*. 2017;102(11):4226-4234. doi:10.1210/jc.2017-01250

70. Hiroshima Y, Yamamoto T, Watanabe M, Baba Y, Shinohara Y. Effects of cold exposure on metabolites in brown adipose tissue of rats. *Mol Genet Metab reports*. 2018;15:36-42. doi:10.1016/j.ymgmr.2018.01.005

71. Lu X, Solmonson A, Lodi A, et al. The early metabolomic response of adipose tissue during acute cold exposure in mice. *Sci Rep*. 2017;7(1):3455. doi:10.1038/s41598-017-03108-x

72. Mota M, Banini BA, Cazanave SC, Sanyal AJ. Molecular mechanisms of lipotoxicity and glucotoxicity in nonalcoholic fatty liver disease. *Metabolism*. 2016;65(8):1049-1061. doi:10.1016/j.metabol.2016.02.014

73. Mendez-Sanchez N, Cruz-Ramon VC, Ramirez-Perez OL, Hwang JP, Barranco-Fragoso B, Cordova-Gallardo J. New Aspects of Lipotoxicity in Nonalcoholic Steatohepatitis. *Int J Mol Sci*. 2018;19(7). doi:10.3390/ijms19072034

74. Neuschwander-Tetri BA. Hepatic lipotoxicity and the pathogenesis of nonalcoholic steatohepatitis: The central role of nontriglyceride fatty acid metabolites. *Hepatology*. 2010;52(2):774-788. doi:10.1002/hep.23719

75. Utzschneider KM, Kahn SE. The Role of Insulin Resistance in Nonalcoholic Fatty Liver Disease. *J Clin Endocrinol Metab*. 2006;91(12):4753-4761. doi:10.1210/jc.2006-0587

76. Kumashiro N, Erion DM, Zhang D, et al. Cellular mechanism of insulin resistance in nonalcoholic fatty liver disease. *Proc Natl Acad Sci U S A*. 2011;108(39):16381-16385. doi:10.1073/pnas.1113359108

77. Duseja A, Chalasani N. Epidemiology and risk factors of nonalcoholic fatty liver disease (NAFLD). *Hepatol Int*. 2013;7(2013):S755-S764. doi:10.1007/s12072-013-9480-x

78. Younossi ZM, Koenig AB, Abdelatif D, Fazel Y, Henry L, Wymer M. Global epidemiology of nonalcoholic fatty liver disease-Meta-analytic assessment of prevalence, incidence, and outcomes. *Hepatology*. 2016;64(1):73-84. doi:10.1002/hep.28431

79. Targher G, Byrne CD, Lonardo A, Zoppini G, Barbui C. Non-alcoholic fatty liver disease and risk of incident cardiovascular disease: A meta-analysis. *J Hepatol*. 2016;65(3):589-600. doi:10.1016/j.jhep.2016.05.013

80. Rich NE, Oji S, Mufti AR, et al. Racial and Ethnic Disparities in Nonalcoholic Fatty Liver Disease Prevalence, Severity, and Outcomes in the United States: A Systematic Review and Meta-analysis. *Clin Gastroenterol Hepatol*. 2018;16(2):198-210.e2. doi:10.1016/j.cgh.2017.09.041

81. Bruschi FV, Tardelli M, Claudel T, Trauner M. PNPLA3 expression and its impact on the liver: current perspectives. *Hepat Med*. 2017;9:55. doi:10.2147/HMER.S125718

82. Ong JP, Younossi ZM. Epidemiology and Natural History of NAFLD and NASH. *Clin Liver Dis*. 2007;11(1):1-16. doi:10.1016/j.cld.2007.02.009

83. Ballestri S, Nascimbeni F, Baldelli E, Marrazzo A, Romagnoli D, Lonardo A. NAFLD as a Sexual Dimorphic Disease: Role of Gender and Reproductive Status in the Development and Progression of Nonalcoholic Fatty Liver Disease and Inherent Cardiovascular Risk. *Adv Ther*. 2017;34(6):1291-1326. doi:10.1007/s12325-017-0556-1

84. PARK SH, JEON WK, KIM SH, et al. Prevalence and risk factors of non-alcoholic fatty

liver disease among Korean adults. *J Gastroenterol Hepatol*. 2006;21(1):138-143. doi:10.1111/j.1440-1746.2005.04086.x

85. Loomba R, Sanyal AJ. The global NAFLD epidemic. *Nat Rev Gastroenterol Hepatol*. 2013;10(11):686-690. doi:10.1038/nrgastro.2013.171

86. Rockey DC, Caldwell SH, Goodman ZD, Nelson RC, Smith AD. Liver biopsy. *Hepatology*. 2009;49(3):1017-1044. doi:10.1002/hep.22742

87. Loomba R. Role of imaging-based biomarkers in NAFLD: Recent advances in clinical application and future research directions. *J Hepatol*. 2018;68(2):296-304. doi:10.1016/j.jhep.2017.11.028

88. Reeder SB, Cruite I, Hamilton G, Sirlin CB. Quantitative assessment of liver fat with magnetic resonance imaging and spectroscopy. *J Magn Reson Imaging*. 2011;34(4):spcone-spcone. doi:10.1002/jmri.22775

89. Imajo K, Kessoku T, Honda Y, et al. Magnetic Resonance Imaging More Accurately Classifies Steatosis and Fibrosis in Patients With Nonalcoholic Fatty Liver Disease Than Transient Elastography. *Gastroenterology*. 2016;150(3):626-637.e7. doi:10.1053/j.gastro.2015.11.048

90. Permutt Z, Le T-A, Peterson MR, et al. Correlation between liver histology and novel magnetic resonance imaging in adult patients with non-alcoholic fatty liver disease - MRI accurately quantifies hepatic steatosis in NAFLD. *Aliment Pharmacol Ther*. 2012;36(1):22-29. doi:10.1111/j.1365-2036.2012.05121.x

91. Batheja M, Vargas H, Silva AM, et al. Magnetic resonance elastography (MRE) in assessing hepatic fibrosis: performance in a cohort of patients with histological data. *Abdom Imaging*. 2015;40(4):760-765. doi:10.1007/s00261-014-0321-8

92. Clark JM, Brancati FL, Diehl AM. The prevalence and etiology of elevated

aminotransferase levels in the United States. *Am J Gastroenterol*. 2003;98(5):960-967. doi:10.1111/j.1572-0241.2003.07486.x

93. Fracanzani AL, Valenti L, Bugianesi E, et al. Risk of severe liver disease in nonalcoholic fatty liver disease with normal aminotransferase levels: A role for insulin resistance and diabetes. *Hepatology*. 2008;48(3):792-798. doi:10.1002/hep.22429

94. Verma S, Jensen D, Hart J, Mohanty SR. Predictive value of ALT levels for non-alcoholic steatohepatitis (NASH) and advanced fibrosis in non-alcoholic fatty liver disease (NAFLD). *Liver Int*. 2013;33(9):1398-1405. doi:10.1111/liv.12226

95. Angulo P, Hui JM, Marchesini G, et al. The NAFLD fibrosis score: A noninvasive system that identifies liver fibrosis in patients with NAFLD. *Hepatology*. 2007;45(4):846-854. doi:10.1002/hep.21496

96. Pirola CJ, Sookoian S. Multiomics biomarkers for the prediction of nonalcoholic fatty liver disease severity. *World J Gastroenterol*. 2018;24(15):1601-1615. doi:10.3748/wjg.v24.i15.1601

97. Sahebkar A, Sancho E, Abelló D, Camps J, Joven J. Novel circulating biomarkers for non-alcoholic fatty liver disease: A systematic review. *J Cell Physiol*. 2018;233(2):849-855. doi:10.1002/jcp.25779

98. Gitto S, Schepis F, Andreone P, Villa E. Study of the Serum Metabolomic Profile in Nonalcoholic Fatty Liver Disease: Research and Clinical Perspectives. *Metabolites*. 2018;8(1). doi:10.3390/metabo8010017

99. Kalhan SC, Guo L, Edmison J, et al. Plasma metabolomic profile in nonalcoholic fatty liver disease. *Metabolism*. 2011;60(3):404-413. doi:10.1016/j.metabol.2010.03.006

100. Gaggini M, Carli F, Rosso C, et al. Altered amino acid concentrations in NAFLD: Impact of obesity and insulin resistance. *Hepatology*. 2018;67(1):145-158. doi:10.1002/hep.29465

101. Miwa Kawanaka M, Nishino K, Oka T, et al. Tyrosine levels are associated with insulin resistance in patients with nonalcoholic fatty liver disease. *Hepatic Med Evid Res*. 2015;7:29. doi:10.2147/hmer.s79100

102. Sunny NE, Kalavalapalli S, Bril F, et al. Cross-talk between branched-chain amino acids and hepatic mitochondria is compromised in nonalcoholic fatty liver disease. *Am J Physiol Endocrinol Metab*. 2015;309(4):E311-9. doi:10.1152/ajpendo.00161.2015

103. Jin R, Banton S, Tran VT, et al. Amino Acid Metabolism is Altered in Adolescents with Nonalcoholic Fatty Liver Disease-An Untargeted, High Resolution Metabolomics Study. 2016. doi:10.1016/j.jpeds.2016.01.026

104. Mardinoglu A, Bjornson E, Zhang C, et al. Personal model-assisted identification of NAD+ and glutathione metabolism as intervention target in NAFLD. *Mol Syst Biol*. 2017;13(3):916. doi:10.15252/msb.20167422

105. Aragonès G, Auguet T, Berlanga A, et al. Increased Circulating Levels of Alpha-Ketoglutarate in Morbidly Obese Women with Non-Alcoholic Fatty Liver Disease. *PLoS One*. 2016;11(4):e0154601. doi:10.1371/journal.pone.0154601

106. Rodríguez-Gallego E, Guirro M, Riera-Borrull M, et al. Mapping of the circulating metabolome reveals α-ketoglutarate as a predictor of morbid obesity-associated non-alcoholic fatty liver disease. *Int J Obes*. 2015;39(2):279-287. doi:10.1038/ijo.2014.53

107. Puri P, Wiest MM, Cheung O, et al. The plasma lipidomic signature of nonalcoholic steatohepatitis. *Hepatology*. 2009;50(6):1827-1838. doi:10.1002/hep.23229

108. Barr J, Caballería J, Martínez-Arranz I, et al. Obesity dependent metabolic signatures associated with nonalcoholic fatty liver disease progression. *J Proteome Res*. 2012;11(4):2521-2532. doi:10.1021/pr201223p

109. Puri P, Baillie RA, Wiest MM, et al. A lipidomic analysis of nonalcoholic fatty liver

disease. *Hepatology*. 2007;46(4):1081-1090. doi:10.1002/hep.21763

110. Kakisaka K, Cazanave SC, Fingas CD, et al. Mechanisms of lysophosphatidylcholine-induced hepatocyte lipoapoptosis. *Am J Physiol Gastrointest Liver Physiol*. 2012;302(1):G77-84. doi:10.1152/ajpgi.00301.2011

111. Papandreou C, Bullò M, Tinahones FJ, et al. Serum metabolites in non-alcoholic fatty-liver disease development or reversion; a targeted metabolomic approach within the PREDIMED trial. *Nutr Metab (Lond)*. 2017;14. doi:10.1186/S12986-017-0213-3

112. Zhou Y, Orešič M, Leivonen M, et al. Noninvasive Detection of Nonalcoholic Steatohepatitis Using Clinical Markers and Circulating Levels of Lipids and Metabolites. *Clin Gastroenterol Hepatol*. 2016;14(10):1463-1472.e6. doi:10.1016/j.cgh.2016.05.046

113. Cano A, Alonso C. Deciphering non-alcoholic fatty liver disease through metabolomics. *Biochem Soc Trans*. 2014;42(5):1447-1452. doi:10.1042/BST20140138

114. Lake AD, Novak P, Shipkova P, et al. Branched chain amino acid metabolism profiles in progressive human nonalcoholic fatty liver disease. *Amino Acids*. 2015;47(3):603-615. doi:10.1007/s00726-014-1894-9

115. Schooneman MG, Vaz FM, Houten SM, Soeters MR. Acylcarnitines: reflecting or inflicting insulin resistance? *Diabetes*. 2013;62(1):1-8. doi:10.2337/db12-0466

116. Li H, Wang L, Yan X, et al. A Proton Nuclear Magnetic Resonance Metabonomics Approach for Biomarker Discovery in Nonalcoholic Fatty Liver Disease. *J Proteome Res*. 2011;10(6):2797-2806. doi:10.1021/pr200047c

117. Toye AA, Dumas ME, Blancher C, et al. Subtle metabolic and liver gene transcriptional changes underlie diet-induced fatty liver susceptibility in insulin-resistant mice. *Diabetologia*. 2007;50:1867-1879. doi:10.1007/s00125-007-0738-5

118. Hyötyläinen T, Jerby L, Petäjä EM, et al. ARTICLE Genome-scale study reveals reduced

metabolic adaptability in patients with non-alcoholic fatty liver disease. *Nat Commun*. 2016. doi:10.1038/ncomms9994

119. Sookoian S, Castaño GO, Scian R, et al. Serum aminotransferases in nonalcoholic fatty liver disease are a signature of liver metabolic perturbations at the amino acid and Krebs cycle level. *Am J Clin Nutr*. 2016;103(2):422-434. doi:10.3945/ajcn.115.118695
120. Jiao N, Baker SS, Chapa-Rodriguez A, et al. Suppressed hepatic bile acid signalling despite elevated production of primary and secondary bile acids in NAFLD. *Gut*. 2018;67(10):1881-1891. doi:10.1136/gutjnl-2017-314307
121. Chiang JYL. Bile acid metabolism and signaling. *Compr Physiol*. 2013;3(3):1191-1212. doi:10.1002/cphy.c120023
122. García-Cañaveras JC, Donato MT, Castell J V., Lahoz A. A Comprehensive Untargeted Metabonomic Analysis of Human Steatotic Liver Tissue by RP and HILIC Chromatography Coupled to Mass Spectrometry Reveals Important Metabolic Alterations. *J Proteome Res*. 2011;10(10):4825-4834. doi:10.1021/pr200629p
123. Lake AD, Novak P, Shipkova P, et al. Decreased hepatotoxic bile acid composition and altered synthesis in progressive human nonalcoholic fatty liver disease. *Toxicol Appl Pharmacol*. 2013;268(2):132-140. doi:10.1016/j.taap.2013.01.022
124. Goffredo M, Santoro N, Tricò D, et al. A Branched-Chain Amino Acid-Related Metabolic Signature Characterizes Obese Adolescents with Non-Alcoholic Fatty Liver Disease. *Nutrients*. 2017;9(7). doi:10.3390/nu9070642
125. Lu LP, Wan YP, Xun PC, et al. Serum bile acid level and fatty acid composition in Chinese children with non-alcoholic fatty liver disease. *J Dig Dis*. 2017;18(8):461-471. doi:10.1111/1751-2980.12494
126. Khusial RD, Cioffi CE, Caltharp SA, et al. Development of a Plasma Screening Panel for

Pediatric Nonalcoholic Fatty Liver Disease Using Metabolomics. *Hepatol Commun*. 2019;3(10):1311-1321. doi:10.1002/hep4.1417

127. Mills EL, Pierce KA, Jedrychowski MP, et al. Accumulation of succinate controls activation of adipose tissue thermogenesis. *Nature*. 2018;560(7716):102-106. doi:10.1038/s41586-018-0353-2

128. Crane JD, Palanivel R, Mottillo EP, et al. Inhibiting peripheral serotonin synthesis reduces obesity and metabolic dysfunction by promoting brown adipose tissue thermogenesis. *Nat Med*. 2015;21(2):166-172. doi:10.1038/nm.3766

129. Robinson LJ, Law J, Astle V, et al. Sexual Dimorphism of Brown Adipose Tissue Function. *J Pediatr*. April 2019. doi:10.1016/J.JPEDS.2019.03.003

130. Gilsanz V, Smith ML, Goodarzian F, Kim M, Wren TAL, Hu HH. Changes in Brown Adipose Tissue in Boys and Girls during Childhood and Puberty. *J Pediatr*. 2012;160(4):604-609.e1. doi:10.1016/j.jpeds.2011.09.035

131. World Health Organization. Body mass index - BMI. http://www.euro.who.int/en/health-topics/disease-prevention/nutrition/a-healthy-lifestyle/body-mass-index-bmi. Published 2019. Accessed January 5, 2019.

132. World Health Organization. Growth reference 5-19 years: Weight-for-age (5-10 years). https://www.who.int/growthref/who2007_bmi_for_age/en/. Published 2007. Accessed January 31, 2019.

133. World Health Organization (WHO). WHO AnthroPlus for Personal Computers Manual: Software for assessing growth of the world's children and adolescents. 2009.

134. Idilman IS, Aniktar H, Idilman R, et al. Hepatic Steatosis: Quantification by Proton Density Fat Fraction with MR Imaging versus Liver Biopsy. *Radiology*. 2013;267(3):767-775. doi:10.1148/radiol.13121360

135. Hu HH, Perkins TG, Chia JM, Gilsanz V. Characterization of Human Brown Adipose Tissue by Chemical-Shift Water-Fat MRI. *Am J Roentgenol*. 2013;200(1):177-183. doi:10.2214/AJR.12.8996

136. Ang QY, Goh HJ, Cao Y, et al. A new method of infrared thermography for quantification of brown adipose tissue activation in healthy adults (TACTICAL): a randomized trial. *J Physiol Sci*. 2017;67(3):395-406. doi:10.1007/s12576-016-0472-1

137. Gashi G, Madoerin P, Maushart CI, et al. MRI Characteristics of Supraclavicular Brown Adipose Tissue in Relation to Cold-Induced Thermogenesis in Healthy Human Adults. *J Magn Reson Imaging*. 2019. doi:10.1002/jmri.26733

138. Zingaretti MC, Crosta F, Vitali A, et al. The presence of UCP1 demonstrates that metabolically active adipose tissue in the neck of adult humans truly represents brown adipose tissue. *FASEB J*. 2009;23(9):3113-3120. doi:10.1096/fj.09-133546

139. van der Lans AAJJ, Hoeks J, Brans B, et al. Cold acclimation recruits human brown fat and increases nonshivering thermogenesis. *J Clin Invest*. 2013;123(8):3395-3403. doi:10.1172/JCI68993

140. Cypess AM, Chen Y-C, Sze C, et al. Cold but not sympathomimetics activates human brown adipose tissue in vivo. *Proc Natl Acad Sci*. 2012;109(25):10001-10005. doi:10.1073/pnas.1207911109

141. Chalfant JS, Smith ML, Hu HH, et al. Inverse association between brown adipose tissue activation and white adipose tissue accumulation in successfully treated pediatric malignancy. *Am J Clin Nutr*. 2012;95(5):1144-1149. doi:10.3945/ajcn.111.030650

142. Ellis KJ, Shypailo RJ, Pratt JA, Pond WG. Accuracy of dual-energy x-ray absorptiometry for body-composition measurements in children. *Am J Clin Nutr*. 1994;60(5):660-665. doi:10.1093/ajcn/60.5.660

143. Shah NR, Braverman ER. Measuring adiposity in patients: The utility of body mass index (BMI), percent body fat, and leptin. *PLoS One*. 2012;7(4). doi:10.1371/journal.pone.0033308

144. Mazess RB, Barden HS, Bisek JP, Hanson J. Dual-energy x-ray absorptiometry for total-body and regional bone-mineral and soft-tissue composition. *Am J Clin Nutr*. 1990;51(6):1106-1112. doi:10.1093/ajcn/51.6.1106

145. Ceniccola GD, Castro MG, Piovacari SMF, et al. Current technologies in body composition assessment: advantages and disadvantages. *Nutrition*. 2019;62:25-31. doi:10.1016/J.NUT.2018.11.028

146. Ghasemi A, Zahediasl S. Normality Tests for Statistical Analysis: A Guide for Non-Statisticians. *Int J Endocrinol Metab*. 2012;10(2):486-495. doi:10.5812/ijem.3505

147. Broadhurst DI, Kell DB. Statistical strategies for avoiding false discoveries in metabolomics and related experiments. *Metabolomics*. 2006;2(4):171-196. doi:10.1007/s11306-006-0037-z

148. Pike N. Using false discovery rates for multiple comparisons in ecology and evolution. *Methods Ecol Evol*. 2011;2(3):278-282. doi:10.1111/j.2041-210X.2010.00061.x

149. Newbern D, Gumus Balikcioglu P, Balikcioglu M, et al. Sex differences in biomarkers associated with insulin resistance in obese adolescents: metabolomic profiling and principal components analysis. *J Clin Endocrinol Metab*. 2014;99(12):4730-4739. doi:10.1210/jc.2014-2080

150. Buckley JP, Doherty BT, Keil AP, Engel SM. Statistical Approaches for Estimating Sex-Specific Effects in Endocrine Disruptors Research. *Environ Health Perspect*. 2017;125(6):067013. doi:10.1289/EHP334

151. Liland KH. Multivariate methods in metabolomics – from pre-processing to dimension

reduction and statistical analysis. *TrAC Trends Anal Chem*. 2011;30(6):827-841. doi:10.1016/j.trac.2011.02.007

152. Ringnér M. What is principal component analysis? *Nat Biotechnol*. 2008;26(3):303-304. doi:10.1038/nbt0308-303

153. Mundfrom DJ, Shaw DG, Ke TL. Minimum Sample Size Recommendations for Conducting Factor Analyses. *Int J Test*. 2005;5(2):159-168. doi:10.1207/s15327574ijt0502_4

154. Perng W, Gillman MW, Fleisch AF, et al. Metabolomic profiles and childhood obesity. *Obesity*. 2014;22(12):n/a-n/a. doi:10.1002/oby.20901

155. Fernández-Alvira JM, Bammann K, Pala V, et al. Country-specific dietary patterns and associations with socioeconomic status in European children: the IDEFICS study. *Eur J Clin Nutr*. 2014;68(7):811-821. doi:10.1038/ejcn.2014.78

156. Lewis GD, Farrell L, Wood MJ, et al. Metabolic signatures of exercise in human plasma. *Sci Transl Med*. 2010;2(33). doi:10.1126/scitranslmed.3001006

157. Wilson Van Voorhis CR, Morgan BL. Understanding Power and Rules of Thumb for Determining Sample Sizes. *Tutor Quant Methods Psychol*. 2007;3(2):43-50. doi:10.20982/tqmp.03.2.p043

158. Bartelt A, Bruns OT, Reimer R, et al. Brown adipose tissue activity controls triglyceride clearance. *Nat Med*. 2011;17(2):200-205. doi:10.1038/nm.2297

159. Kazak L, Chouchani ET, Jedrychowski MP, et al. A Creatine-Driven Substrate Cycle Enhances Energy Expenditure and Thermogenesis in Beige Fat. *Cell*. 2015;163(3):643-655. doi:10.1016/J.CELL.2015.09.035

160. Labbé SM, Mouchiroud M, Caron A, et al. mTORC1 is Required for Brown Adipose Tissue Recruitment and Metabolic Adaptation to Cold. *Sci Rep*. 2016;6:37223.

doi:10.1038/srep37223

161. Delong Meng X, Yang Q, Huanyu Wang X, et al. Glutamine and asparagine activate mTORC1 independently of Rag GTPases. 2020. doi:10.1074/jbc.AC119.011578

162. Bianchi G, Marchesini G, Brunetti N, et al. Impaired insulin-mediated amino acid plasma disappearance in non-alcoholic fatty liver disease: A feature of insulin resistance. *Dig Liver Dis*. 2003;35(10):722-727. doi:10.1016/S1590-8658(03)00416-X

163. Vanderlinde RE. Review of pyridoxal phosphate and the transaminases in liver disease. *Ann Clin Lab Sci*. 16(2):79-93. http://www.ncbi.nlm.nih.gov/pubmed/3008634. Accessed March 24, 2020.

164. Gregory JF, DeRatt BN, Rios-Avila L, Ralat M, Stacpoole PW. Vitamin B6 nutritional status and cellular availability of pyridoxal 5′-phosphate govern the function of the transsulfuration pathway's canonical reactions and hydrogen sulfide production via side reactions. *Biochimie*. 2016;126:21-26. doi:10.1016/j.biochi.2015.12.020

165. Xu C, Yu C, Xu L, Miao M, Li Y. High serum uric acid increases the risk for nonalcoholic fatty liver disease: A prospective observational study. *PLoS One*. 2010;5(7):1-6. doi:10.1371/journal.pone.0011578

166. Sirota JC, McFann K, Targher G, Johnson RJ, Chonchol M, Jalal DI. Elevated serum uric acid levels are associated with non-alcoholic fatty liver disease independently of metabolic syndrome features in the United States: Liver ultrasound data from the National Health and Nutrition Examination Survey. *Metabolism*. 2013;62(3):392-399. doi:10.1016/j.metabol.2012.08.013

167. Xu C, Wan X, Xu L, et al. Xanthine oxidase in non-alcoholic fatty liver disease and hyperuricemia: One stone hits two birds. *J Hepatol*. 2015;62(6):1412-1419. doi:10.1016/j.jhep.2015.01.019

168. Cheung KJ, Tzameli I, Pissios P, et al. Xanthine Oxidoreductase Is a Regulator of Adipogenesis and PPARγ Activity. *Cell Metab*. 2007;5(2):115-128. doi:10.1016/J.CMET.2007.01.005

169. Pettegrew JW, Levine J, McClure RJ. Acetyl-L-carnitine physical-chemical, metabolic, and therapeutic properties: relevance for its mode of action in Alzheimer's disease and geriatric depression. *Mol Psychiatry*. 2000;5(6):616-632. doi:10.1038/sj.mp.4000805

170. Pandhare J, Donald SP, Cooper SK, Phang JM. Regulation and function of proline oxidase under nutrient stress. *J Cell Biochem*. 2009;107(4):759-768. doi:10.1002/jcb.22174

171. Lettieri Barbato D, Aquilano K, Baldelli S, et al. Proline oxidase–adipose triglyceride lipase pathway restrains adipose cell death and tissue inflammation. *Cell Death Differ*. 2014;21(1):113-123. doi:10.1038/cdd.2013.137

172. Marmol-Carrasco P, Ibáñez CF. Control of brown adipose tissue adaptation to nutrient stress by the activin receptor ALK7. *bioRxiv*. December 2019:861609. doi:10.1101/861609

173. Galinier A, Carrière A, Fernandez Y, et al. Adipose tissue proadipogenic redox changes in obesity. *J Biol Chem*. 2006;281(18):12682-12687. doi:10.1074/jbc.M506949200

174. Lettieri Barbato D, Tatulli G, Cannata SM, Bernardini S, Aquilano K, Ciriolo MR. Glutathione Decrement Drives Thermogenic Program in Adipose Cells. *Sci Rep*. 2015;5:1-11. doi:10.1038/srep13091

175. Elshorbagy AK, Refsum H, Smith AD, Graham IM. The association of plasma cysteine and γ-glutamyltransferase with BMI and obesity. *Obesity*. 2009;17(7):1435-1440. doi:10.1038/oby.2008.671

176. Czech MP, Fain JN. Cu ++ -dependent thiol stimulation of glucose metabolism in white fat cells. *J Biol Chem*. 1972;247(19):6218-6223.

177. Sengupta S, Wehbe C, Majors AK, Ketterer ME, DiBello PM, Jacobsen DW. Relative Roles of Albumin and Ceruloplasmin in the Formation of Homocystine, Homocysteine-Cysteine-mixed Disulfide, and Cystine in Circulation. *J Biol Chem*. 2001;276(50):46896-46904. doi:10.1074/jbc.M108451200

178. Pastore A, Alisi A, di Giovamberardino G, et al. Plasma levels of homocysteine and cysteine increased in pediatric NAFLD and strongly correlated with severity of liver damage. *Int J Mol Sci*. 2014;15(11):21202-21214. doi:10.3390/ijms151121202

179. Gulsen M, Yesilova Z, Bagci S, et al. Elevated plasma homocysteine concentrations as a predictor of steatohepatitis in patients with non-alcoholic fatty liver disease. *J Gastroenterol Hepatol*. 2005;20(9):1448-1455. doi:10.1111/j.1440-1746.2005.03891.x

180. Sunny NE, Parks EJ, Browning JD, Burgess SC. Excessive hepatic mitochondrial TCA cycle and gluconeogenesis in humans with nonalcoholic fatty liver disease. *Cell Metab*. 2011;14(6):804-810. doi:10.1016/j.cmet.2011.11.004

181. Goodacre R, Broadhurst D, Smilde AK, et al. Proposed minimum reporting standards for data analysis in metabolomics. *Metabolomics*. 2007;3(3):231-241. doi:10.1007/s11306-007-0081-3

182. Van Herck MA, Vonghia L, Francque SM. Animal Models of Nonalcoholic Fatty Liver Disease-A Starter's Guide. *Nutrients*. 2017;9(10). doi:10.3390/nu9101072

APPENDIX

A. Supplementary Figures and Tables (Methods)

Appendix A1. Adult GETBAT exclusion criteria.

1. Any contradictions for MRI (claustrophobia, implanted metal, metallic injuries, recent tattoo or weight > 300lbs)
2. Prior bariatric surgery or liver transplant
3. Use of any of the following medications: β adrenergic, steatogenic, anti-hyperglycemic, antidepressant, anti-psychotic, anxiolytic, thyroid, antiemetic – 5HT3 antagonists or serotonergic drug - *[see **Appendix A3**]*
4. Any condition associated with brown adipose tissue, hepatic steatosis or liver disorders - *[see **Appendix A4**]*
5. Self-reported alcohol intake greater than 7 drinks/week without exceeding 3 drinks/day (men) and 2 drinks/day (women)
6. Nicotine or tobacco use (smoking, nicotine patch, chew tobacco, nicotine gum, e-cigarette or cigar)
7. Pregnant or nursing

Appendix A2. Pediatric GETBAT exclusion criteria.

1. Any contradictions for MRI (claustrophobia, implanted metal, metallic injuries, recent tattoo or weight > 300lbs)
2. Prior bariatric surgery or liver transplant

3. Use of any of the following medications: β adrenergic, steatogenic, anti-hyperglycemic, antidepressant, anti-psychotic, anxiolytic, thyroid, antiemetic – 5HT3 antagonists or serotonergic drug - *[see **Appendix A3**]*
4. Any condition associated with brown adipose tissue, hepatic steatosis or liver disorders - *[see **Appendix A4**]*

Appendix A3. List of excluded medications.

Class of Drugs	List
Drugs affecting β-adrenergic receptor	**β -Blockers** • Acebutolol (Sectral) • Atenolol (Tenormin) • Bisoprolol (Zebeta) • Metoprolol (Lopressor, Toprol-XL) • Nadolol (Corgard) • Propranolol (Inderal LA, InnoPran XL) **Asthma/COPD beta-adrenergic agonists** • Bambuterol (Bambec, Oxeol) • Bitolterol mesylate (Tornalate) • Clenbuterol (Dilaterol, Spiropent, Ventipulmin) • Fenoterol (Berotec N) • Formoterol (Foradil, Zenhale, Symbicort, Forpack Discair, Oxeze/Oxis) • Isoprenaline/ Isoproterenol (Isuprel) • Levosalbutamol (Levalbuterol, Xopenex) • Metaproterenol (Alupent) • Olodaterol (Striverdi) • Pirbuterol (Maxair) • Procaterol • Salbutamol (Albuterol, Ventolin) • Salmeterol (Serevent Diskus) • Terbutaline (Bricanyl) • Vilanterol (Breo Ellipta, Relvar Ellipta) **Others** • Mirabegron (Myrbetriq) • Methylphenidate (Ritalin)
Steatogenic medications	**Corticosteroids** • Betamethasone (Celestone) • Budesonide (Pulmicort, Entocort EC)

	• Cortone Acetate (Cortone) • Cotolone • Dexamethasone (Decadron) • Fludrocortisone (Florinef Acetate) • Methylprednisolone (Medrol, Methylpred-DP) • Prednisone (Bubbli-Pred, Deltasone, Prednicot, Prelone, Pediapred 5, Pms-prednisolone) • Triamcinolone (Aristocort) **Tetracycline** • Demeclocycline (Declomycin) • Doxycycline (Doryx, Vibramycin) • Minocycline (Dynacin, Minocin, Monodox) • Oxytetracycline (Terramycin) • Tetracycline (Achromycin) • Tigecycline (Tygacil) **Other** • Amiodarone (Cordarone, Nexterone, Pacerone) • L-asparaginase (Elspar) • Methotrexate (Rheumatrex, Trexall) • Tamoxifen(Nolvadex) • Valproic acid (Depakote, Depakote ER, Depakote Sprinkle, Depakene, Depacon, Stavzor)

Anti-hyperglycemic drugs	**Alpha-Glucosidase Inhibitor**
	• Acarbose (Precose)
	• Miglitol (Glyset)
	
	Biguanides
	• Metformin (Glucophage, Glucophage XR, Glumetza, Fortamet, Riomet)
	• Metformin combination drugs
	  o Actoplus Met
	  o Avandamet
	  o Duetact
	  o Glucovance
	  o Janumet
	  o Jentadueto
	  o Komboglyze
	  o Metaglip
	  o PrandiMet
	
	Dipeptidyl peptidase-4 (DPP-4) inhibitor
	• Alogliptin (Nesina)
	• Canagliflozin (Invokana)

	● Dapagliflozin (Farxiga) ● Linagliptin (Tradjenta) ● Saxagliptin (Onglyza) ● Sitagliptin (Januvia) **Glucagon-like peptide** ● Exenatide (Exendin-4, Byetta) ● Liraglutide (Victoza) ● Lixisenatide (Lyxumia) **Meglitinides** ● Repaglinide (GlucoNorm, Prandin, NovoNorm) ● Nateglinide (Starlix) **Insulin** **Sulfonylurea** ● Chlorpropamide (Diabinese) ● Glimepiride (Amaryl) ● Glipizide (Glucotrol, Glucotrol XL) ● Glyburide (DiaBeta, Glynase PresTab, Micronase) ● Tolbutamide ● Yolazamide **Thiazolidinediones** ● Pioglitazone (Actos) ● Rosiglitazone (Avandia)
HIV drugs	• HAART
Antidepressants, anxiolytic drugs, anti-psychotic drugs	**5-HT2 Receptor Antagonists** ● Trazodone (Desyrel, Oleptro, Trazorel, Trialodine, Trittico) **5-HT3 Receptor Antagonists** ● Vortioxetine (Brintellix, Trintellix) **Dopamine Reuptake Blocker** ● Bupropion (Wellbutrin) **MAOIs (Monoamine oxidase inhibitors)** ● Isocarboxazid (Marplan) ● Phenelzine (Nardil) ● Selegiline (Emsam) ● Tranylcypromine (Parnate)

	SNRIs (Serotonin and norepinephrine reuptake inhibitors) ● Desvenlafaxine (Pristiq) ● Duloxetine (Cymbalta) ● Venlafaxine (Effexor XR) **SSRIs (Selective serotonin reuptake inhibitor)** ● Citalopram (Celexa) ● Escitalopram (Lexapro) ● Fuoxetine (Prozac) ● Fuvoxamine (Luvox) ● Paroxetine (Paxil) ● Sertraline (Zoloft) **Tetracyclic Antidepressant** ● Maprotiline (Teva-Maprotiline) ● Mirtazapine (Tera-Mirtazapine) **Tricyclic medication** ● Amitriptyline (Elavil) ● Amoxapine (Asendin**)** ● Clomipramine (Anafranil) ● Desipramine (Norpramin) ● Doxepin (Silenor) ● Imipramine (Tofranil) ● Nortriptyline (Pamelor) ● Protriptyline (Vivactil) ● Trimipramine (Surmontil)
Thyroid drugs	**Anti-thyroid** ● Methimazole (Tapazole) ● Propylthiouracil (Propyl-Thyracil or PTU) **Thyroid** ● Levothyroxine (T4) (Levothroid, Levoxyl, Synthroid, Tirosint, Unithroid) ● Liothyronine (T3) (Cytomel) ● Liotrix (T3 and T4) (Thyrolar)
Antiemetic (5HT3 antagonists)	● Dolasetron (Anzemet) ● Granisetron (Granisetron Hydrochloride) ● Ondansetron (Zofran) ● Palonosetron (Aloxi)
Drugs affecting serotonin	● Amphetamine ● Dextromethorphan ● Metoclopramide

Table A4. List of excluded conditions.

Conditions	List
Diseases that affects brown adipose tissue	• Adrenal gland disorder (i.e. pheochromocytoma) • Hibernoma
Diseases associated with hepatic steatosis and liver disorders	• Abetalipoproteinemia • Celiac disease • Cystic fibrosis • Galactosemia • Glycogen storage disease • Hemochromatosis • Hepatitis B or C • Hepatocellular carcinoma (HCC) • Homocystinuria • Inflammatory bowel disease • Lipodystrophy • Polycystic liver disease • Tyrosinemia • Weber-Christian syndrome • Wilson's disease

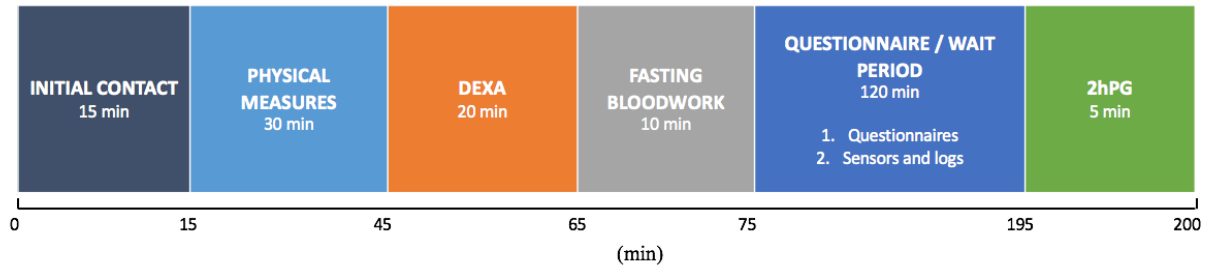

Appendix A5. Visit 1 Timeline (McMaster University Medical Centre).

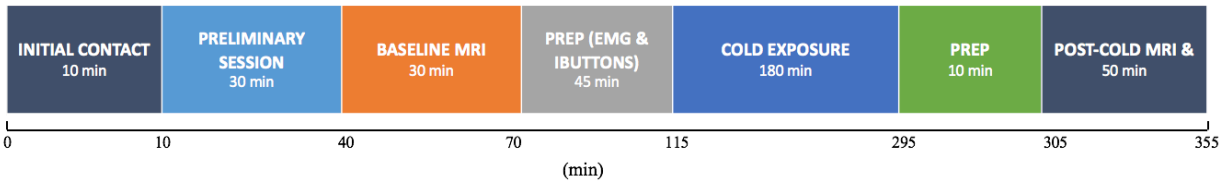

Appendix A6. Adult Visit 2 Timeline (St. Joseph's Healthcare Hamilton).

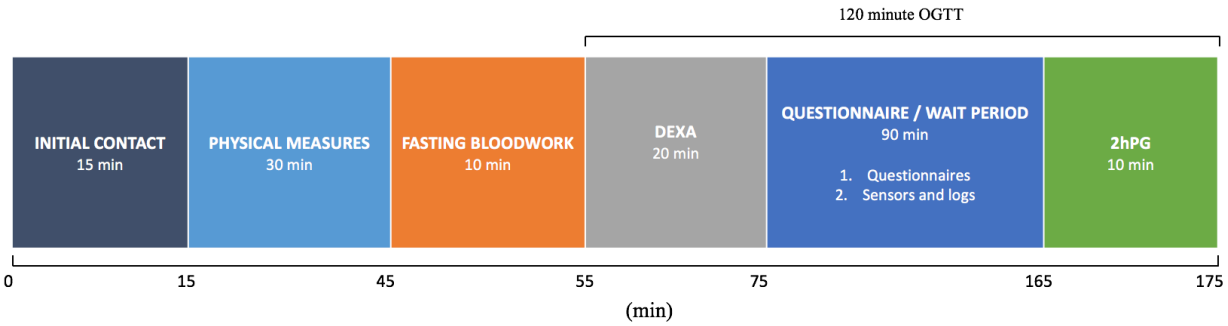

Appendix A7. Pediatric Visit 1 Timeline (McMaster University Medical Centre).

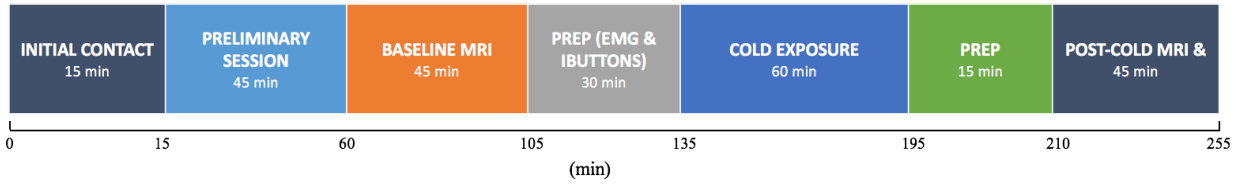

Appendix A8. Pediatric Visit 2 Timeline (St. Joseph's Healthcare Hamilton).

Appendix A9. MRI protocol parameters for IDEAL-IQ sequence.

Pulse Sequence: IDEAL-IQ		
Parameter	**SCV**	**Liver**
Patient Entry	Head First	Feet First
Patient Position	Supine	
Coil	HNS Head/Neck/Chest	NeoCoil 32 Channel Torso Array
Orientation	Axial	
Flip angle	4	3
TE	Min Full	
Number of echoes	6	
Echo Train Length	3	
Number of shots	2	
Bandwidth	111.11	
Frequency axis	Bottom/Up	

Phase axis	Right/Left	
Spatial resolution (mm)	1.48 x 1.48	1.33 x 1.33
Acquired slice thickness (mm)	4	8
Imaging Options	EDR, Fast, IDEAL, ARC	

B. Supplementary Figures and Tables (Results)

Results for the PCA with varimax rotation (see **Results Section 3.2**) for the adult cohort can be seen in **Appendix B1-B4**. Eleven components were selected for analysis prior to the inflection point of the scree plot (**Appendix B2**) which cumulatively explained 75% of the variation (**Appendix B1**). The rotated loadings matrix can be seen in **Appendix B3**, where factor loadings < 0.4 were excluded, and metabolites with a factor loading ≥ 0.4 are considered to constitute that component[149]. Clearly, there is a lack of simple structure on the rotated loadings matrix as many metabolites load highly on more than one component which makes interpretability more difficult. Negative loadings simply imply an inverse correlation between such metabolite and others within the component[152]. Metabolite identities within each component are provided in **Appendix B4**.

Appendix B1. Total variance for 11 identified principal components.

Component	Eigenvalue	% of Variance	Cumulative %
1	9.32	15.53	15.53
2	7.28	12.13	27.66
3	4.82	8.04	35.70
4	4.32	7.20	42.90
5	3.95	6.58	49.48
6	3.69	6.15	55.62
7	2.96	4.94	60.56
8	2.72	4.53	65.09

9	2.44	4.06	69.15
10	1.88	3.13	72.28
11	1.87	3.12	75.40

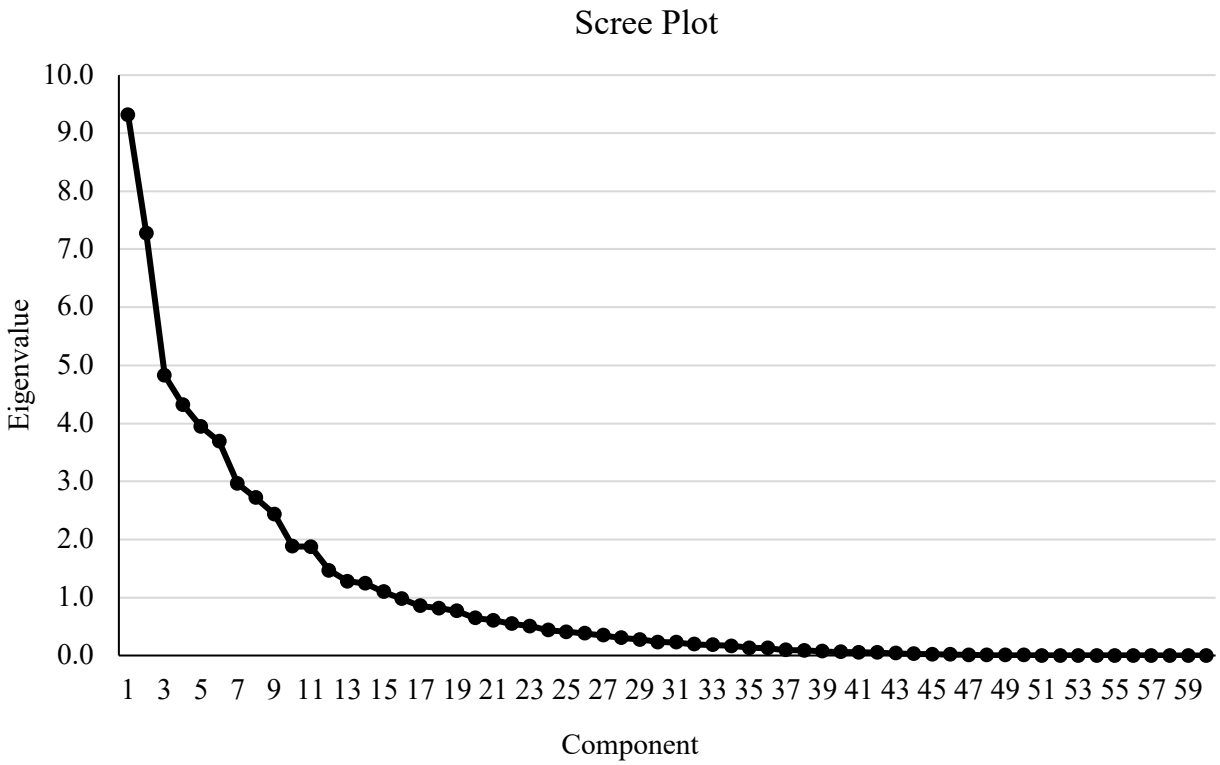

Appendix B2. Scree plot displaying eigenvalues for identified principal components. The inflection point in the scree plot arm was determined to occur at component 11.

Appendix B3. Varimax rotated loadings matrix from PCA in the adult cohort. Loadings < 0.4 were excluded.

	Component										
	1	2	3	4	5	6	7	8	9	10	11
4-Hydroxy-L-proline	**.87**										
Cis-4-Hydroxy-D-proline	**.87**										
Glutamine	**.73**										
D-Glucose	**.71**		**.41**								
Fructose-galactose-glucose-mannose	**.70**		**.46**								
Carnitine	**.68**			**.43**							

Gluconic acid	**.67**										
L-carnitine	**.67**			**.43**							
Xylose-ribose-arabinose	**.55**		**.54**								
Tyrosine	**.53**							**.46**			
Hypoxanthine	**-.48**										
Oleic acid		**.87**									
Linoleic acid		**.85**									
Palmitoleic acid		**.83**									
Ethyl-myristate		**.78**	**-.40**								
Adenonsine-2,3-cyclic-monophosphate		**.46**									
3-Hydrox-butyric acid		**.44**		**.41**							
3-Hydroxy-3-methylglutaric acid			**.83**								
Aconitate			**.65**								
Ocatadecanoyl-carnitine			**-.63**								
Propionate			**.62**						**-.47**		
Succinate			**.57**						**-.49**		
2-Phosphoglycerate			**-.44**					**.43**			
Creatine				**.81**							
Alanine				**.81**							
MDA				**.76**							
Pyridoxal				**.46**							
Xanthine				**.44**							
Acetyl-carnitine		**.41**		**.43**							
D-Glucose-6-phosphate					**.97**						
D-Fructose-6-phosphate					**.97**						
a-D-glucose-1-phosphate					**.97**						
Taurine					**.77**						
Homoserine						**.90**					
Threonine						**.90**					
Asparagine						**.73**					
Serine						**.57**					
Lauryl-L-carnitine							**.92**				
Dodecanoyl-carnitine							**.92**				

Hexanoyl-L-carnitine				**.43**			**.60**				
Uracil							**.57**				
Phosphocreatine											
Proline								**.70**			
Uridine-5-monophophate								**.63**			
Phenylalanine								**.60**		**.41**	
Methionine						**.53**		**.58**			
L-Pyroglutamic acid								**.48**			
a-ketoglutarate			**.43**					**.47**			
Glutamic acid								**.40**			
Thymine									**.75**		
Aminobenzoic acid									**.74**		
Hippurate									**.64**		
Histamine										**.84**	
Histidine										**.81**	
Glycine											
Cysteine											**.81**
Cystine											**.80**
Orotate									**.40**		**-.46**

Appendix B4. Metabolite identities within each principal component. Metabolites with rotated loadings > 0.4 were included. Bolded metabolite names represent positive loadings, non-bolded metabolites represent negative loadings.

Component	Metabolites
1	**Fructose-galactose-glucose-mannose, D-glucose, 4-hydroxy-L-proline, cis-4-hydroxy-D-proline, gluconic acid, xylose-ribose-arabinose, glutamine, carnitine, L-carnitine, tyrosine**, hypoxanthine
2	**Linoleic acid, oleic acid, palmitoleic acid, ethyl-myristate, adenosine-2,3-cyclicmonophosphate, acetyl-carnitine, 3-hydroxybutyric acid**
3	**D-glucose, fructose-galactose-lactose-glucose-mannose, xylose-ribose-arabinose, 3-hydroxy-3-methylglutaric acid, aconitate, propionate, succinate, a-ketoglutarate**, 2-phosphoglycerate, ocatadecanoyl-carnitine, ethyl-myristate
4	**Carnitine, L-carnitine, 3-hydroxybutyric acid, creatine, alanine, MDA, pyridoxal, xanthine, acetyl-carnitine, hexanoyl-L-carnitine**
5	**D-glucose-6-phosphate, D-fructose-6-phosphate, a-D-glucose-1-phosphate, taurine**
6	**Homoserine, threonine, asparagine, serine**

7	**Lauryl-L-carnitine, dodecanoyl-carnitine, hexanoyl-carnitine, uracil**
8	**Tyrosine, 2-phosphoglycerate, proline, uridine-5-monophosphate, phenylalanine, methionine, L-pyroglutamic acid, a-ketoglutarate, glutamic acid**
9	**Thymine, aminobenzoic acid, hippurate, orotate**, propionate, succinate
10	**Histamine, histidine, phenylalanine**
11	**Cysteine, cystine**, orotate

In multivariate linear regression analysis, component 9 significantly negatively predicted pre-cold SCV PDFF%, and positively predicted both SCV PDFF% reduction and percent change in SCV PDFF% independent of age and sex (**Appendix B5-B7**). Other significant models can be identified by grey shading, although there were no other similarities between outcome variables.

Appendix B5. Metabolite component regression models for **Pre-Cold SCV PDFF%.** Grey shading and bolding denote $P<0.05$.

Predictor: Component Scores	**Model 1** Univariate			**Model 2** + Age			**Model 3** + Age + Sex			**Model 4** + Age + Sex + % Body Fat		
	β	t	p-value	β	t	p-value	β	t	p-value	β	t	p-value
1	0.103	0.802	0.426	-0.147	-1.328	0.189	-0.130	-1.132	0.262	**-0.152**	**-2.113**	**0.039**
2	0.042	0.325	0.746	-0.058	-0.557	0.580	-0.098	-0.887	0.379	-0.101	-1.444	0.154
3	**0.313**	**2.557**	**0.013**	0.157	1.474	0.146	0.144	1.328	0.189	0.078	1.107	0.273
4	**0.394**	**3.320**	**0.002**	0.188	1.711	0.092	0.184	1.670	0.100	0.004	0.049	0.961
5	0.136	1.061	0.293	0.100	0.964	0.339	0.121	1.156	0.253	**0.219**	**3.495**	**0.001**
6	**-0.325**	**-2.665**	**0.010**	-0.126	-1.141	0.259	-0.152	-1.354	0.181	-0.023	-0.308	0.759
7	-0.214	-1.695	0.095	-0.129	-1.247	0.217	-0.114	-1.063	0.292	0.042	0.582	0.563
8	-0.117	-0.910	0.367	-0.045	-0.428	0.670	-0.025	-0.236	0.814	-0.029	-0.414	0.680
9	-0.238	-1.898	0.063	**-0.254**	**-2.576**	**0.013**	**-0.274**	**-2.765**	**0.008**	-0.066	-0.922	0.361
10	-0.092	-0.713	0.479	-0.062	-0.595	0.554	-0.073	-0.700	0.487	0.037	0.544	0.588
11	**0.292**	**2.365**	**0.021**	0.190	1.847	0.070	0.182	1.752	0.085	**0.150**	**2.283**	**0.026**

Appendix B6. Metabolite component regression models for **Percent Change SCV PDFF%.** Grey shading and bolding denote $P<0.05$.

Predictor: Component Scores	**Model 1** Univariate	**Model 2** + Age	**Model 3** + Age + Sex	**Model 4** + Age + Sex

										+ % Body Fat		
	β	t	p-value	β	t	p-value	β	t	p-value	β	t	p-value
1	-0.003	-0.023	0.982	0.200	1.534	0.131	0.161	1.174	0.245	0.136	1.248	0.218
2	**-0.259**	**-2.003**	**0.050**	-0.187	-1.539	0.130	-0.149	-1.165	0.249	-0.178	-1.803	0.077
3	-0.203	-1.554	0.126	-0.097	-0.774	0.442	-0.064	-0.500	0.619	-0.062	-0.616	0.541
4	**-0.345**	**-2.754**	**0.008**	-0.211	-1.629	0.109	-0.206	-1.603	0.115	-0.080	-0.754	0.454
5	0.103	0.778	0.440	0.131	1.080	0.285	0.105	0.859	0.394	0.162	1.595	0.117
6	0.217	1.665	0.102	0.076	0.583	0.562	0.117	0.893	0.376	0.008	0.074	0.941
7	0.053	0.398	0.692	-0.019	-0.152	0.879	-0.046	-0.372	0.711	-0.169	-1.740	0.088
8	0.139	1.048	0.299	0.083	0.677	0.501	0.049	0.388	0.699	-0.045	-0.447	0.657
9	0.222	1.700	0.095	**0.241**	**2.047**	**0.045**	**0.264**	**2.265**	**0.028**	0.119	1.193	0.238
10	0.032	0.237	0.814	0.007	0.059	0.953	0.032	0.261	0.795	0.055	0.545	0.588
11	-0.242	-1.865	0.067	-0.168	-1.372	0.176	-0.153	-1.255	0.215	-0.089	-0.916	0.364

Appendix B7. Metabolite component regression models for **SCV PDFF% Reduction**. Grey shading and bolding denote $P<0.05$.

Predictor: Component Scores	**Model 1** Univariate			**Model 2** + Age			**Model 3** + Age + Sex			**Model 4** + Age + Sex + % Body Fat		
	β	t	p-value	β	t	p-value	β	t	p-value	β	t	p-value
1	0.000	-0.003	0.997	0.191	1.441	0.155	0.150	1.080	0.285	0.186	1.518	0.135
2	**-0.296**	**-2.316**	**0.024**	-0.230	-1.890	0.064	-0.197	-1.529	0.132	-0.214	-1.890	0.064
3	-0.179	-1.365	0.178	-0.079	-0.619	0.538	-0.045	-0.343	0.733	-0.006	-0.055	0.956
4	**-0.332**	**-2.638**	**0.011**	-0.208	-1.581	0.120	-0.203	-1.555	0.126	-0.088	-0.719	0.475
5	0.155	1.176	0.245	0.181	1.490	0.142	0.157	1.274	0.208	0.091	0.813	0.420
6	0.203	1.555	0.126	0.071	0.536	0.594	0.112	0.842	0.403	0.013	0.105	0.916
7	0.033	0.244	0.808	-0.036	-0.284	0.777	-0.064	-0.506	0.615	-0.177	-1.569	0.123
8	0.099	0.743	0.461	0.046	0.368	0.714	0.009	0.072	0.942	0.001	0.007	0.994
9	0.241	1.855	0.069	**0.259**	**2.181**	**0.033**	**0.283**	**2.404**	**0.020**	0.159	1.393	0.169
10	0.019	0.140	0.889	-0.004	-0.034	0.973	0.021	0.165	0.869	-0.052	-0.463	0.645
11	-0.223	-1.710	0.093	-0.153	-1.231	0.224	-0.138	-1.114	0.270	-0.118	-1.068	0.290

In the hepatic fat analysis, component 9 was significantly negatively associated with hepatic fat after controlling for all covariates, which is the only common component in both BAT and liver

outcome models (**Appendix B8**). Component 8 was also significantly positively associated with hepatic fat across all models.

Appendix B8. Metabolite component regression models for **Pre-Cold Liver PDFF%.** *Denotes that a quadratic function was used as it fit better than a linear function for labeled variables. Grey shading and bolding denote $P<0.05$.

Predictor: Component Score	**Model 1** Univariate			**Model 2** + Age			**Model 3** + Age + Sex			**Model 4** + Age + Sex + % Body Fat		
	β	t	p-value	β	t	p-value	β	t	p-value	β	t	p-value
1 – Linear*	**0.307**	**2.519**	**0.015**	0.185	1.423	0.160	0.176	1.320	0.192	0.133	1.112	0.271
1 – Quadratic*	**0.260**	**2.128**	**0.038**	0.188	1.533	0.131	0.198	1.557	0.125	0.147	1.263	0.212
2	0.164	1.286	0.203	0.101	0.839	0.405	0.122	0.954	0.344	0.119	1.075	0.287
3	0.155	1.214	0.230	0.046	0.371	0.712	0.053	0.414	0.680	-0.019	-0.169	0.867
4	0.245	1.959	0.055	0.106	0.821	0.415	0.107	0.825	0.413	-0.024	-0.204	0.839
5	-0.175	-1.379	0.173	-0.200	-1.717	0.091	-0.213	-1.782	0.080	-0.106	-0.938	0.352
6	**-0.309**	**-2.518**	**0.014**	-0.190	-1.517	0.135	-0.192	-1.489	0.142	-0.102	-0.876	0.385
7	-0.115	-0.896	0.374	-0.058	-0.484	0.630	-0.068	-0.546	0.587	0.035	0.308	0.759
8	**0.280**	**2.255**	**0.028**	**0.332**	**2.966**	**0.004**	**0.343**	**2.965**	**0.004**	**0.320**	**3.135**	**0.003**
9	**-0.347**	**-2.869**	**0.006**	**-0.358**	**-3.257**	**0.002**	**-0.362**	**-3.231**	**0.002**	**-0.233**	**-2.145**	**0.036**
10	-0.045	-0.347	0.729	-0.025	-0.209	0.835	-0.022	-0.183	0.855	0.105	0.955	0.344
11	0.108	0.843	0.403	0.037	0.308	0.759	0.041	0.331	0.742	0.040	0.365	0.716

Appendix B9. Stepwise linear regression models for **SCV PDFF% Reduction** in children. Grey shading and bolding denote $P<0.05$.

Predictor	**Model 1** Univariate			**Model 2** + % Body Fat		
	β	t	p-value	β	t	p-value
4-Hydroxy-L-Proline	**-.677**	**-4.216**	**< .001**	**-.648**	**-3.589**	**.002**

cis-4-Hydroxy-Proline	**-.675**	**-4.193**	**< .001**	**-.645**	**-3.568**	**.002**

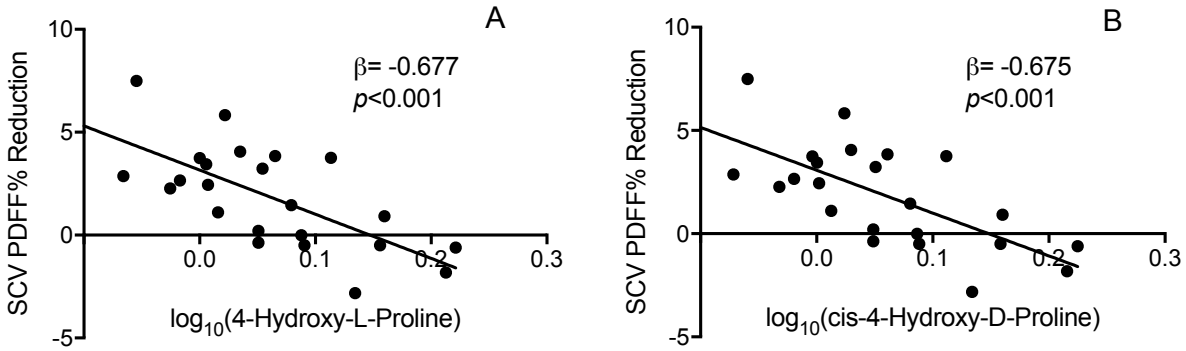

Appendix B10. Correlation scatter plot for **SCV PDFF% Reduction** in children. (A) 4-hydroxy-L-proline, and (B) cis-4-hydroxy-proline.